

UNITED STATES DEPARTMENT OF THE INTERIOR
GEOLOGICAL SURVEY

Alteration and vein mineralization,
Schwartzwalder uranium deposit,
Front Range, Colorado

by
Alan R. Wallace¹
U.S. Geological Survey

Open-file Report 83-417

1983

This report is preliminary and has not been edited or reviewed
for conformity with U.S. Geological Survey
editorial standards and stratigraphic nomenclature.

¹Denver, Colo.

ABSTRACT

The Schwartzwalder uranium deposit, in the Front Range west of Denver, Colorado, is the largest vein-type uranium deposit in the United States. The deposit is situated in a steeply dipping fault system that cuts Proterozoic metamorphic rocks. The host rocks represent a submarine volcanic system with associated chert and iron- and sulfide-rich pelitic rocks. Where faulted, the more competent garnetiferous and quartzitic units behaved brittly and created a deep, narrow conduit.

The ores formed 70-72 m.y. ago beneath 3 km of Phanerozoic sedimentary rocks. Mineralization included two episodes of alteration and three stages of vein mineralization. Early carbonate-sericite alteration pseudomorphically replaced mafic minerals, whereas the ensuing hematite-adularia episode replaced only the earlier alteration assemblage. Early vein mineralization produced a minor sulfide-adularia-carbonate assemblage. Later vein mineralization generated the uranium ores in two successive stages. Carbonates, sulfides, and adularia filled the remaining voids. Clastic dikes composed of fault gouge and, locally, ore were injected into new and existing fractures.

Geologic and chemical evidence suggest that virtually all components of the deposit were derived from major hornblende gneiss units and related rocks. The initial fluids were evolved connate/metamorphic water that infiltrated and resided along the extensive fault zones. Complex fault movements in the frontal zone of the eastern Front Range caused the fluids to migrate to the most permeable segments of the fault zones. Heat was supplied by increased crustal heat flow related to igneous activity in the nearby Colorado mineral belt. Temperatures decreased from 225°C to 125°C during later mineralization, and the pressure episodically dropped from 1000 bars. The CO₂ fugacity was initially near 100 bars, and uranium was carried as a dicarbonate complex. Sudden decreases in confining pressure during fault movement caused

evolution of CO_2 and a consequent increase in pH. Uranium was released with destruction of the uranyl complexes; it was subsequently reduced by aqueous sulfur species, thereby leading to the precipitation of pitchblende.

ACKNOWLEDGMENTS

I wish to express my warmest thanks to Tom Nash, who counselled me through this endeavor, and who provided a wealth of ideas, support, and friendship. Joe Whelan performed the isotopic analyses, and contributed greatly to my interpretations of that data. Ken Ludwig graciously provided the results of his U-Pb isotopic analyses and interpretations. Conversations with Tom, Joe, and Ken, along with those with Dick Taylor, Bob Rye, and Ed Young, provided a plethora of welcome ideas and stimulation.

This study would not have been possible without the tremendous cooperation of the Cotter Corporation and the other companies involved with uranium deposits in the Front Range. Rick Karlson and John Wright, the Chief Mine Geologists at the Schwartzwalder mine during the course of this study, were veritable fountains of information and interest, and kindly tolerated a novice in the subterranean world. Conversations with Rick and John, as well as with John Haley, Jim Paschis, Jack Stark, and Brad Watts, enhanced my understanding of the mines in the district.

This manuscript has benefitted from critical reviews by Cy Field and Tom Nash.

TABLE OF CONTENTS

	<u>Page</u>
1. Introduction	1
Purpose and Scope of Investigations	1
Methods of Investigation	3
Location and Accessibility	4
Mining History	5
Previous Work	6
Description of Mine Workings	7
2. Regional Geologic Setting	9
3. General Geology	12
Introductory Statement	12
Metamorphic Rocks	12
Hornblende Gneiss	15
Petrography and Chemistry	17
Quartz-feldspar Gneiss	21
Quartzite	23
Petrography and Chemistry	24
Garnet-biotite Gneiss	25
Petrography and Chemistry	27
Mica Schist	33
Petrography and Chemistry	33
Metamorphism	35
Metamorphic Rock Precursors	41
Intrusive Rocks	44
Pegmatite	44
Aplite	44
Structural Geology	44
Foliation	45
Folds	45
Faults	47
Rogers Fault System	48
Illinois Fault System	48
Tension Fractures	50
Development of Fault System	51
4. Alteration	55
Carbonate-sericite Alteration	55
Alteration of Hornblende Gneiss	57
Alteration of Garnet-biotite Gneiss	59
Alteration of Quartzite	61
Alteration of Mica Schist	61

	Hematite-adularia Alteration	61
	Chemical Effects of Alteration	65
	Volume Relations	65
	Chemical Gains and Losses	66
	Carbonate-sericite Zone	66
	Hematite-adularia Zone	69
5.	Vein Mineralogy and Paragenesis	71
	Descriptive Mineralogy	72
	Stage I Mineralogy	72
	Stage II Mineralogy	75
	Stage III Mineralogy	84
	Clastic Dikes	87
	Effects of Fault Movement on Ores	92
	Bottom of the Ore Deposit	93
	Supergene Processes	94
	Trace Elements	95
6.	Age of Mineralization and Tectonic Implications	103
7.	Geochemistry of Alteration and Vein Mineralization	107
	Estimates of Pressure and Temperature	107
	Stable Isotopes	111
	Oxygen Isotope Data	112
	Unaltered and altered wall rocks	112
	Vein carbonates	114
	Carbon Isotope Data	114
	Sulfur Isotope Data	116
	Processes of Alteration and Vein Mineralization	118
8.	Proposed Genesis of the Uranium Deposits	136
	Structural Development	136
	Origin of Clastic Dikes	137
	Source of Fluid and Mineral Components	138
	Carbon	138
	Sulfur	140
	Oxygen	141
	Uranium and Lead	142
	Possible Source Rocks	142
	The Hydrothermal System	146
9.	Summary and Conclusions	149
10.	References	153
11.	Appendix	167

LIST OF TABLES

<u>Table</u>	<u>Page</u>
1. Modal analyses of hornblende gneiss.	18
2. Microprobe analyses of minerals from hornblende gneiss.	19
3. Chemical analyses of hornblende gneiss.	20
4. Modal and chemical analyses of quartz-feldspar gneiss.	22
5. Modal analyses of quartzite.	25
6. Chemical analyses of quartzite.	26
7. Modal analyses of garnet-biotite gneiss.	28
8. Microprobe analyses of minerals from garnet-biotite gneiss.	29
9. Chemical analyses of garnet-biotite gneiss.	32
10. Modal analyses of mica schist.	34
11. Chemical analyses of mica schist.	36
12. Metamorphic mineral assemblages.	37
13. Chemical summary of fresh and altered rocks carbonate-sericite zone.	67
14. Microprobe analyses of vein carbonates.	84
15. Microprobe analyses of clastic dikes.	91
16. Summary of trace element chemistry of veins.	96
17. Correlation matrices for trace elements.	97
18. Trace element composition of clastic dikes.	102
19. Fluid inclusion data.	110
20. Oxygen and carbon isotope data for altered rocks.	113
21. Sulfur isotope data.	118

<u>Table</u>	<u>Page</u>
A1. Chemical analyses of altered hornblende gneiss.	168
A2. Chemical analyses of altered garnet-biotite gneiss.	169
A3. Trace element data for Illinois vein system.	170
A4. Trace element data for horsetail vein system.	171
A5. Trace element data for Rogers vein system.	172

LIST OF FIGURES

<u>Figure</u>	<u>Page</u>
1. Location of the Schwarzwaldler mine in the Front Range, Colorado.	2
2. Cross-section of the Schwarzwaldler mine, showing veins and mine workings.	8
3. Geologic map of the east-central Front Range.	10
4. Generalized geologic map of the area surrounding the Schwarzwaldler mine.	13
5. Schematic stratigraphic section of the major metamorphic rock units and members.	14
6. Photographs of the major rock units.	16
7. ACF-AKF diagrams for major rock units.	38
8. Fe-Mg-Mn diagram showing compositions of metamorphic minerals.	39
9. Sketch of surficial distribution of major lithologic units, faults, and folds.	46
10. Sketch of alteration zones in relationship to veins and other structures.	56
11. Photographs of carbonate-sericite alteration.	58
12. Photographs of hematite-adularia alteration.	62
13. Graph showing gains and losses of major oxides during carbonate-sericite alteration.	68
14. Graph showing chemical compositions of fresh hornblende gneiss, and of equivalent samples in carbonate-sericite and hematite-adularia zones.	70
15. Paragenetic diagram of alteration and vein mineralization.	73
16. Paragenetic diagram for Stage II mineralization.	77
17. Photomicrograph of Stage IIa pitchblende.	80

<u>Figure</u>	<u>Page</u>
18. Photographs of Stage IIb and IIc mineralization.	82
19. Photographs of breccias produced by high-pressure fluids.	86
20. Photographs of clastic dikes.	89
21. Cluster analyses of trace elements from horse-tail, Illinois, and Rogers vein systems.	99
22. Log $f(\text{CO}_2)$ - log $f(\text{O}_2)$ diagram showing stabilities of iron-bearing minerals.	108
23. Oxygen and carbon isotopic data for vein carbonates, and oxygen isotopic data for depositing fluids.	115
24. Diagram showing the stabilities of sodium and potassium silicates.	122
25. Diagrams showing the stability fields for minerals formed during alteration and early vein mineralization.	126
26. Diagrams showing the stability fields for minerals formed during Stage IIc mineralization.	128
27. Diagram showing the stability fields for uranyl carbonate complexes.	130

ALTERATION AND VEIN MINERALIZATION, SCHWARTZWALDER URANIUM DEPOSIT, FRONT RANGE, COLORADO

CHAPTER 1. INTRODUCTION

The Schwartzwald uranium mine, in the Front Range west of Denver, Colorado (Figure 1), is the largest known vein-type uranium deposit in the United States. The deposit is one of more than twenty mines and prospects along the eastern flank of the range. Discovered in 1949, the mine has been in nearly continuous production since 1953.

Known uranium reserves in the world occur in sandstone, quartz-pebble conglomerate, and vein types of deposits in approximately equal amounts (Nash et al., 1981). However, major recent discoveries of vein-type deposits in Australia and Canada will increase reserves in that category. The new discoveries have spurred interest in hardrock uranium districts in the United States, including those along the eastern flank of the Front Range. Evaluation of those districts and exploration for new deposits requires an understanding of the geologic processes responsible for the formation of large deposits such as that at the Schwartzwald mine.

Purpose and Scope of Current Investigations

As part of a program by the U.S. Geological Survey to study hard-rock uranium deposits in the United States, a new study was initiated in 1978 of the geology and geochemistry of the uranium deposits in the Front Range, with particular emphasis on the Schwartzwald mine. Kenneth R. Ludwig investigated the uranium-lead isotopies and determination of the age of the deposit. Joseph F. Whelan and Robert O. Rye studied the light stable isotope geochemistry of the deposit and wall rocks. This study has

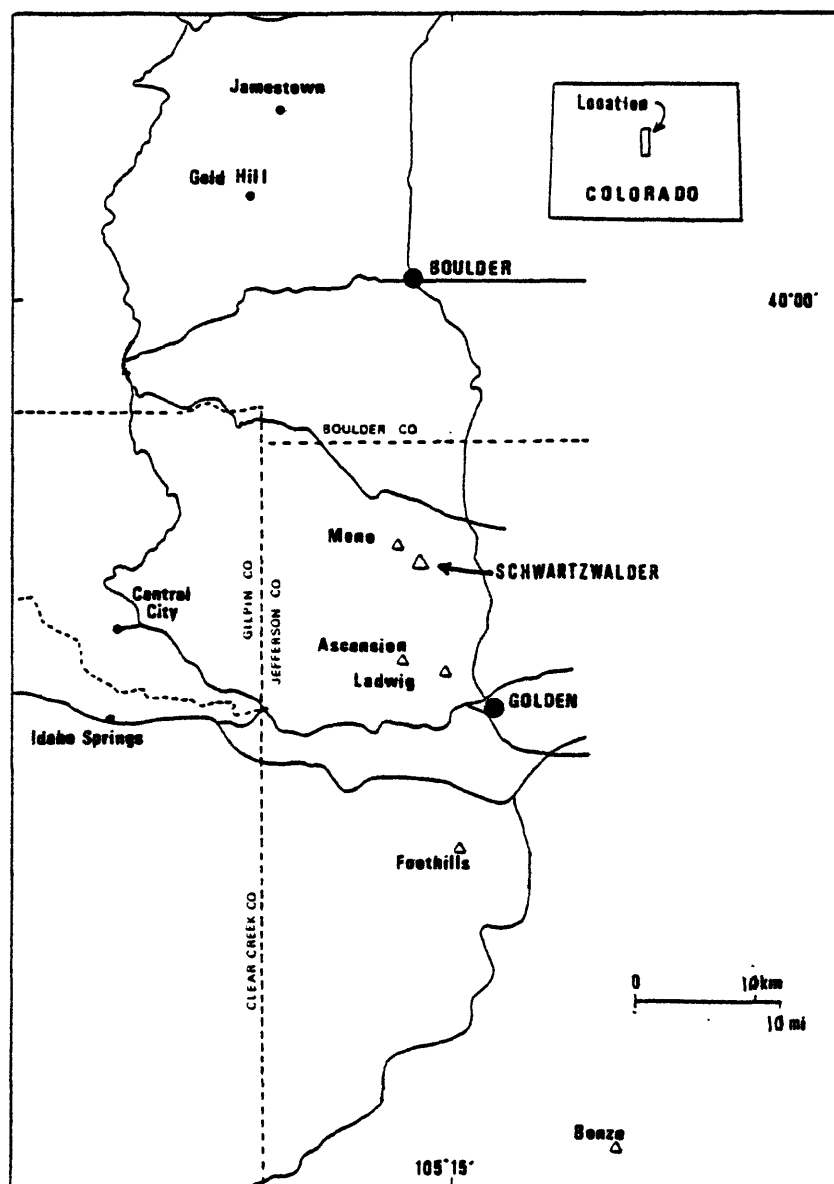


Figure 1. Location of the Schwartzwalder mine and other uranium mines in the east-central Front Range, Colorado.

concentrated on the regional setting, metamorphic petrology, hydrothermal alteration, vein mineralization, and trace element geochemistry. Each project benefitted from the excellent geologic framework provided by various geologists and mining companies who had worked or were still working in the area.

The purpose of this study is to define the environment of wallrock alteration and vein mineralization at the Schwartzwald deposit. The conclusions are based largely upon the specific results of this investigation, but also draw upon available geologic maps and the preliminary data obtained by the other investigators in the project. The ultimate goal of the study was to generate a model for the genesis of this type of deposit that can be used for evaluating other prospects in similar geologic settings in the foothills of the Front Range and elsewhere.

Methods of Investigation

Field work was done, as weather and mine access permitted, during parts of 1978, 1979, and the summers of 1980 and 1981. All field work utilized existing published and company surface and underground maps. Local maps and sketches were drawn to provide information for sample localities or where additional detail was necessary to describe a particular feature. Underground studies concentrated on and samples were collected from the host rocks, alteration zones, and veins; veins were sampled both laterally and vertically. In addition, diamond drill cores of wall rocks and veins were studied and sampled.

Samples collected in the field were used for mineralogical and chemical studies. Over two hundred thin, polished thin, and polished sections were examined optically with transmitted and reflected light. The electron beam microprobe (ARL, model SEM-Q) and scanning electron microscope (Cambridge Stereoscan 180) were used to verify mineral identification and provided quantitative and semi-quantitative analyses, respectively, of mineral species.

X-ray powder diffraction studies (Philips-Norelco diffractometer, Ni-filtered CuK radiation) also aided mineral identifications.

Chemical analyses of more than 150 samples were performed in the U.S. Geological Survey laboratories. Major oxide concentrations were determined by X-ray fluorescence. Quantitative and semiquantitative analyses for more than fifty trace elements were determined utilizing X-ray fluorescence, delayed neutron, emission spectrographic, atomic absorption, and other specific analytical techniques.

Fluid inclusion studies were attempted on selected samples of gangue minerals. The fluid inclusions in doubly polished sections were first studied optically and described. A Chaix M.E.C.A. heating-freezing stage was then used to determine freezing and homogenization temperatures for the inclusions. This information provided estimates of the salinity of the fluid and temperature of formation of the mineral.

Location and Accessibility

The Schwartzwalder mine is 11 km north-northwest of Golden, Colorado, in section 25, T.2S., R.71W. of the Ralston Buttes 7 1/2-minute topographic quadrangle (Figure 1). It can be reached year-round from Golden to the south along paved and dirt roads. The mine is situated on the west side of Ralston Creek, and the main haulage adit is at an elevation of 1996 m.

Mining activity dictated access to underground workings. Mined-out and subeconomic veins in the mine were sealed off for ventilation purposes, thereby restricting access to many workings in the upper half of the mine. During the course of this study, mining activity ceased along some veins, whereas development along other veins continually exposed fresh rock. Hazards related to blasting, mucking, and ventilation allowed only cursory inspection of some veins.

Other uranium deposits in the east-central Front Range (Figure 1; see also Sims and Sheridan, 1964) are accessible by paved or dirt roads; some can be reached only on foot. All properties are on private land; permission was required for access, and was not available for some prospects. Underground workings were accessible at only the Bonzo, Ladwig, and Mena mines. Flooding, caving, and high radon levels in the air prevented access to other deposits. Many prospects are nothing more than a small pit or adit.

Mining History

Ore has been produced and shipped from seven mines along the eastern foothills of the Front Range, and more than a dozen smaller prospects were taken to various stages of development. Several deposits were initially prospected for copper. In 1949, Fred Schwartzwalder discovered uranium at the present sites of the Mena and Schwartzwalder mines (Sheridan et al., 1967). Numerous other deposits and uranium occurrences were discovered and developed within the ensuing ten years. By 1960, seven mines had shipped ore; the largest producer was the Schwartzwalder mine (Sims and Sheridan, 1964).

A decrease in the market for uranium in the 1960's halted production at all but the Schwartzwalder mine, and only that mine has shipped ore since then. Exploration and property development have continued at all properties in the area, although most properties have changed ownership several times. Current owners or lessees of the major properties are as follows: Ascension (Exxon Corp.), Bonzo (Energy Fuels Nuclear), Schwartzwalder and Foothills mines (Cotter Corp.), Ladwig (Energy Fuels Nuclear and Reserve Oil and Minerals), and Mena (Western Nuclear and Reserve Oil and Minerals). In addition, Rocky Mountain Energy is doing exploratory drilling on two properties.

Production figures are largely unavailable for the deposits. Young (1979b) reported that total production from the Schwartzwald-

er mine exceeded five million kilograms of U_3O_8 .

Previous Work

The uranium deposits along the eastern foothills of the Front Range are within the bounds of ten 7 1/2-minute topographic quadrangles, the geology of which have been mapped by personnel of the U.S. Geological Survey. These maps, along with the regional studies by Lovering and Goddard (1950), Peterman and Hedge (1968), and Tweto (1975) provide a regional framework for more specific studies related to the uranium deposits.

Many studies have dealt with various aspects of one or more of the uranium deposits. Sims and Sheridan (1964) described all of the deposits as they were known in the late 1950's, and Sheridan et al. (1967) concentrated on those within the Ralston Buttes quadrangle. Reports dealing with specific desoposits include those for the Ladwig (Ferris and Bennett, 1977; Wallace, 1979), Mena (Stark, 1979), and Golden Gate Canyon (Adams and Stugard, 1956) mines.

The Schwartzwalder mine has been the subject of many studies. The geology of the deposit, as it became progressively more exposed and understood, was described by A. G. Bird (Bird, 1958, 1979; Downs and Bird, 1965), E. J. Young (Young, 1977, 1979a, 1979b), J. A. Paschis (Paschis, 1979; DeVoto and Paschis, 1980), and J. H. Wright (Wright, 1980; Wright et al., 1981). Many studies concentrated on specific aspects of ore genesis, including regional setting (Maslyn, 1978; Wallace, in press), ore mineralogy (Honea and Ferris, unpub. report; Heyse, 1972; Wallace and Karlson, 1982), and fluid inclusions (Rich and Barabas, 1976). All companies have internally-prepared reports and geologic maps of their respective deposits, many of which were made available for this study on a confidential basis.

Description of Mine Workings

The original mining at the Schwartzwalder deposit utilized five adits at several levels on the steep hillside southwest of Ralston Creek. Drifts and stopes extending from the five crosscuts followed the veins. Mining eventually descended below the bottom of the canyon, and a 300-meter shaft was sunk from the Steve level at a sill elevation of 1996 m. Crosscuts were driven northwest to the veins approximately every 30 m down the shaft. Each crosscut represented a level, and the levels were numbered sequentially downward from the Steve (First) Level. Two more shafts were ultimately sunk, one from the Steve Level to the 12th Level, and the second from the 10th to the 20th Levels. An exhaust borehole to the surface was drilled northwest of the other shafts in 1977, and crosscuts were driven to connect the borehole to the other workings. All mining to date has been in the Illinois and horsetail fault systems. Current development is beginning to exploit new ores in the Rogers vein system to the northwest.

Crosscuts from the shafts intersect the veins, and drifts extend laterally along the veins. The veins are mined by room and pillar, shrinkage stoping, and block caving methods (Wright, 1980). The ore is routed through ore passes and loaders to the hoists, which carry the ore to small trains on the Steve Level. The ore is ultimately shipped to the Cotter Corporation mill in Canon City, Colorado.

A general cross-section of the mine is shown in Figure 2.

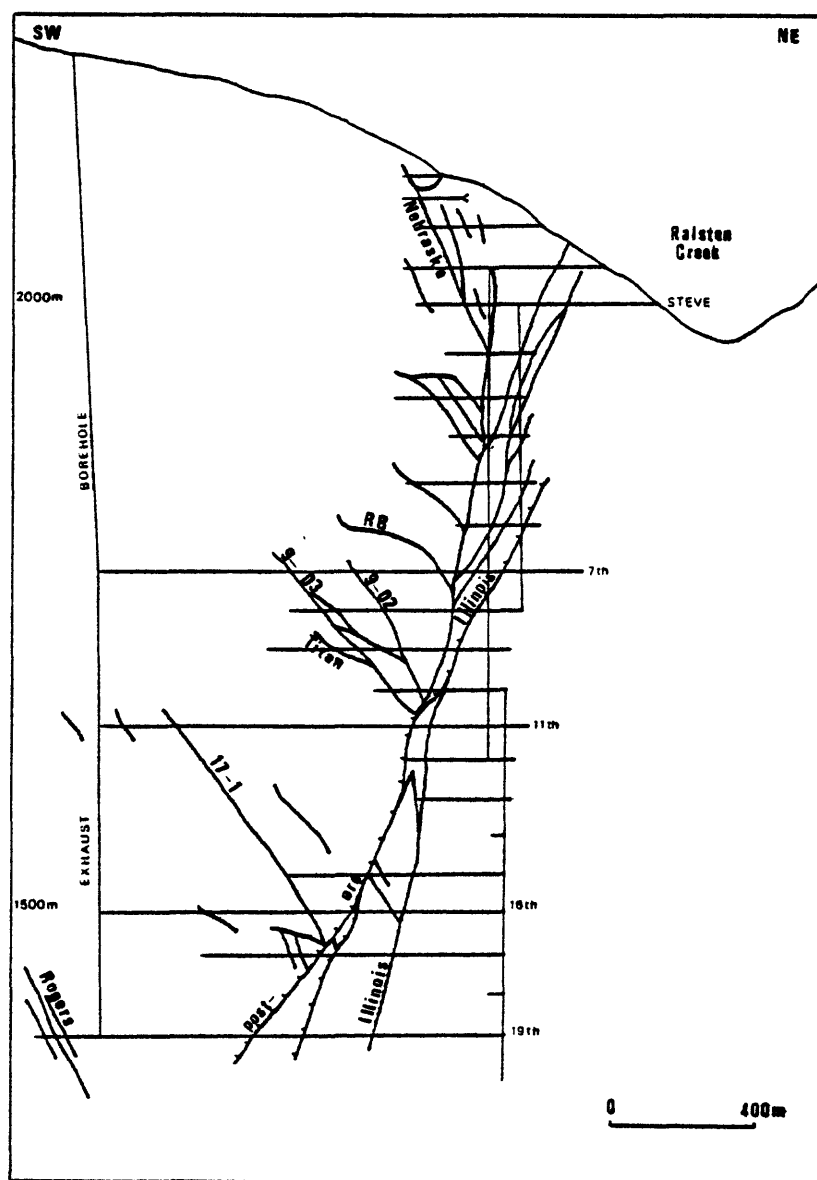


Figure 2. Cross-section of the Schwartzwalder mine, showing veins and mine workings (from unpub. Cotter Corp. data).

CHAPTER 2. REGIONAL GEOLOGIC SETTING

The north-trending Front Range of Colorado is a structural block composed of igneous and metamorphic rocks of dominantly Proterozoic age (Figure 3). A thick section of Paleozoic and younger continental and marine sedimentary rocks unconformably flanks and partially overlies the exposed basement complex. Intrusive bodies of Late Cretaceous and younger age form an elongate, northeast-trending belt through the Proterozoic basement. Ore deposits associated with plutons comprise the Colorado mineral belt, which intersects the range front 30 km north of the Schwartzwalder mine.

Protoliths of the metamorphic rocks were originally deposited in a volcanic arc-backarc basin environment prior to 1730 m.y. ago (Hills and Houston, 1979). Regional and dynamic metamorphism 1750-1700 m.y. ago transformed the mixed sedimentary and volcanic assemblage into a medium- to high-grade metamorphic terrane, and accompanied the intrusion of the Boulder Creek Granodiorite (Hedge and Peterman, 1968). Regional folding and metamorphism accompanied the intrusion of the Silver Plume Granite 1400 m.y. ago, but no regional metamorphic event was related to the emplacement of the Pikes Peak Batholith 1041 m.y. ago (Hedge and Peterman, 1968).

The Front Range block was uplifted and stripped of its sedimentary veneer at least twice during Phanerozoic time. Block uplifts related to the development of the Ancestral Rocky Mountains during Pennsylvanian time (Kluth and Coney, 1981) induced erosion and peneplanation of the basement rocks. Coarse arkosic sediments derived from the exposed basement were deposited unconformably on the flanks of the block uplifts. Major uplift of the basement block during the Late Cretaceous - early Tertiary Laramide orogeny again caused erosion of the overlying sedimentary rocks and exposed the Proterozoic rocks (Tweto, 1975).

Cataclastic deformation 1200 m.y. ago (Abbott, 1972) generated large northeast-trending shear zones and smaller, but laterally extensive, northwest-trending faults (Tweto and Sims, 1963).

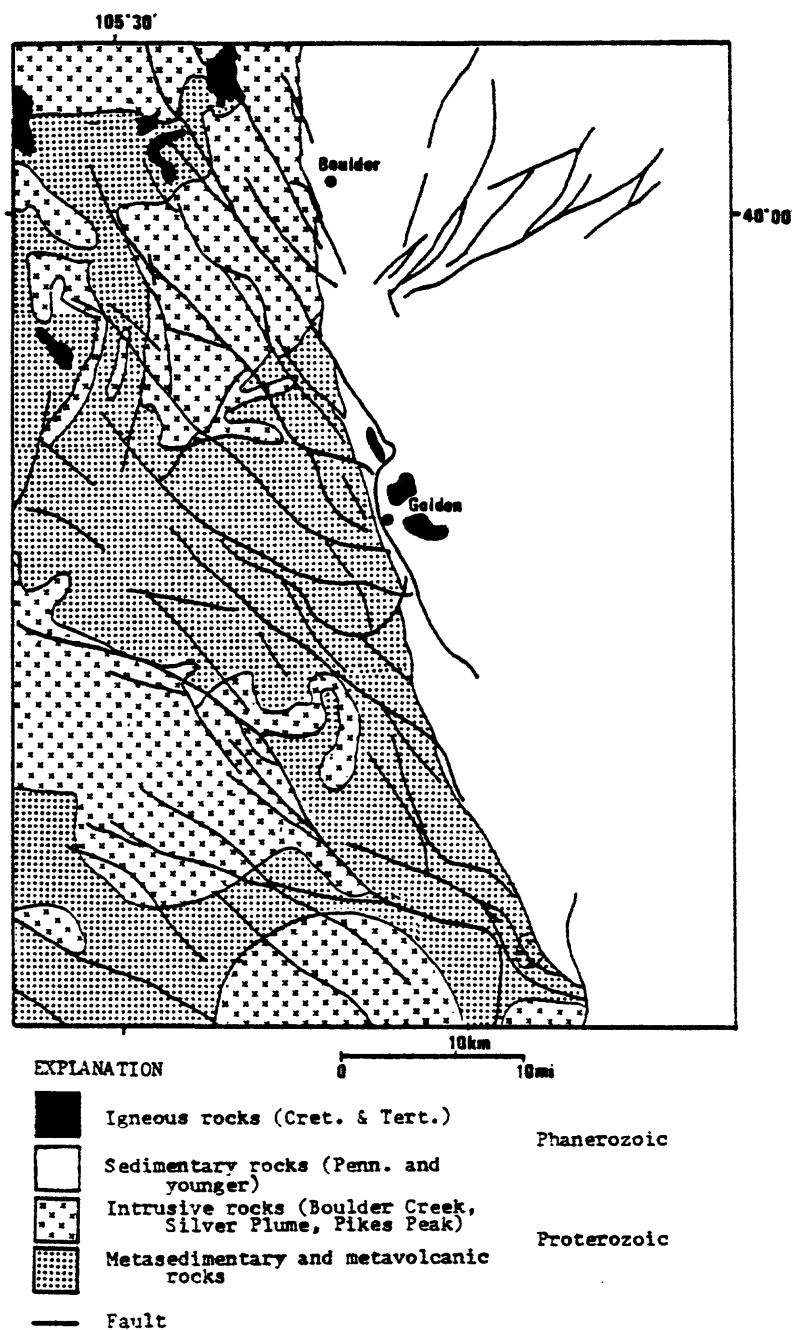


Figure 3. Geologic map of the east-central Front Range, Colorado (from Tweto, 1979).

Proterozoic movement along the northwest-trending faults produced cataclastic to mylonitic textures, and Late Proterozoic dikes of aplite, diabase, and pegmatite invaded some of the fault zones. Renewed movement along the faults facilitated the uplift of the Front Range during the Laramide orogeny (Tweto, 1975). In addition, major reverse faults formed along the flanks of the Front Range, and repeated movement along those faults continued during the Laramide orogeny.

The northwest-trending faults cut both granitic and metamorphic terranes in the east-central Front Range. Quartz and hematite cement the fault-generated breccias in the granitic terrane. In contrast, carbonates and adularia cement the breccias in the metamorphic terrane (Wallace, in press). In areas where both cements are present, the carbonate indurates brecciated fragments of the quartz-hematite cement.

CHAPTER 3. GENERAL GEOLOGY

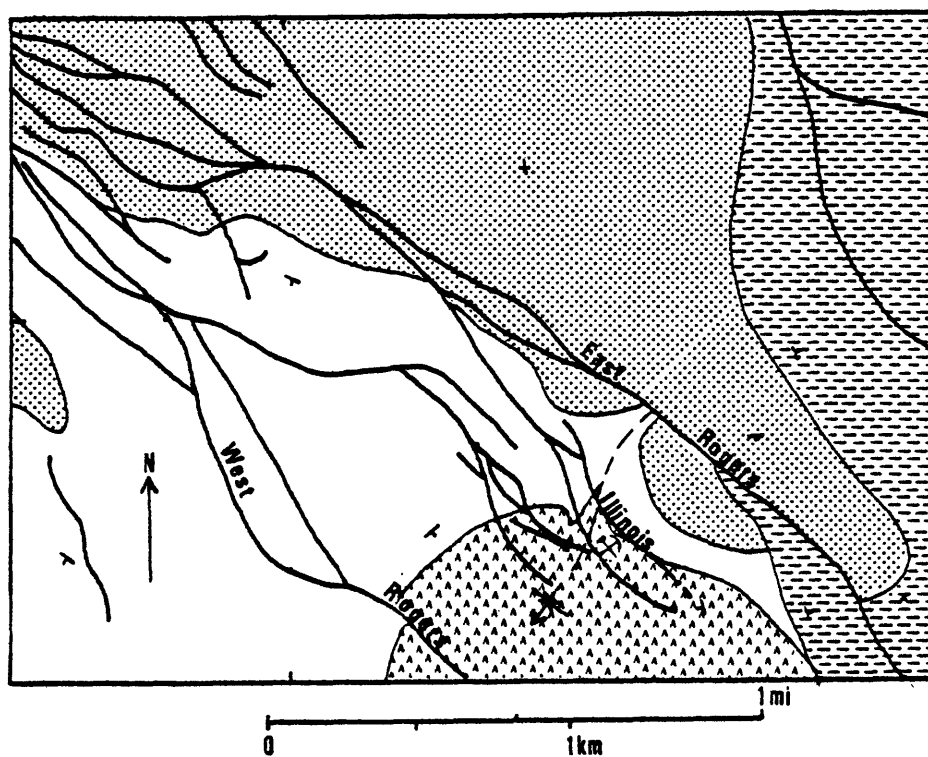
Introductory Statement

The veins of uranium at the Schwartzwalder mine are situated in a complex array of faults and fractures related to the Rogers fault system, one of the northwest-trending faults of Proterozoic ancestry (Figure 4). The host rocks are part of a multilithic sequence of metasedimentary and metavolcanic rocks that was folded during Proterozoic deformation into a steeply plunging, isoclinal fold (Sheridan et al., 1967). Subsequent development of the northwest fault system truncated the nose of the fold. The Phanerozoic sedimentary rocks once covered the study area, and the unconformity between the crystalline basement and the overlying Pennsylvanian Fountain Formation is less than two kilometers east of the deposit. The east segment of the Rogers fault cuts the unconformity 1 km southeast of the mine.

Metamorphic Rocks

The metamorphic rocks form four major units, each one of which contains one or more lithologic varieties (Figure 5). The major units include hornblende gneiss, quartzite, garnet-biotite gneiss, and mica schist. The quartzite and garnet-biotite gneiss constitute a relatively narrow transition zone between the regionally more extensive hornblende gneiss and mica schist units described by Sheridan et al. (1967). The width of the transition zone varies due to both tectonic thickening and variations in the thickness of the original sedimentary sequence. An average of 50-100 meters is a good approximation for the width of the transition zone.

The metasedimentary rocks were originally included in the Idaho Springs Formation (Lovering and Goddard, 1950). That name has been discarded, and rock units are now named on the basis of



Explanation:




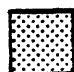





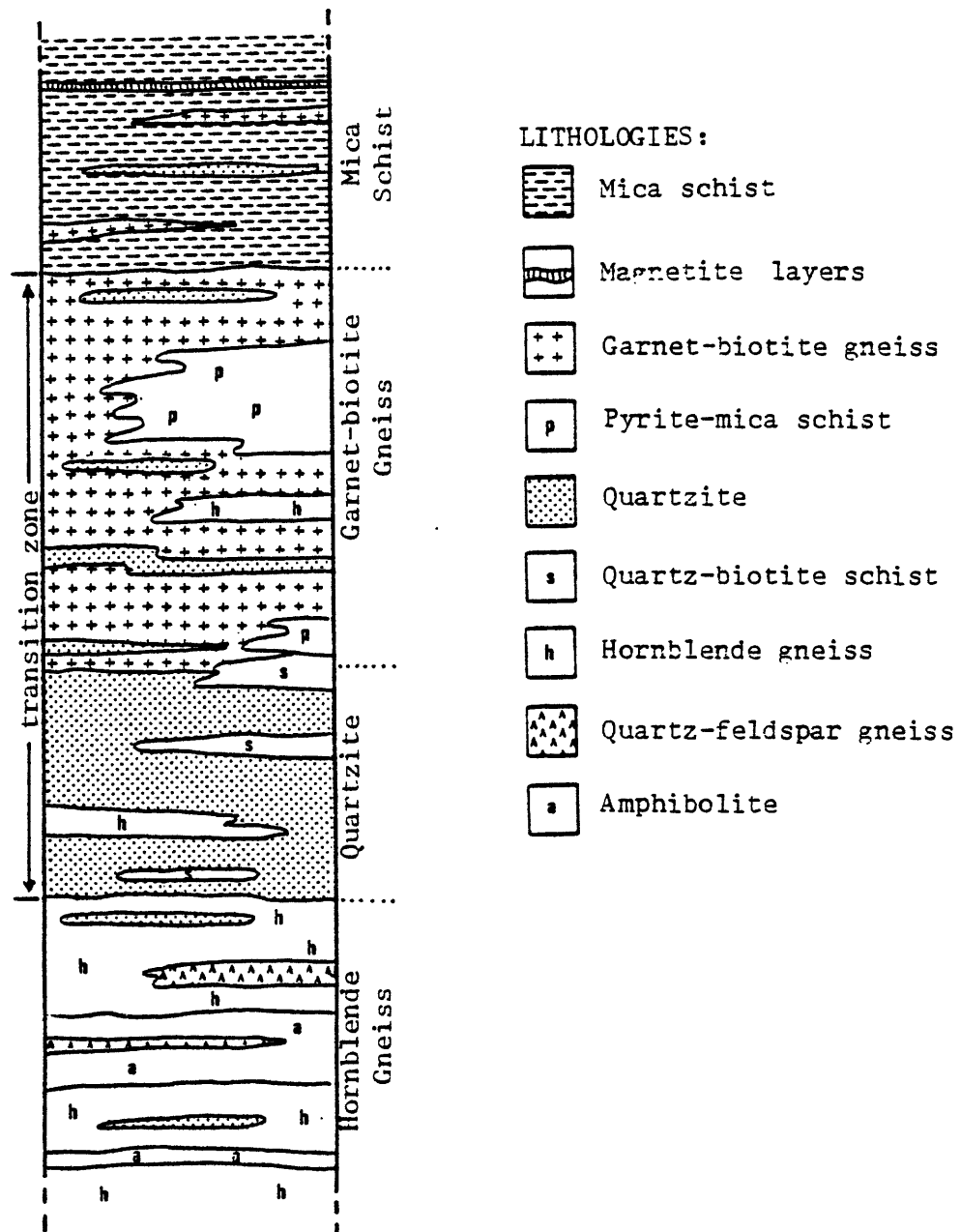
	Sedimentary rocks - undivided	} Phanerozoic
	Mica schist	
	Hornblende gneiss	} Proterozoic
	Interlayered microcline gneiss and calc-silicate gneiss	
	Contact	
	Fault	
	Synform, showing direction of plunge	
	Strike and dip of bedding and layering	
	Schwartzwalder mine	

Figure 4. Generalized geologic map of the area surrounding the Schwartzwalder mine (modified from Sheridan et al., 1967).



their principal lithology (Tweto, 1977).

Hornblende Gneiss

The hornblende gneiss unit is part of the regionally more extensive hornblende gneiss mapped by Sheridan et al. (1967). At the mine, the unit is lithologically diverse, and includes calc-silicate gneiss, massive amphibolite, and quartz-flooded hornblende gneiss. The calc-silicate gneiss is the dominant lithology; the other two lithologies form thin to thick beds within the calc-silicate gneiss.

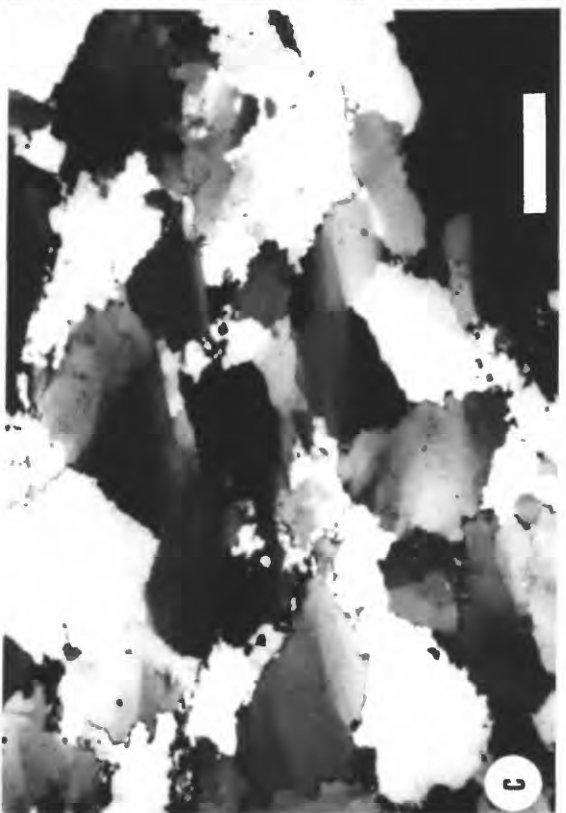
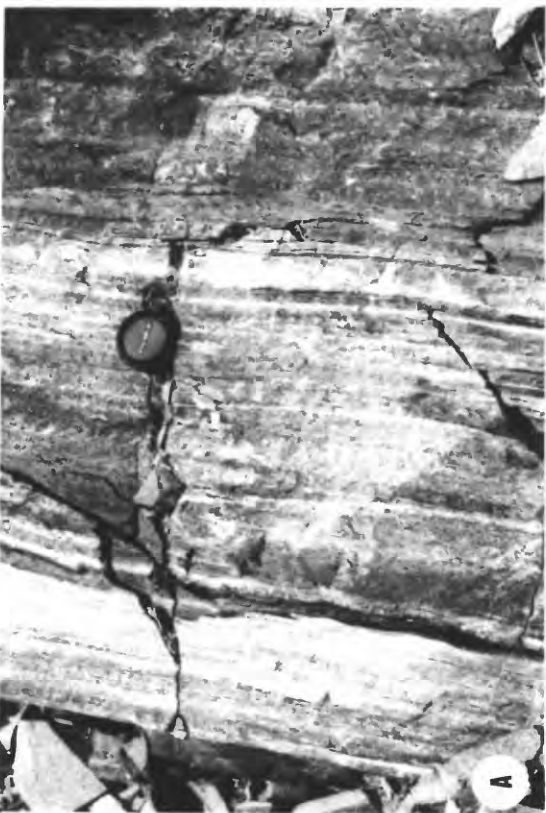
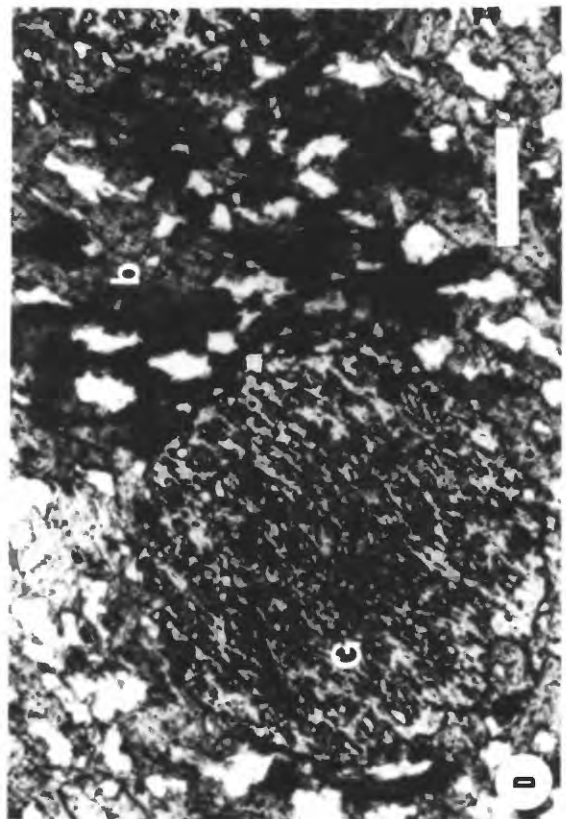
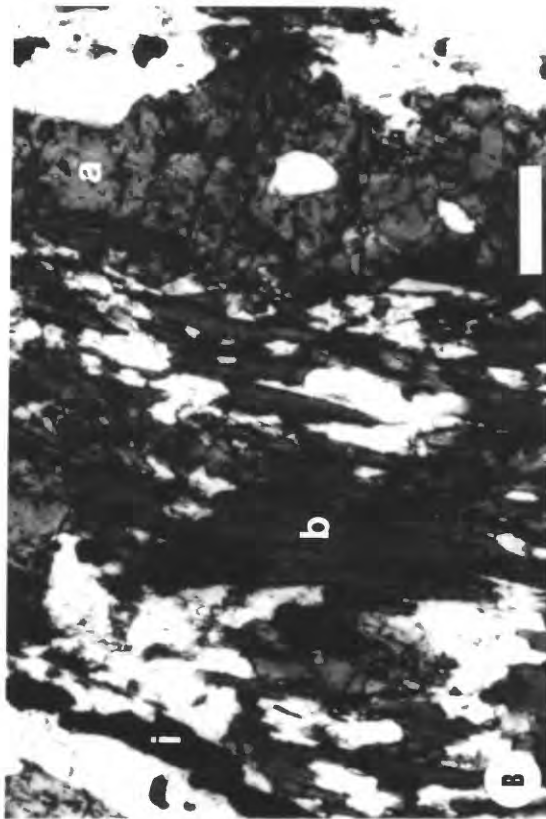
Distinct compositional layering characterizes the calc-silicate gneiss (Figure 6a). Dark layers composed of amphibole and biotite alternate with lighter layers of quartz or calcite. Layers range in thickness from several millimeters to several centimeters, although the thickness of some dark layers exceeds several meters. Layering parallels foliation in the mafic zones, and banding visually accentuates folds at all scales. Biotite-rich layers are locally common, and other layers contain coarse crystals of pink garnet, black tourmaline, or potassium feldspar.

The amphibolite is very dark green, fine grained, and massive, and is lithologically similar to the dark layers in the calc-silicate gneiss. Foliation is indistinct owing to the massive texture. Layers of quartz and calcite are locally common, but they are thin and more widely spaced than those in the calc-silicate gneiss.

"Quartz-flooded" describes calc-silicate gneiss with abundant layers of quartzite and veins of quartz. This lithology is both gradational into the major quartzite unit and locally enclosed by the calc-silicate gneiss. Most layers of quartzite resemble the blue-white microcrystalline rock in the quartzite unit, and are parallel to foliation and other layering. In striking contrast, however, are anastomosing layers and veins of milky white quartz which cut and replace both calc-silicate gneiss and quartzite

Figure 6. Major lithologies at the Schwartzwalder deposit.

- a. Calc-silicate gneiss member of hornblende gneiss. Light-colored bands are felsic gneiss and marble; dark layers are amphibolite and hornblende gneiss.
- b. Photomicrograph of hornblende gneiss, with hornblende (a) and biotite (b). Felsic minerals include quartz and plagioclase feldspar. Abundant opaque is ilmenite (i). Bar is 0.20 mm long.
- c. Photomicrograph of quartzite. Note dimensional-preferred orientation, undulatory extinction, and serrate contacts. Bar is 1.0 mm long.
- d. Photomicrograph of garnet-biotite gneiss. Garnet (g) contains quartz inclusions. Bar is 1.0 mm long.



layers. These zones are uncommon, and are truncated by the Laramide faults containing uranium ores. They may represent Proterozoic quartz veins of either hydrothermal or metamorphic origin.

Petrography and Chemistry

The mineralogy and textures of the hornblende gneiss are extremely variable. All rocks are fine-grained and foliated, and compositional layering is usually present. Hornblende is always a major component, and biotite, calcite, clinopyroxene, actinolite, quartz, and feldspars all may be abundant in the various lithologies (Table 1).

Pleochroic green hornblende forms fine- to coarse-grained subhedral crystals. The average composition is that of ferroedenite (Leake, 1978), based upon microprobe analyses (Table 2). Ferro-actinolite and grunerite are interleaved with hornblende. Pleochroic brown biotite (Table 2) is interleaved with amphiboles (Figure 6b), and also forms amphibole-free layers. Very pale blue salite (Table 2) is locally common, and forms coarse corroded porphyroblasts, some of which are strongly resorbed by amphibole and quartz. Undulatory quartz forms medium-grained layers parallel to foliation and grains interstitial to the mafic minerals. Plagioclase feldspar (An_{40}) occurs as small grains with quartz, or, more rarely, relatively coarse porphyroblasts aligned parallel to foliation. Microcline is twinned and medium-grained, whereas orthoclase is commonly untwinned and fine-grained. Calcite, although not always present, is a major component of some rocks. In such cases the calcite forms a coarse matrix in which other minerals are embedded. It does not invade or flood quartz layers, and is confined to mafic layers. When present in smaller amounts, calcite is fine-grained and intergrown with all minerals. Spene and ilmenite are ubiquitous but mutually exclusive, as are ilmenite and calcite. Primary muscovite is notably absent from the hornblende gneiss.

Table 1. Modal analyses (volume percent) of rocks of hornblende gneiss unit.¹

	80S31	80S35	80S8
Quartz	7.0%	3.0%	—
Plagioclase	16.0	26.0	tr
Microcline	tr	—	3.0%
Biotite	13.0	3.0	17.0
Hornblende	62.0	51.0	24.0
Actinolite	—	8.0	—
Clinopyroxene	—	tr	17.0
Calcite	—	3.0	40.0
Ilmenite	2.0	—	—
Sphene	—	2.0	tr
Scapolite	—	4.0	—
Epidote	—	tr	—
Apatite	tr	tr	tr
Zircon	tr	tr	tr
Total	100.00	100.00	100.00

¹Modes based upon counts totalling 800-1,000 points. (-): not present; (tr): trace.

The parallel arrangement of biotite, amphiboles, and local porphyroblasts of plagioclase define the foliation. Compositional layering parallels foliation, although some small felsic- or carbonate-rich lenses are oblique. The contacts of calcite-rich layers are more diffuse than those of quartz-rich layers. There is no evidence that conformable layers of quartz or calcite formed as a result of post-metamorphic veining.

Major oxide analyses of the hornblende gneiss illustrate the compositional variability of the unit (Table 3). All lithologies are rich in calcium and iron. Variations in SiO₂, CaO, and CO₂ controlled the abundances of quartz, hornblende, actinolite, and calcite. Concentrations of TiO₂, CaO, and CO₂ apparently controlled the formation of ilmenite and sphene. At constant TiO₂, rocks with high CO₂ or CaO contain sphene and those with low CO₂ or CaO contain ilmenite, a relationship demonstrated by the occurrence of sphene in calcite-rich rocks.

Table 2. Microprobe analyses of minerals from hornblende gneiss unit.

Mineral	Biotite	Biotite	Pyroxene
Sample	80S59	79S31	79S31
# spots anal.	3	4	2
SiO ₂ %	36.3	36.3	51.0
Al ₂ O ₃	15.5	16.8	0.31
FeO	23.2	22.2	15.7
MgO	9.9	9.75	9.51
CaO	0.01	0.04	23.8
Na ₂ O	0.34	0.12	0.05
K ₂ O	9.03	9.58	0.02
TiO ₂	2.16	1.76	0.02
MnO	0.12	0.13	0.36
Total	96.58	96.68	100.70

Numbers of ions on basis of 24 O (6 O for pyroxene)

Si	6.073	8.000	6.034	8.000	Si	1.96	
Al	1.927		1.966		Al	0.01	2.00
Al	1.118	1.384	1.320	1.539	Ti	0.00	
Ti	0.271		0.219		Fe	0.03	
Fe	3.237		3.085		Fe	0.48	
Mn	0.017	5.726	0.019	5.518	Mg	0.55	2.02
Mg	2.472		2.414		Mn	0.01	
Ca	0.001		0.007		Ca	0.98	
Na	0.109	2.036	0.038	2.077	Na	0.00	
K	1.926		2.032		K	0.00	

* * * * *

Mineral	Amphibole	Amphibole	Amphibole
Sample	80S59	79S31	79S31
# spots anal.	4	1	1
SiO ₂ %	43.12	49.40	46.20
Al ₂ O ₃	10.89	1.99	6.46
FeO	20.38	19.00	20.00
MgO	8.45	12.20	10.60
CaO	11.08	12.50	12.30
Na ₂ O	2.07	0.29	0.65
K ₂ O	0.58	0.15	0.67
TiO ₂	0.86	0.04	0.39
MnO	0.44	0.20	0.21
Total	97.87	95.78	97.49

Numbers of ions on basis of 24 O

Si	6.852	8.00	7.879	8.00	7.322	8.00
Al	1.148		0.121		0.678	
Al	0.891		2.901		0.529	
Ti	0.102		0.004		0.046	5.000
Mg	2.001	5.00	2.901	5.00	2.507	
Fe	2.006		1.840		1.918	
Mn	—		—		—	
Fe	0.702		0.703		0.735	
Mn	0.059	2.00	0.028		0.029	3.197
Ca	1.239		2.140	2.990	2.096	
Na	0.637		0.088		0.201	
Ca	0.648	1.402	—		—	
K	0.117		0.31		0.136	

Table 3. Chemical analyses of hornblende gneiss unit.

	79S28	79S31	80S8	80S15	80S28	80S31	80S35	80S40	80S67	80S81	80S90	80S124
SiO ₂ (%)	40.70	45.70	13.10	42.00	50.00	45.70	44.50	46.20	48.10	30.30	44.00	49.60
Al ₂ O ₃	4.80	13.00	12.60	14.30	15.00	15.80	16.10	15.30	14.20	16.80	15.80	13.70
Fe (total)	7.36	13.00	9.32	9.92	9.24	14.40	12.90	9.93	9.97	13.20	9.98	10.60
FeO	5.95	10.70	7.69	7.93	7.46	11.50	10.40	7.94	—	—	8.38	7.54
Fe ₂ O ₃	1.57	2.55	1.63	2.20	1.98	3.22	2.78	2.21	—	—	1.78	3.40
MgO	2.30	5.48	5.89	3.80	3.60	5.56	4.60	4.50	4.70	4.20	3.70	3.70
CaO	26.90	9.31	21.50	9.42	10.20	8.15	10.30	13.00	11.30	11.40	5.47	8.53
Na ₂ O	0.20	<0.20	0.30	2.40	4.40	2.80	3.10	4.10	3.30	<0.20	0.30	3.10
K ₂ O	0.39	4.39	3.03	3.83	0.77	1.51	2.01	0.62	1.80	5.93	4.99	1.86
TiO ₂	0.51	1.27	0.79	1.75	0.87	1.93	1.87	0.95	1.25	1.64	1.49	1.93
P ₂ O ₅	<0.10	0.40	0.20	0.20	0.20	0.30	0.20	0.20	0.20	0.40	0.40	0.62
MnO	0.27	0.08	0.13	0.18	0.16	0.20	0.13	0.11	0.70	0.16	0.10	0.13
LOI	16.66	6.78	13.10	11.32	4.45	1.85	3.74	4.41	4.38	14.68	14.10	5.34
C (total)	4.38	1.71	3.07	3.05	1.04	0.34	0.84	1.04	1.2	3.49	—	—
C (org.)	0.05	0.39	0.28	0.53	0.15	0.13	0.01	0.01	0.40	0.21	—	—
C (carb.)	4.33	1.32	2.79	2.52	0.89	0.21	0.83	1.02	0.80	3.28	—	—
S	0.01	0.05	0.06	0.02	0.03	0.16	0.02	0.04	0.02	0.07	—	—
Hg (ppm)	0.01	<0.01	<0.01	0.01	<0.01	<0.01	0.01	0.01	<0.01	0.01	0.03	0.04
Ag	<5	<5	<5	<5	<5	<5	<5	<5	<5	6	<5	<5
As	<1	5	<1	30	10	7	1	1	<1	50	100	10
B	N	N	N	L	N	N	N	N	N	N	30	N
Ba	100	500	500	150	150	300	150	100	300	200	150	1500
Be	N	L	N	70	N	N	N	N	N	L	10	2
Bi	<0.20	0.50	0.20	1.50	<0.20	<0.20	0.50	<0.20	<0.20	<0.20	<0.20	0.70
Cd	1	0.30	0.20	2	0.20	0.50	0.50	0.20	0.20	0.30	0.30	0.20
Co	3	22	23	37	23	37	41	30	26	26	77	23
Cr	150	300	100	150	150	70	200	200	200	150	300	100
Cu	2	150	30	5	100	70	30	20	70	100	150	100
F	300	1500	500	1000	300	700	900	400	800	1400	3100	1200
Ga	7	20	20	20	15	20	30	20	20	20	20	20
La	N	N	N	N	N	N	N	N	N	N	N	70
Mo	2	<2	25	16	3	2	<5	<5	7.40	5.40	14	42
Ni	15	77	36	65	46	38	67	62	48	77	120	41
Pb	10	N	N	20	N	10	N	N	10	10	50	N
Sb	<1	50	<1	15	<1	2	<1	<1	<1	3	3	3
Sc	10	30	20	30	20	30	30	30	30	20	30	20
Sr	150	150	70	200	N	150	150	150	150	150	150	1500
Th	<2.80	<3.20	<2.30	<15	<2.90	<2.10	<2.40	2.64	<2.50	<3.20	<2.50	<11
Tl	<1	<1	<1	<1	<1	<1	<1	<1	<1	2	<1	<1
U	1.80	2.66	1.08	52	1.74	0.74	<2.10	2.03	2.97	3.75	3.46	37.50
V	70	300	70	300	150	200	300	150	300	100	300	150
Y	20	30	15	20	15	20	30	15	30	15	20	30
Yb	2	3	1.50	3	1.50	2	3	1.50	3	1.50	3	3
Zn	30	70	50	20	70	70	150	100	50	100	100	200
Zr	30	70	30	70	70	50	70	70	100	30	100	100
density (g/cm ³)	2.77	2.90	2.95	2.71	2.77	2.87	2.82	2.77	2.89	2.87	2.63	2.54

Analyzed for but not detected in any sample: Au, Ca, Eu, Ge, Hf, In, Li, Nb, Nd, Pd, Pr, Pt, Ra, Se, Sm, Sn, Ta, Te, W. N: not detected; L: detected but below accurate detection limit; (-): not analyzed for.

Quartz-feldspar Gneiss

Quartz-feldspar gneiss forms conformable layers exclusively within the hornblende gneiss. As such, it is a subunit of the hornblende gneiss. However, on a regional scale it forms a distinct and separate unit (Sheridan et al., 1967; Stark, 1979), and will be considered as such in this report.

The quartz-feldspar gneiss is medium-grained, foliated, and reddish black. Individual layers vary in width from one to several meters, and are always conformable to the foliation and layers of the enclosing hornblende gneiss. Pink feldspars impart the distinctive reddish hue to the rock.

Quartz, plagioclase feldspar (An_{28}), biotite, and microcline are the major minerals (Table 4). Some units are devoid of alkali feldspars, in contrast to microcline-rich units elsewhere in the region. Plagioclase feldspar is always the dominant feldspar. Biotite is olive-green in samples containing microcline, but reddish brown in those devoid of microcline. The preferred orientation of the mica imparts a foliated texture to the rock.

The quartz-feldspar gneiss has two dominant textures. Most rocks contain equigranular felsic minerals with oriented flakes of brown biotite (sample 1; Table 4). Other samples have an aplitic texture with patches and diffuse linear zones of fine-grained quartz, plagioclase feldspar, green biotite, and minor epidote, which replace primary quartz and feldspars (sample 2; Table 4). These diffuse linear zones may represent shearing during Proterozoic tectonism, although they were not observed in any other units.

The major oxide composition of the quartz-feldspar gneiss is given in Table 4. The rock is relatively silicic, and is compositionally similar to a rhyolite (Le Maitre, 1976).

Table 4. Modes (volume percent) and chemical analyses (weight percent) of rocks of quartz-feldspar gneiss unit.

Modes	1	2
	Qtz-feld Gneiss	Qtz-feld gneiss with aplitic zones
Quartz	36%	47%
Microcline	2	10
Plagioclase	50	31
Biotite	12	10
Carbonate	--	1
Magnetite	tr	1
Epidote	--	tr
Apatite	tr	tr
Zircon	tr	tr
Total	100.00	100.00

Chemical	
Analyses	80S63
SiO ₂ (%)	71.20
Al ₂ O ₃	14.00
Fe (Total)	2.79
MgO	0.62
CaO	1.62
Na ₂ O	3.40
K ₂ O	4.22
TiO ₂	0.30
P ₂ O ₅	0.10
MnO	0.04
LOI	1.43
Total	99.71

¹Modes based upon counts totalling 800 points. (-): not present;
(tr): trace.

Quartzite

The quartzite unit is bounded stratigraphically by the hornblende gneiss and garnet-biotite gneiss units, and is part of the transition zone. Layers and lenses of quartzite are also present in the quartz-flooded zones of the hornblende gneiss and in all other units. The unit varies in thickness, probably due both to original variations in stratigraphic thickness and to later tectonic thickening. True thicknesses of 3-15 meters are most common. The contact with the hornblende gneiss may either have an intervening zone of quartz-flooded hornblende gneiss, or may grade directly into the calc-silicate gneiss lithology. Contacts with the garnet-biotite gneiss are both sharp or gradational, with a gradual increase in non-quartzitic material towards the gneiss.

The geologic staff at the Schwartzwalder mine has defined two lithologies in the quartzite: the dominant quartzite unit, and a quartz-biotite schist unit. The quartzite member is predominantly a massive, fine-grained quartzite, but contains thin, locally abundant layers of hornblende gneiss and mica schist. The massive variety is blue-white to white, although layers and patches of red quartzite, independent of hydrothermal alteration, are common. These layers are aligned and impart an apparent foliation to the quartzite. In many exposures, the quartzite contains very thin to thick lenses and bands of schist, all of which are preferentially oriented. Garnet- and hornblende-rich layers are also common. The most extreme cases of contamination occur where quartzite and carbonate-rich layers form zones, several meters in width, of alternating 1-8 mm-wide bands. Isolated layers in the quartzite contain abundant magnetite and sulfides; pyrite is the dominant sulfide.

The quartz-biotite schist member is lithologically similar to the major mica schist unit, but occurs sporadically between the garnet-biotite gneiss and hornblende gneiss. It is entirely absent in some sections. The rock is dark and fine-grained. It is

locally garnet-rich, resembling the garnet-biotite gneiss unit, and locally pyrite-rich, resembling the pyrite-mica schist member of the garnet-biotite gneiss. Oriented micas, parallel bands of pyrite, and compositional layers define the foliation. Zones composed of thin, alternating bands of mafic and felsic layers are common. Layers of quartzite are prevalent in some sections.

Petrography and Chemistry

The quartzite is composed dominantly of quartz with minor and variable amounts of other minerals (Table 5). Although the quartz is fine to medium grained, it is noticeably finer-grained in rocks containing other minerals. Quartz crystals have pronounced undulatory extinction and a dimensional-preferred orientation parallel to foliation (Figure 6c). Grain contacts are irregular to sutured. Small flakes of brown biotite are oriented parallel to foliation. Colorless to green actinolite is predominantly fine-grained and fibrous, but may form coarser, euhedral crystals. Green chlorite replaces both biotite and actinolite, and may be of retrograde metamorphic origin. Carbonate is usually associated with the chlorite, but is also scattered throughout the rock as small patches interstitial to quartz. Magnetite, which forms small grains and elongate mineral trains parallel to foliation, is the most common opaque mineral. The opaque minerals in sample 2 of Table 5 include magnetite, pyrrhotite, specular hematite, chalcopyrite, pyrite, and marcasite. All form clots and stringers parallel to foliation. Well-rounded grains of zircon and apatite are ubiquitous accessory minerals.

Major oxide analyses (Table 6) attest to the quartz-rich composition of the unit. Over ninety percent of the rock is SiO_2 .

Table 5. Modal analyses (volume percent) of rocks of quartzite unit.¹

	1	2
	79S30	80S125
Quartz	86%	88%
Actinolite	tr	tr
Biotite	5	tr
Muscovite	tr	—
Opaque	1	10
Tourmaline	tr	1
Chlorite	5	1
Apatite	tr	tr
Zircon	tr	tr
Total	100.00	100.00

¹Modes based upon counts totalling 600 points; (-): not present; (tr): trace.

Garnet-biotite Gneiss

The garnet-biotite gneiss comprises the major portion of the transition zone, and, owing to its propensity to fracture during faulting, it is the dominant host rock for uranium ores. The unit has two subunits: a garnet-biotite gneiss member that is the dominant lithology, and a pyrite-mica schist member that is much less extensive and ranges from many meters in thickness to being completely absent. A hornblende-rich variety of the garnet-biotite gneiss member has been recognized by the mine geologists, but its presence is sporadic. Contacts between members and with the bounding units are commonly gradational, and are defined by the predominance of one mineral (garnet, pyrite) or lithology.

The garnet-biotite gneiss member is dark, relatively massive, and fine-grained (Figure 6d). It is composed of pink garnet, brown to green biotite, and quartz. The relative abundances of biotite and garnet vary considerably, and resulting lithologies range from mica schist to garnet-quartz gneiss. Numerous conformable layers of quartz and/or sulfides are parallel to foliation.

Table 6. Chemical analyses of quartzite unit.

	79S30	80S91
SiO ₂ (%)	92.00	97.40
Al ₂ O ₃	0.87	0.70
Fe (total)	4.03	0.37
FeO	3.12	0.25
Fe ₂ O ₃	1.01	0.13
MgO	0.74	0.20
CaO	0.90	0.25
Na ₂ O	<0.20	<0.20
K ₂ O	0.15	0.09
TiO ₂	0.05	<0.02
P ₂ O ₅	<0.10	<0.10
MnO	<0.02	<0.02
LOI	1.09	0.31
C (total)	0.31	—
C (org.)	<0.01	—
C (carb.)	0.31	—
S	0.27	—
Hg (ppm)	0.01	0.11
Ag	<5	<5
As	1	50
B	N	N
Ba	50	50
Be	N	N
Bi	<0.20	<0.20
Cd	0.20	<0.20
Co	<2	<2
Cr	2	2
Cu	50	3
F	100	100
Ga	N	N
La	N	N
Mo	2	11
Ni	6	<5
Pb	N	N
Sb	1	<1
Sc	N	N
Sr	10	N
Th	<2.60	<6.90
Tl	<1	<1
U	1.73	26.8
V	15	7
Y	N	N
Yb	N	N
Zn	20	10
Zr	N	N
density (g/cm ³)	2.83	2.70

Analyzed for but not detected in any sample: Au, Ce, Eu, Ge, Hf, In, Li, Nb, Nd, Pd, Pr, Pt, Re, Se, Sm, Sn, Ta, Te, W.
 N: not detected; L: detected but below accurate detection limit; (-): not analyzed for

Thin layers and lenses of quartzite are rare to ubiquitous, and locally comprise a substantial volume of the member. Quartz layers on the Upper Level have selvages of pink feldspar and garnet. Sulfides, where present, are either disseminated or form conformable stringers and small discontinuous clots in the gneiss. Pyrite is the dominant sulfide; pyrrhotite and smaller amounts of chalcopyrite and bornite are evident as well.

The pyrite-mica schist member is dark silver, fine- to medium grained, and strongly foliated. The major minerals are muscovite, biotite, pyrite, and quartz. Thin layers of pyrite and thicker layers of quartz parallel the foliation. The micaceous minerals emphasize the foliation, small-scale crenulations, and folds. Layers of pyrite maintain roughly uniform thicknesses through the axes of the folds. Numerous thin to and thick lenses of sulfide-poor garnet-biotite gneiss are interlayered with the pyrite-mica schist. The gradation between the pyrite-mica schist and the quartz-biotite schist member of the quartzite is marked by a decrease in the abundance of sulfides.

The garnet-biotite gneiss member locally contains layers of hornblende-rich gneiss. Many layers are identical to those of the major hornblende gneiss unit, whereas others form hybrid rock containing both garnet and green amphibole. Layers range in thickness from several centimeters to several meters.

Petrography and Chemistry

Fine-grained (0.5 mm) biotite and quartz with poikiloblastic almandine garnet characterize the garnet-biotite gneiss. Muscovite, pyrite, and orthoclase are locally abundant (samples 1, 2, and 3; Table 7). Lepidoblastic biotite accentuates the strong foliation, and compositional layers parallel the foliation. Biotite is predominantly yellow-brown, but some layers contain only olive green biotite; both varieties were not observed in any single sample. Electron microprobe analyses given in Table 8 indicate

Table 7. Modal analyses (volume percent) of rocks of the garnet-biotite gneiss unit.

Modes ¹	Garnet-biotite Gneiss			Pyrite-mica schist	Hornblende-rich garnet biotite gneiss
	1 79S19	2 80S84	3 80S107	4 80S74	5 80S48
Quartz	39%	29%	20%	36%	42%
Orthoclase	tr	7	—	—	—
Plagioclase	—	tr	—	16	3
Biotite	27	41	44	29	20
Muscovite	6	9	2	8	—
Hornblende	—	—	—	—	10
Garnet	23	14	29	—	25
Pyrite	4	—	—	9	tr
Tourmaline	—	tr	2	—	tr
Chlorite	—	—	tr	—	—
Carbonate	1	—	2	2	tr
Apatite	tr	tr	tr	tr	tr
Zircon	tr	tr	1.0	tr	tr
Total	100.00	100.00	100.00	100.00	100.00

¹Modes based upon counts totalling 800-1000 points. (-): not present; (tr): trace.

Table 8. Microprobe analyses of garnet and biotite in the garnet-biotite gneiss unit.

Mineral	Garnet	Garnet	Garnet	Garnet	Garnet
Sample	79S24	79S18	Rim 79S21	Middle 79S21	Core 79S21
#spots anal.	8	4	1	1	1
SiO ₂ %	39.40	39.70	36.70	35.80	36.50
Al ₂ O ₃	20.90	21.50	21.40	20.90	21.60
FeO	31.70	31.70	31.60	28.60	26.30
MgO	1.26	2.33	1.25	0.88	0.82
CaO	1.97	1.92	3.75	3.83	3.82
Na ₂ O	0.02	0.01	0.00	0.00	0.10
K ₂ O	0.01	0.01	0.01	0.02	0.00
TiO ₂	0.03	0.07	0.14	0.03	0.04
MnO	3.11	1.41	4.43	9.08	10.1
Total	98.41	98.65	99.27	98.15	99.28

Numbers of ions on basis of 24 O

Si	6.000	6.000	6.318	6.318	5.973	6.000	5.935	6.000	5.953	6.000
Al	—	—	—	—	0.027	—	0.065	—	0.047	—
Al	3.963	3.967	4.040	4.048	4.078	4.096	4.020	4.024	4.096	4.101
Ti	0.004	—	0.0078	—	0.018	—	0.004	—	0.005	—
Mg	4.272	—	0.5513	—	0.303	—	0.218	—	0.199	—
Fe	0.303	5.338	4.2180	5.286	4.294	5.861	3.960	5.994	3.587	5.853
Mn	0.340	—	0.1900	—	0.611	—	1.136	—	1.399	—
Ca	0.423	—	0.3270	—	0.653	—	0.680	—	0.668	—

Almandine	80.00%	79.80%	73.30%	66.10%	61.30%
Andradite	0.07	0.15	0.44	0.10	0.12
Grossular	6.30	6.06	10.70	11.20	11.30
Pyrope	5.68	10.40	5.17	3.64	3.40
Spessartine	7.92	3.59	10.40	19.00	23.90

* * * * *

Mineral	Green	Brown	Brown
Sample	biotite 79S24	biotite 79S18	biotite 79S21
# spots anal.	9	4	2
SiO ₂ %	36.60	35.70	33.90
Al ₂ O ₃	19.60	20.70	18.20
FeO	26.40	17.60	25.50
MgO	6.35	9.03	6.17
CaO	0.04	0.04	0.01
Na ₂	0.14	0.27	0.09
K ₂ O	8.12	7.61	9.58
TiO ₂	0.98	1.34	1.37
MnO	0.13	0.03	0.10
Total	98.36	92.32	94.84

Numbers of ions on basis of 24 O

Si	6.01	8.000	5.976	8.000	5.862	8.000
Al	1.99	—	2.024	—	2.138	—
Al	1.77	—	2.066	—	1.573	—
Ti	0.12	—	0.170	—	0.179	—
Fe	3.62	7.080	2.457	6.953	3.682	7.035
Mn	0.02	—	0.004	—	0.015	—
Mg	1.55	—	2.256	—	1.586	—
Ca	0.01	—	0.007	—	0.001	—
Na	0.04	1.750	0.078	1.711	0.029	2.144
K	1.70	—	1.626	—	2.114	—

that the green biotites contain more iron and manganese and less magnesium than the brown biotites; the amount of titanium is slightly less in the green biotites (Table 8). Garnets coexisting with biotite in both rocks are iron-rich (approximately 80 percent almandine), and relative Mn and Mg concentrations mimic those of the biotites. They are largely unzoned and poikiloblastic with few to numerous inclusions of quartz. Some have a poikiloblastic core and a subhedral idioblastic rim. Others are optically homogeneous, but microprobe analyses show a pronounced increase in Fe and decrease in Mn from core to rim (Table 8). Inclusions of quartz and lesser biotite are so abundant in a few garnets that no discrete garnet porphyroblast is evident. Foliation in all samples wraps around and is never truncated by the garnets. Muscovite is intimately intergrown with biotite. Fine-grained aggregates of muscovite, with distinct contacts with adjacent quartz and biotite, are common and may represent the original presence of sillimanite (Sheridan et al., 1967). Orthoclase, where present, is fine-grained and untwinned. Plagioclase feldspar (An_{37}) is rare, but has distinct polysynthetic twinning where present. Pyrite is the dominant sulfide, and is both disseminated and in veinlets parallel to foliation. Veinlets of chalcopyrite locally truncate the pyrite, and appear to predate Laramide alteration and brecciation. Zoned black to yellow sphalerite is intergrown with pyrite in samples from the 12th level. Pyrrhotite is rare, and small magnetite grains are locally included in garnet and disseminated through biotite. Graphite is abundant in many sulfide-rich layers, and forms small blades parallel to foliation. Coarse- to fine-grained green tourmaline is a common accessory mineral.

Although the garnet-biotite gneiss is relatively massive, variations in the relative abundances of one or more minerals create layers enriched or depleted in those phases. This mineral layering is ubiquitous and visible at all scales. Monomineralic layers of quartz or pyrite are conspicuous but relatively less common.

Some quartz layers have thin selvages of mafic silicates, pyrite, or potassium feldspar. Layers of pyrite may contain pyrrhotite, chalcopyrite, and various other sulfides.

The pyrite-mica schist is a strongly foliated two-mica schist with abundant pyrite. Lepidoblastic muscovite is intimately intergrown with brown biotite. Quartz, the most abundant mineral in the rock, and plagioclase feldspar are equigranular and interstitial to the micas. Pyrite, with inclusions of pyrrhotite, forms fine to coarse disseminated grains as well as discontinuous lenses and nodules. When disseminated, it is usually associated with muscovite-rich zones. Monomineralic layers of quartz conformable to foliation are common. Some micaceous layers contain only biotite, but none contain only muscovite.

Layers of hornblende gneiss in the garnet-biotite gneiss member are identical to those of the major hornblende gneiss unit. Of particular interest are those smaller layers of garnet-biotite gneiss which contain amphiboles. Although forest-green hornblende is the predominant amphibole, some layers contain grunerite. Brown biotite is partially replaced by green biotite, and muscovite is absent from these layers. Tourmaline is coarse-grained and blue.

The rocks of the garnet-biotite gneiss are iron-rich, as shown by the major oxide analyses and reflected by the mineralogy (Table 9). Total iron generally exceeds 15 percent, and some samples contain more than 20 percent. A modal increase of garnet is correlative with an increase in the total iron content of the rock. The pyrite-mica schist contains less iron and considerably more sulfur than the garnet-biotite gneiss, but the two members are otherwise compositionally similar. The hornblende-bearing varieties of the garnet-biotite gneiss are iron-rich, but are more calcic and less potassic and aluminous than the enclosing garnet gneiss. The distinct decrease in the abundance of micas in the amphibole-bearing rocks reflects the lower concentrations of potassium and aluminum.

Table 9. Chemical analyses of garnet-biotite gneiss unit.

	79S19	80S19	80S25	80S48	80S71	80S77	80S84	80S87	80S97	80S107	80S117	79S24
SiO ₂ (%)	59.50	39.10	58.70	53.70	55.40	47.30	59.60	51.90	57.00	54.10	58.60	52.30
Al ₂ O ₃	11.70	13.50	10.90	9.93	11.10	10.60	13.70	12.90	15.00	13.30	12.60	13.50
Fe (total)	17.00	19.10	14.10	19.30	21.10	20.70	15.70	22.70	18.30	20.40	14.90	22.00
FeO	13.00	15.40	10.50	15.30	20.50	17.10	—	18.60	15.50	17.40	12.30	19.10
Fe ₂ O ₃	4.40	4.11	4.00	4.44	0.56	3.60	—	4.55	3.11	3.30	2.90	3.22
MgO	3.00	5.99	2.40	3.40	3.30	3.40	3.00	2.00	3.10	3.20	2.70	3.40
CaO	1.56	2.60	1.80	4.12	1.61	1.22	0.48	1.00	0.98	0.70	0.85	1.12
Na ₂ O	0.20	0.90	0.30	0.40	<0.20	0.30	0.30	<0.20	<0.20	< 0.20	0.70	<0.20
K ₂ O	3.18	3.75	3.71	1.59	2.85	3.69	4.11	2.44	3.54	3.40	3.23	4.88
TiO ₂	0.48	3.90	0.30	0.38	0.49	0.45	0.56	0.53	0.62	0.62	0.49	0.59
P ₂ O ₅	0.40	0.65	0.20	0.20	0.30	0.40	0.10	<0.10	0.10	0.20	0.20	0.20
MnO	0.48	1.06	0.66	1.05	1.03	1.18	0.21	0.48	0.47	0.37	0.35	0.58
LOI	3.35	8.31	7.15	4.92	3.02	10.49	1.86	5.35	1.50	4.02	5.55	1.88
C (total)	0.53	2.25	2.41	1.34	1.02	2.33	0.28	—	—	—	—	0.35
C (org.)	0.14	0.26	1.32	0.30	0.98	1.12	0.22	—	—	—	—	<0.01
C (carb.)	0.39	1.99	1.07	1.04	0.04	1.21	0.06	—	—	—	—	0.35
S	1.74	0.59	1.66	0.53	1.98	4.77	<0.01	—	—	—	—	0.03
Hg (ppm)	0.01	<0.01	0.02	0.02	<0.01	0.04	<0.01	0.09	0.02	0.01	0.02	<0.01
Ag (ppm)	<5	<5	<5	<5	<5	<5	<5	<5	<5	<5	<5	<5
As	10	20	30	15	1	50	3	20	<1	2	20	<1
B	N	N	20	N	N	L	N	100	200	300	30	N
Ba	300	500	200	200	300	300	200	150	700	500	300	700
Ba	N	L	5	N	L	L	N	1.50	2	2	2	1.50
Bi	1.50	1	2	1.50	1	<0.20	0.70	<0.20	<0.20	<0.20	<0.20	<0.20
Cd	0.50	2	5	2	1	10	0.20	0.20	0.70	0.30	<0.20	0.70
Co	35	22	20	25	13	8	17	18	17	18	15	16
Cr	50	70	20	30	50	50	50	70	70	70	70	70
Cu	200	30	300	100	150	150	3	70	1	2	100	2
F	1300	1700	900	600	900	1200	1300	1400	1300	1300	1100	800
Ga	20	20	20	15	—	20	15	20	20	30	20	20
La	L	N	N	N	L	50	L	N	50	50	50	L
Mo	5	5	7	5	5	5	35	86	12	5.50	<5	7
Ni	47	49	75	40	25	30	32	32	41	38	29	36
Pb	50	70	150	50	50	70	30	100	70	30	50	30
Sb	3	<1	5	1	<1	7	1	10	<1	<1	<1	2
Sc	10	20	10	7	10	7	15	10	15	15	15	15
Sr	30	150	70	150	15	50	30	30	50	100	70	70
Th	<9.10	<4.10	<11	<8.93	<12.90	<7.70	<11	<17	<17.80	<16.80	<13.20	<8.20
Tl	<1	<1	3	<1	<1	<1	2	<1	<1	<1	<1	<1
U	6.21	5.34	9.37	6.32	7.36	23.30	40.20	88	6.52	4.58	4.73	18.40
V	150	200	700	70	150	150	70	150	150	200	150	150
Y	20	50	30	15	30	20	30	10	15	10	15	15
Yb	2	—	—	2	—	3	2	—	—	—	3	—
Zn	100	30	200	150	100	100	150	200	200	200	150	150
Zr	100	100	150	70	70	70	100	70	100	100	70	150
density (g/cm ³)	3.02	3.10	2.88	2.90	3.02	3.03	2.95	3.07	2.95	3.05	3.00	3.25

Analyzed for but not detected in any sample: Au, Ce, Eu, Ga, Hf, In, Li, Nb, Nd, Pd, Pt, Re, Se, Sm, Sn, Ta, Te, W. N: not detected; L: detected by below accurate detection limit; (—): not analyzed for.

Mica Schist

The mica schist unit at the mine is part of the more extensive unit mapped by Sheridan et al. (1967). As discussed later, the unit is rarely a host for the uranium ores, and underground exposures are consequently limited. Most information comes from surface exposures and drill cores.

The mica schist is a dark, strongly foliated rock composed of quartz and mica. Thin layers of quartzite are common, as are zones rich in garnet, magnetite, or sulfides. Sulfides, including pyrite and pyrrhotite, are disseminated throughout much of the schist, and locally form laterally continuous layers several centimeters in thickness. Both quartz and sulfide layers locally exhibit boudinage structures. A quartz-magnetite layer conformable to foliation is exposed on the surface. Flanigan (1977) demonstrated, using electrical resistivity measurements, the presence of abundant magnetite-rich layers in the mica schist.

Petrography and Chemistry

The mica schist is fine-grained and foliated. The major minerals include quartz, biotite, muscovite, and microcline. Unlike the quartzite unit, the quartz crystals are neither elongate nor aligned. Both microcline and plagioclase feldspar are twinned and intergrown with quartz. Fine to coarse flakes of muscovite are intimately intergrown with green or brown biotite. The micas are aligned, and impart a schistose texture to the rock. Garnets in garnet-rich layers are identical to those in the garnet-biotite gneiss unit. The ratio of biotite to muscovite increases substantially in those layers containing garnet (compare samples 1 and 2; Table 10).

Several layers are composed primarily of magnetite with lesser amounts of garnet and grunerite (sample 3; Table 10). The garnet is coarse and euhedral, and contains inclusions of magne-

Table 10. Modal analyses (volume percent) of rocks of mica schist.¹

	1	2	3
	79S22	80S103	80S127
Quartz	35%	39%	tr
Microcline	14	12	tr
Plagioclase	tr	1	tr
Biotite	11	26	--
Muscovite	32	15	--
Grunerite	--	--	16
Magnetite	6	3	70
Tourmaline	--	tr	--
Garnet	--	4	14
Zircon	tr	tr	--
Apatite	tr	tr	--
Epidote	2	--	--
Total	100.00	100.00	100.00

¹Modes based upon counts totalling 800-1000 points. (-): not detected; (tr): trace.

tite comprising up to one-half its volume. Subhedral, medium-grained grunerite is pleochroic green and twinned. Some amphiboles contain minute inclusions of chalcopyrite. Massive granular magnetite is interstitial to the other minerals. Hematite is exsolved from magnetite along octahedral planes of parting.

The mica schist is chemically similar to rocks of the garnet-biotite gneiss unit and quartz-biotite schist in the quartzite unit. Unlike the other units, the iron in the mica schist is dominantly ferric (Table 11). However, as noted for the garnet-biotite gneiss, an increase in ferrous iron is accompanied by an increase in the amount of almandine garnet.

Metamorphism

Regional metamorphism produced mineral assemblages (Table 12) characteristic of the amphibolite grade described by Turner (1981) and medium grade outlined by Winkler (1974). Because the distribution of chemical analyses of hornblende gneiss, garnet-biotite gneiss, and mica schist plotted on ACF-AKF diagrams (Figure 7) correspond to the mineral assemblages noted in thin sections of the rock types, most of the minerals presumably represent equilibrium assemblages. Quartz and amphiboles locally resorb the few pyroxenes in the rocks, suggesting some retrograde metamorphism. However, minerals in other rocks have sharp grain contacts and do not show any evidence of resorption.

Not all assemblages are in equilibrium. Microprobe analyses of aggregates of garnets (Table 8) indicate manganese-rich cores with a progressive decrease in the Mn/Fe ratio towards the rims. Plots of both the garnets and coexisting biotites on a Fe-Mg-Mn diagram (Figure 8), the biotites are clearly compositionally similar to those in other samples, and that the trend of decreasing Mn/Fe ratios in the garnets projects directly towards the general compositions of garnets in other samples. These compositional trends suggest that garnets in some layers began to form relatively

Table 11. Chemical analyses of mica schist unit.

	79S21	79S22	79S25	80S95	80S103
SiO ₂ %	60.90	62.40	53.10	62.30	57.10
Al ₂ O ₃	13.70	13.70	12.70	11.20	14.30
Fe (total)	13.40	13.10	18.40	11.20	12.30
FeO	4.28	4.07	15.80	6.34	7.36
Fe ₂ O ₃	10.00	10.00	2.89	5.39	5.48
MgO	2.00	2.40	3.20	2.10	2.60
CaO	1.20	1.16	0.67	1.50	1.18
Na ₂ O	2.80	1.70	<0.20	1.60	1.50
K ₂ O	2.71	4.08	4.38	2.87	3.72
TiO ₂	0.54	0.51	0.54	0.47	0.58
P ₂ O ₅	0.10	0.10	0.10	<0.10	0.20
MnO	0.31	0.25	0.62	0.27	0.71
LOI	1.55	1.94	6.99	6.44	5.44
C (total)	0.34	0.36	1.73	—	—
C (org.)	0.09	0.04	0.27	—	—
C (carb.)	0.25	0.35	1.46	—	—
S	0.01	0.01	0.01	—	—
Hg (ppm)	<0.01	<0.01	0.01	<0.01	0.03
Ag	<5	<5	<5	<5	<5
As	1	1	5	1	1
B	N	N	20	70	30
Ba	150	300	300	150	700
Be	N	L	3	2	5
Bi	0.70	1.50	0.70	<0.20	<0.20
Cd	0.70	0.20	0.50	<0.20	<0.20
Co	16	23	18	13	14
Cr	20	70	50	70	70
Cu	1000	3	1.50	5	70
F	1100	1400	1700	1100	1600
Ga	20	20	20	20	20
La	N	70	L	N	L
Mo	<2	2	4	<5	<5
Ni	24	29	36	20	24
Pb	20	50	30	30	20
Sb	<1	<1	<1	<1	<1
Sc	5	10	15	10	20
Sr	200	150	150	150	200
Th	<15.00	<16.70	<13.50	<7.92	<9.13
Tl	<1	<1	<1	<1	<1
U	3.13	2.27	5.79	3.58	5.46
V	50	70	100	70	100
Y	10	20	20	20	30
Yb	2	3	2	2	—
Zn	70	70	70	200	150
Zr	30	100	100	100	150
density (g/cm ³)	3.05	2.93	3.05	2.57	2.78

Analyzed for but not detected in any sample: Au, Ce, Eu, Ge, Hf, In, Li, Nb, Nd, Pd, Pr, Pt, Ra, Se, Sm, Sn, Ta, Te, W. N: not detected; L: detected but below accurate detection limit; (-): not analyzed for

Table 12. Mineral assemblages in metamorphic rocks of the Schwartzwalder Mine.

Pelitic rocks:

quartz-biotite-almandine-muscovite-pyrite
biotite-quartz-almandine-muscovite
biotite-almandine-quartz
quartz-biotite-plagioclase-pyrite-muscovite
quartz-muscovite-microcline-biotite-magnetite
quartz-garnet-biotite-hornblende-plagioclase
quartz-biotite-muscovite-microcline-garnet

Calcareous rocks:

hornblende-plagioclase-biotite-quartz
hornblende-plagioclase-actinolite-biotite-quartz-(calcite)
calcite-hornblende-biotite-clinopyroxene-scapolite-micro-
cline

Quartzitic rocks:

quartz-biotite
quartz-magnetite-pyrrhotite

Quartz-feldspar rocks:

plagioclase-quartz-biotite
quartz-plagioclase-microcline-biotite

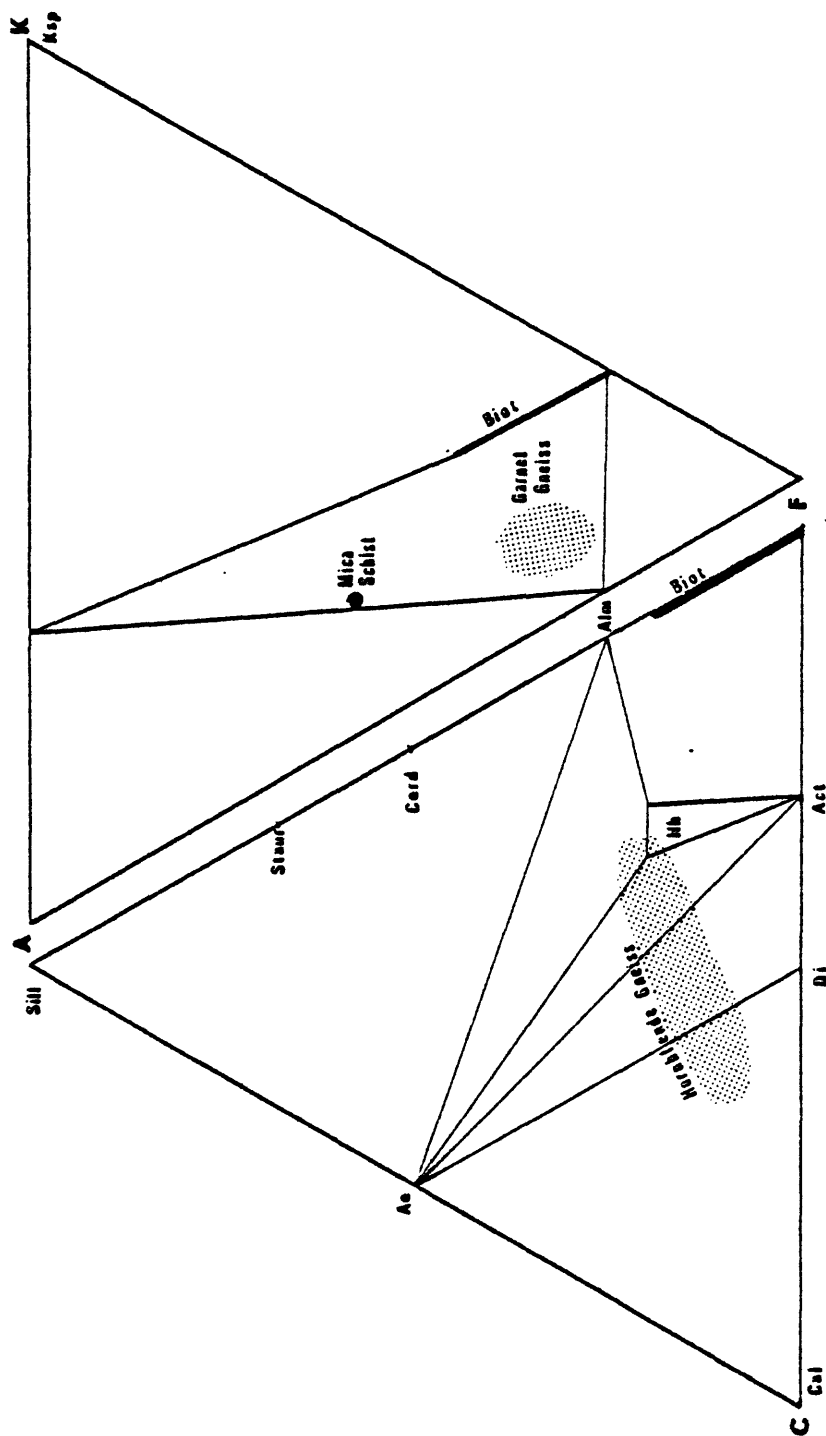


Figure 7. ACF-AKF diagram, showing the major rock types of the Schwartzwalder deposit. Minerals and tie-lines from Winkler (1974).

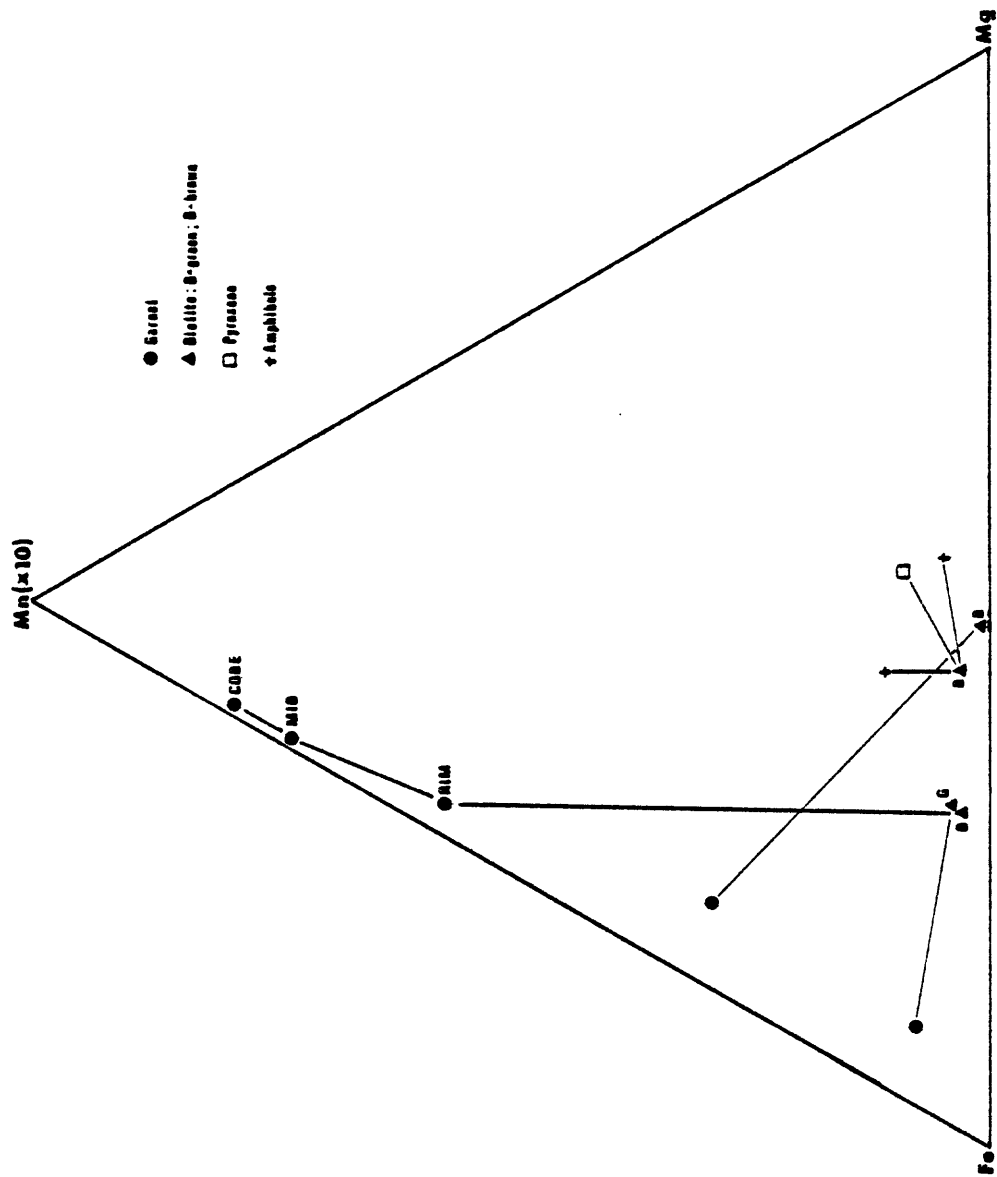


Figure 8. Fe-Mg-Mn diagram showing the compositions and trends of metamorphic minerals, based upon microprobe analyses.

early and partitioned Mn into the cores, as described by Hollister (1968). These garnets, coincidentally, do not contain inclusions of biotite. Garnets with biotite inclusions and sieve textures are chemically unzoned and iron-rich (Figure 8), and must have formed later than the zoned garnets.

Cordierite, staurolite, or polymorphs of Al_2SiO_5 were not observed in the micaceous rocks, as expected from the ACF-AKF diagrams. Sheridan et al. (1967) reported both sillimanite and andalusite from the mica schist unit. In those rocks, sillimanite was associated with muscovite, not microcline, which thereby places the assemblage below the sillimanite-microcline isograd.

Quartz-biotite-garnet and quartz-muscovite-biotite-magnetite are the two major assemblages of the pelitic rocks. Ferric iron is dominant in the magnetite-rich rocks, and ferrous iron predominates in the garnet-rich rocks (compare Tables 9 and 11). However, the compositions of the two assemblages are otherwise similar. Thin lenses of garnet-biotite gneiss in the mica schist have a considerably greater $\text{Fe}^{+2}/\text{Fe}^{+3}$ ratio than that of the enclosing schist (compare samples 1 and 2, Table 11). The oxygen fugacity was therefore extremely variable from layer to layer and unit to unit, but oxygen was clearly not mobile. The original mineral assemblage, not subsequent metamorphism, must have determined the oxygen fugacity (Klein, 1966).

Iron-rich amphiboles dominate the mineralogy of the calcareous rocks, but variations in the bulk rock composition strongly influenced the resultant mineralogy of the metamorphosed rocks. For example, calcite and sphene coexist to the exclusion of ilmenite, and rocks with abundant potassium contain biotite. CO_2 was erratically mobile. Several units contain contemporaneous carbonate and quartz; if the system was open to CO_2 loss, the carbonate and quartz should have reacted during metamorphism to form diopside (Klein, 1966). Other units contain clinopyroxene without quartz, indicating that CO_2 was able to escape, allowing diopside to form.

Despite evidence of elemental immobility, selvages around some small quartz layers in all rock units suggest that some layers may have formed as a result of metamorphism. All however, are conformable to foliation.

Metamorphic Rock Precursors

Regional mapping in the east-central Front Range by previous workers (Sheridan et al., 1967; Sims and Gable, 1967; Moench, 1964; and many others) has demonstrated the sedimentary and possibly volcanic origin for many of the non-plutonic Proterozoic rocks in the area. In the Ralston Buttes quadrangle and adjoining areas, compositional layering is, in most instances, representative of the original lithologic units (Lickus and LeRoy, 1968; Sheridan et al., 1967). With the exception of regional unconformities, the contacts of all units are generally conformable.

The mica schist and hornblende gneiss units, which form a transitional contact at the Schwartzwalder mine, are both areally extensive. The mica schist contains numerous beds of quartzite, and conglomeritic layers contain granitic clasts (Lickus and LeRoy, 1968). The schist likely represents a widespread, possibly near-shore, shale sequence. The hornblende gneiss is as lithologically diverse elsewhere as it is at the mine. Sheridan et al. (1967) suggested that protoliths may have included calcareous shales, impure carbonates, and possibly mafic volcanic and volcanioclastic units. Lickus and LeRoy (1968) concluded that the hornblende gneiss was originally stratigraphically older than the mica schist. Sheridan et al. (1967) equivocated about the relative age relationships in the vicinity of the mine.

At the Schwartzwalder mine, the hornblende gneiss grades into the mica schist through a transition zone of quartzite and garnet-biotite gneiss. Most contacts are conformable, and many are gradational. The rocks of the mica schist and garnet-biotite gneiss are clearly of pelitic ancestry, as shown by the high concentra-

tions of aluminum and potassium, and were locally carbonaceous. Some zones contain abundant sulfides and, locally, metals other than iron. The rocks of the pelitic sequence are notable for their iron-rich compositions: most contain more than 10 percent total iron; some contain more than 20 percent; and some layers in the mica schist contain more than 60 percent total iron. The mica schist grades into the garnet-biotite gneiss with an increase in the $\text{Fe}^{+2}/\text{Fe}^{+3}$ ratio, and thin to thick layers of both lithologies are intercalated.

The quartzite forms a distinct unit in the transition zone, and is intercalated with all other units. As such, it is likely of sedimentary origin. Relict cobbles or pebbles were not observed to confirm a fluvial origin, but the unit contains rounded grains of zircon and apatite. The thin, persistent banding of quartzite and carbonates in several underground exposures strongly suggests a low-energy depositional environment for those rocks. The unit is locally sulfidic and hematitic.

The hornblende gneiss, as exposed at the mine, has several prominent lithologies, all of which are complexly interlayered. Some layers contain abundant carbonates, which, combined with various amounts of silica, potassium, and aluminum, suggests that they were originally calcareous argillites. Many of the amphibolites, however, have relatively low concentrations of carbonate and between one and two percent TiO_2 . The rocks are mineralogically similar to iron formations described by Immege and Klein (1976) and Klein (1973). However, those rocks, as well as most iron-formations (James, 1966), contain less than one percent TiO_2 and in excess of 20 percent total iron. The amphibolites at the Schwartzwalder mine more closely resemble mafic to intermediate volcanic or volcanoclastic rocks, based upon analyses summarized by Nockolds (1954) and Le Maitre (1976). The association of high titanium with amphibolites has been noted elsewhere in the east-central Front Range, and rutile-rich zones in some of those units may represent metamorphosed soil horizons developed on top of

mafic volcanic or volcanoclastic units (Marsh and Sheridan, 1976). Although the evidence is equivocal, the high titanium concentrations combined with the conformable position of the unit suggest that the amphibolite was originally a mafic volcanoclastic deposit interbedded with the calcareous sediments of the calc-silicate gneiss. Sheridan et al. (1967) suggested that the amphibolite might represent sills of hornblende diorite.

If indeed the hornblende gneiss is the oldest unit (Lickus and LeRoy, 1968), the base of the sequence was a heterogeneous mixture of mafic volcanoclastic units intermixed with calcareous muds, some of which likely contained volcanoclastic material. Quartz was deposited near the top of this unit, either as clastic quartzite or as chemically precipitated chert in a relatively quiet environment. The quartzite locally contained laminations of sulfides, shales, and carbonates, and graded laterally into a shale unit, now represented by the quartz-biotite schist member. As deposition continued, the quartzite graded upward into extremely iron-rich pelitic sediments. These sediments locally contained abundant sulfides or were somewhat more carbonaceous. Scattered layers of hornblende gneiss suggest sporadic volcanism. Deposition of the iron-rich shale continued with a gradual increase in the oxidation state of the iron. However, beds rich in ferrous iron indicate periodic reversals of that trend. Local layers of hematitic or siderite-rich chert were deposited in the shale.

This sequence is similar to Precambrian iron-formations described by James (1954) and many others. Additional work is clearly needed on the regional sedimentology of the units in the east-central Front Range. However, it is evident at this stage of research that the host rocks for the uranium ores at the Schwartzwalder mine were once a sulfur-rich iron-formation associated with mafic volcanism.

Intrusive Rocks

Dikes of pegmatite and aplite are the only intrusive units that have been recognized in the mine workings or drill cores. Both are of Proterozoic age (Sheridan et al., 1967).

Pegmatite

Pegmatites, confined exclusively to the mica schist and hornblende gneiss units, form tabular bodies centimeters to meters in width. The pegmatites are grossly conformable to foliation and layering in the gneiss. Contacts with the enclosing schists and gneisses are distinct to diffuse, possibly suggesting both intrusive and metasomatic origins for the pegmatites (Wright, 1980).

The pegmatites are extremely coarse-grained and unfoliated. Quartz, pink perthite, microcline, muscovite, and sodic plagioclase are the major minerals. Black tourmaline and red garnet are common accessory minerals. Quartz is ubiquitous, but either microcline or plagioclase may be completely absent in some rocks.

Aplite

Dikes of aplite are scattered through the metamorphic rocks. The dikes are less than a meter in width, and are conformable to layering. The rocks are foliated and locally difficult to distinguish from quartzitic units. Quartz, plagioclase, and microcline are the dominant minerals, and oriented flakes of biotite define the foliation. Small grains of pyrite are elongate parallel to the foliation of the biotite.

Structural Geology

The structures at the Schwartzwalder mine include foliation and folds that formed during Proterozoic deformation, and a comp-

lex system of faults produced during both Proterozoic and Laramide tectonism. Uranium ores were emplaced in the faults approximately 70 m.y. ago (Chapter 6) during Laramide uplift of the Front Range. However, the morphology of those faults was influenced by the presence of foliation and folds in the host rocks.

Foliation

Foliation encompasses the planar features, including compositional layering and schistosity, that formed during Proterozoic metamorphism. All of the units contain at least some compositional layering. However, as described in previous sections, the thicknesses of individual layers vary considerably from unit to unit.

Schistosity is pronounced in all units except the quartzite, and schistosity and layering are generally coplanar. Pelitic rocks with modally abundant micas are extremely schistose. Hornblende crystals are aligned, producing moderate linearity in amphibole-rich layers. Elongate quartz grains in some quartzite layers are preferentially oriented parallel to schistosity.

Folds

The metamorphic rock units are compressed into a tight synform (Figure 4). The axial plane of the fold is nearly vertical, and the fold axis plunges steeply to the south (Downs and Bird, 1965). As a result, the dip of the layering in the metamorphic rocks is steep to vertical everywhere on the synform. The mica schist forms the core of the fold. As a result of folding, the rocks of the transition zone were nearly doubled in thickness in the nose of the synform. Faulting truncated the nose of the fold, and apparently dragged the southwest limb northward (Figure 9; Wright, 1980).

Small folds are ubiquitous in the rock units. Detailed map-

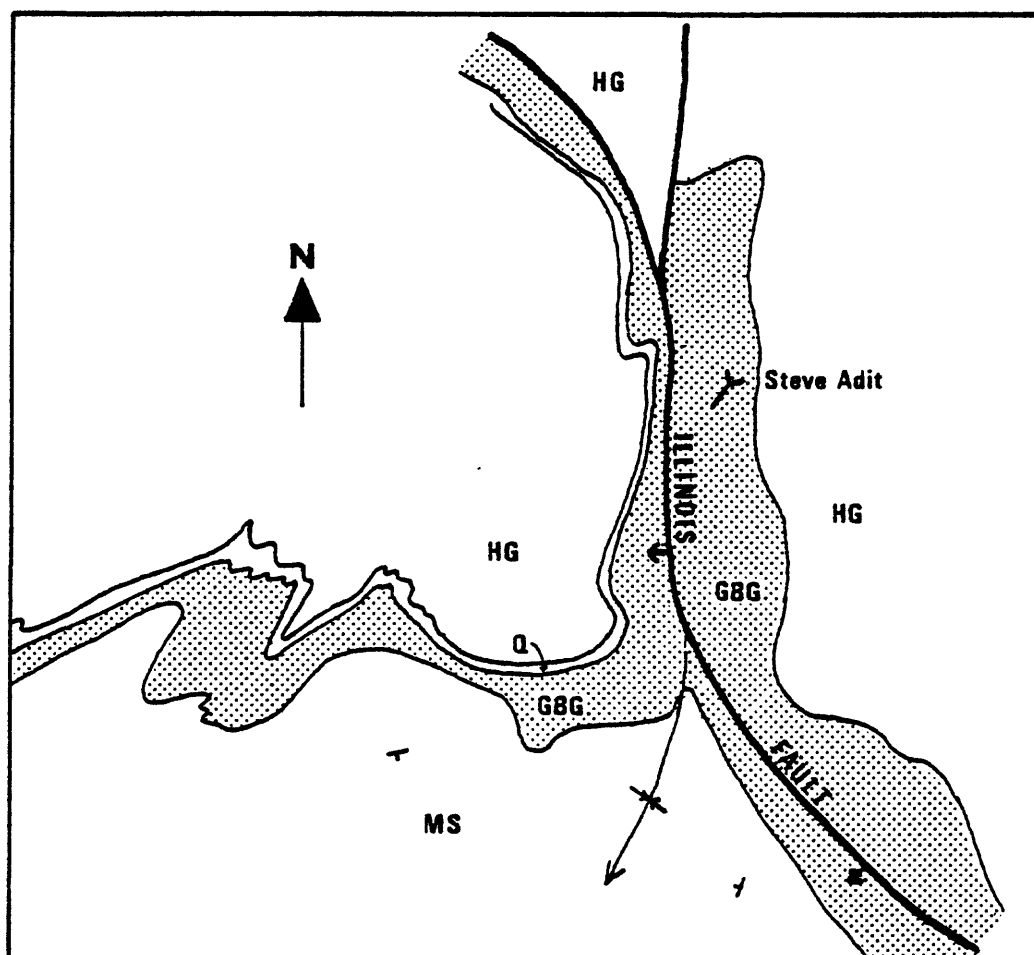


Figure 9. Schematic sketch of the surface distribution of the four major lithologic units, the synform, and the Illinois fault. HG: hornblende gneiss; Q: quartzite; GBG: garnet-biotite gneiss; MS: mica schist. From Wright (1980).

ping (Cotter Corp., unpublished maps) indicates that the fold axes dip steeply, and may be parasitic to the large synform. The folds are broad to isoclinal, and may occur singly or in multiple sets. Folds in the transition zone units commonly double the original thickness of the sequence. Fold crenulations are common, but are difficult to see in rocks that have poorly developed layering or schistosity.

Faults

The faults and fractures at the Schwartzwalder Mine comprise three distinct systems: (1) the Rogers fault, (2) the Illinois fault, and (3) tension fractures related to both the Illinois and Rogers faults. The Rogers fault is one of several laterally extensive, northwest-trending faults in the Front Range. The Illinois fault and the tension fractures are believed to be related to movement along the Rogers fault system. The Illinois fault and the tension fractures in the hangingwall of the Illinois fault are readily visible in mine workings, but only along the relatively short strike lengths of the mineralized zones. The Rogers fault system is only partly exposed in recent mine workings, although several drill holes have penetrated the west segment of the fault.

Both the lithologies of the rocks and the relative orientation of metamorphic structures strongly influenced the development of the observed fault morphologies and textures during Laramide fault movement. Faulting in relatively brittle rocks, such as the quartzite and garnet-biotite gneiss units, created fault zones filled with angular, poorly sorted breccia fragments. In contrast, similar movement in relatively ductile rocks, such as the mica schist, generated diffuse, gouge-filled fault zones. Movement in rock units with thin-bedded, heterogeneous lithologies, such as some rocks of the hornblende gneiss unit, formed discrete to diffuse zones of both breccia and gouge. The orienta-

tion of foliation with respect to that of the fault also influenced the development of the zones: fractures parallel to foliation contain much more fault gouge than those oblique to foliation.

The most essential factor in ground preparation for subsequent ore deposition was the combination of fault movement in obliquely-foliated units and the tendency of the transition zone rocks to brecciate. Faults splay into several gouge-filled strands upon entering the bounding rock units. Uranium-rich hydrothermal fluids readily moved through the permeable brecciated zones, whereas the relatively impermeable gouge impeded the lateral movement of the fluids.

Rogers Fault System

The Rogers fault system in the vicinity of the mine contains two parallel segments 1000 m apart (Young, 1977). Both segments strike to the northwest and dip approximately 65°NE. The fault is composed of many closely spaced, anastomosing strands covering a total width of one meter to tens of meters. Reverse dip-slip and right-lateral strike-slip movement along the east segment displaced the Proterozoic-Phanerozoic unconformity near the mine more than one hundred meters (Figure 4). Data from exploratory drilling into the west segment of the fault indicate both right-lateral drag folding in the hangingwall and reverse dip-slip displacement of rock units. Although similar to the observed movement along the east segment, some of this movement is probably of pre-Laramide origin.

Illinois Fault System

The Illinois fault system dips steeply to the west, and forms a north-trending diagonal fault between the east and west segments of the Rogers fault. The Illinois fault cannot be traced on the

surface to either strand of the Rogers fault, largely because of poor exposures. The inferred intersection downdip of the Illinois and the west segment of the Rogers fault would be present several hundred meters below the lowest workings in the mine, based upon projections of the two faults.

The Illinois fault system is composed of a pre-ore fault and a subparallel post-ore fault. The pre-ore fault dips $70-75^{\circ}$ to the west. In its simplest form, especially in the lowest levels of the mine, the fault is a single strand a meter or more in width. Elsewhere, the fault forms a broad zone composed of many closely spaced and anastomosing faults and fractures. These fractures commonly diverge, leaving large horses of wallrock between strands. Pegmatites parallel the fault in the footwall, suggesting a Proterozoic origin for the fault (Paschis, 1979). Subsequent Proterozoic right-lateral movement created the apparent drag of the synform (Wright, 1980). The fault follows the southeast limb of the synform to the nose of the fold, and then bends north and trends northwest out of the synform. On the surface, both sides of the fault are bounded by units of the transition zone. The fault dips less steeply than the layering of the host rocks, and, with increased depth, leaves the transition zone units along the southeast limb and nose of the synform. At deeper levels, the fault transects the southwest limb of the synform. Complex fault movements juxtaposed hornblende gneiss in the footwall against transition zone units and mica schist in the hangingwall.

The post-ore Illinois fault formed after Laramide mineralization along the pre-ore Illinois fault. It dips 60° to the west and strikes north-northwesterly. The pre-ore and post-ore faults intersect between the 10th and 13th levels of the mine, with the post-ore fault entering the hangingwall of the older fault below this interval (Figure 2). The zone of intersection is extremely fractured and brecciated, making it difficult to precisely define the major faults. The post-ore fault splays into two subparallel strands below the 15th level, but the entire fault zone is charac-

teristically composed of numerous small anastomosing fractures. Movement along the fault was predominantly dip-slip, with a normal displacement of over 100 m (Wright, 1980). This is inferred from the reconstruction of offset tension fractures. Displacement of the pre-ore Illinois fault is much less evident, although the anastomosing character of both faults, the wide zone of intersection, and the shallow angle of intersection make reconstruction difficult.

The post-ore Illinois fault is a very open structure, and forms a watercourse throughout much of its extent in the mine. Although locally sealed by late-stage calcite, continuous openings in the fault are up to a meter or more in width, and large blocks that spalled from the walls locally form rubble in the opening. This mega-vug texture contrasts sharply with the matrix-filled breccia of the pre-ore Illinois fault, and may indicate a very different mechanism and much shallower depth of fault movement for the later fault.

Tension Fractures

Major east-dipping horsetail-type fractures are present on the hangingwall of the pre-ore Illinois fault. Wright (1980) described two sets of fractures: one which strikes due north, and another which strikes more northwesterly. Both sets apparently root in the pre-ore Illinois fault, and both are mineralized. The dips of the fractures are variable and range from steep to flat, even along the same structure. The RB vein (Figure 2) flattens before again steepening updip, and parts of the Upper vein dip to the west. Movement along the post-ore Illinois fault truncated many of the veins below the 13th level.

Several episodes of movement that took place before, during, and after ore mineralization are usually evident, but none created major displacement. Drag folds in adjacent rocks indicate both strike-slip and dip-slip movement. The faults commonly juxtaposed

different rock types, usually with the hornblende gneiss emplaced below the garnet-biotite gneiss. Some fractures, including those in brittle transition zone rocks, are relatively narrow. Most fractures, however, are typically wide where they cut the rocks of the transition zone. Several of the veins in the upper levels of the mine are more than ten meters wide (Downs and Bird, 1965). Portions of the Titan and RB veins are more than a meter in width, and are partially to completely filled with uncompacted breccia. The relatively small amount of offset and the large, dilated zones indicate that these faults formed as a result of tension in the hangingwall of the Illinois fault. It is notable that, in the bounding mica schist and hornblende gneiss units, nearly all tension fractures are extremely diffuse and filled with gouge regardless of the width of the structure in the rocks of the transition zone.

Development of Fault System

The fracture system at the Schwartzwalder mine originated during Proterozoic tectonism, but subsequent Laramide movement modified the system to its present form. On a regional scale, it is apparent that Laramide movement produced the modern fault textures (Tweto and Sims, 1963; Wallace, in press), despite the Proterozoic ancestry. However, the pre-existing structures undoubtedly influenced the later development of the fault system.

The Schwartzwalder deposit is situated near the junction of two major fault systems: (1) the northwest-trending Rogers fault and related fractures, and (2) the north-trending, range bounding Golden fault (Figure 3). Laramide movement along the Rogers fault was predominantly reverse dip-slip, although early activity was strike-slip (Warner, 1980). The eastern segment of the fault cuts the basal units of the overlying Phanerozoic sedimentary rocks, and produced flexural folding in the upper, unfaulted strata. The basal units are welded to the crystalline basement,

and dip about 40°E along the range front, implying rotation of the basement as well. Kellogg (1973) demonstrated that vertical Laramide uplift rotated basement blocks to the north around a N20W axis, with an increase in the amount of rotation in blocks immediately adjacent to the range front. Rotation requires a curved fault surface (Stearns, 1978), but both segments of the Rogers fault are relatively planar. Therefore, although reverse movement along the Rogers fault may have offset the basal units during rotation, other faults in the basement were responsible for the observed rotation.

Rotation and faulting took place in the upper plate of the Golden fault, one of several reverse faults that parallel the range front south of Boulder (Bryant et al., 1981). The fault dips steeply to the west, and total displacement exceeded 2700 m (Van Horn, 1976). Several of the northwest-trending faults extend through the sedimentary rocks and intersect, but never cut, the reverse fault (Scott, 1972; Van Horn, 1972). Both the Golden fault and the northwest faults were probably active at the same time, concentrating movement along the latter pre-existing planes of weakness. In places, such as at the Schwartzwalder deposit where the major fault has more than one segment, intervening zones must have been subjected to extremely complex stress, thereby producing equally intricate fracture patterns. It is notable that all of the uranium deposits along the foothills are situated in the northwest-trending fault systems and within a few kilometers of the range front. The interaction between the two sets of faults during uplift clearly produced complex fracture systems in the crystalline upper plate. This decreased in apparent complexity away from the frontal zone as the influences of the reverse faults diminished.

The pre-ore Illinois fault is situated between the two strands of the Rogers fault system. Proterozoic pegmatites fill what was probably a proto-Illinois fault that may have formed as a cymoid fracture between the bounding faults (Paschis, 1979).

During subsequent movement of unknown age, the Illinois fault apparently dragged the nose of the synform (Wright, 1980), and juxtaposed hornblende gneiss against the rocks of the transition zone. The former effect was caused by right-lateral movement (Wright, 1980), but the latter effect could have been due to either right-lateral movement or major normal displacement.

A few pegmatitic dikes in the hangingwall of the Illinois fault suggest Proterozoic precursors to the tension fractures (Paschis, 1979). However, it is unreasonable to assume that the dilatant zones, in some places more than two meters in width, survived deep burial and tectonism since late Proterozoic time. As such, the modern system of horsetail fractures in the mine must have developed during Laramide time as a result of dominantly normal movement along the pre-ore Illinois fault. The two slightly dissimilar sets of fractures suggest that the Illinois fault may have had two slightly dissimilar periods of displacement. Offsets observed along the tension fractures attest to adjustments in many directions, as might be expected if one set formed and was subsequently disrupted by the other. At this time, there is little evidence for the relative ages of the two fault sets. The primary causes of dilation along the horsetail fractures was tension and changes in the strike and (or) dip of the fracture. Lateral changes in the orientation caused the fractures to pinch and swell abruptly. Similarly, changes in vein widths accompany changes in the dip of the fracture.

Although of roughly the same age and orientation, the morphologies of the pre-ore and post-ore Illinois faults are remarkably different. The materials in the pre-ore fault zone are strongly brecciated, and repeated movement locally pulverized the fragments and ores. Although the fault was originally a relatively open conduit for hydrothermal fluids, the textures preserved in brecciated vein materials suggest that the original breccia was fairly close-packed. In contrast, the post-ore fault is characteristically open, with dilations over a meter in width and tens

of meters in length. Although both are approximately the same age, have the same orientation, and moved in the same direction, the difference in forms may be due to different mechanisms of formation. The change from a tighter to more open fracture may instead reflect a shallower, essentially near-surface, origin for the post-ore fault.

CHAPTER 4. FEATURES AND MINERALOGY OF ALTERATION

Hydrothermal fluids invaded faults and fractures, and altered many of the surrounding rocks prior to the deposition of uranium in the veins. Two successive assemblages of alteration, shown schematically in Figure 10, were produced. Carbonate and sericite characterize the early assemblage, which forms a bleached halo around the fractures. The ensuing episode of alteration produced a distinctive hematite-adularia assemblage superimposed upon the earlier assemblage immediately adjacent to the veins. The hematite-adularia zone is locally absent, and some vein segments have no associated alteration. However, the hematite-adularia zone is never present without the carbonate-sericite zone. The mineralogy and sequence of hydrothermal alteration is uniform throughout the 900 vertical meters of mine workings.

Carbonate-sericite Alteration

Carbonate-sericite alteration forms a halo up to two meters in width around most veins and fractures, regardless of the grade or presence of ore in the veins. Ca-Mg-Fe carbonates and sericite characterize the assemblage. Chlorite, epidote, paragonite, albite, leucoxene, and kaolinite are minor alteration products. The altered rocks are pale yellow-green, in striking contrast to the dark hue of the fresh rocks. Alteration preserved all primary rock textures, including foliation, layering, and mineral shapes. Carbonate and sericite pseudomorphically replace the primary mafic minerals in the rocks, but do not severely alter the felsic minerals. Thus, the abundance of mafic minerals in a particular host rock influenced the relative intensity of alteration.

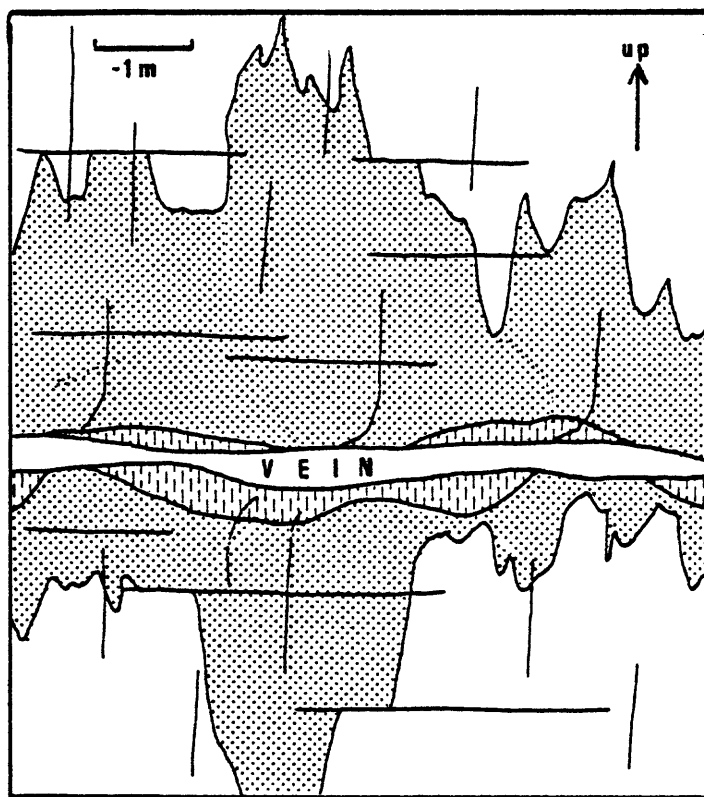


Figure 10. Schematic drawing to illustrate the relative distribution of the carbonate-sericite (stippled) and hematite-adularia (vertical short dashes) to the vein. Vertical foliation represented by thin vertical lines, some of which show drag along the fault.

Alteration of Hornblende Gneiss

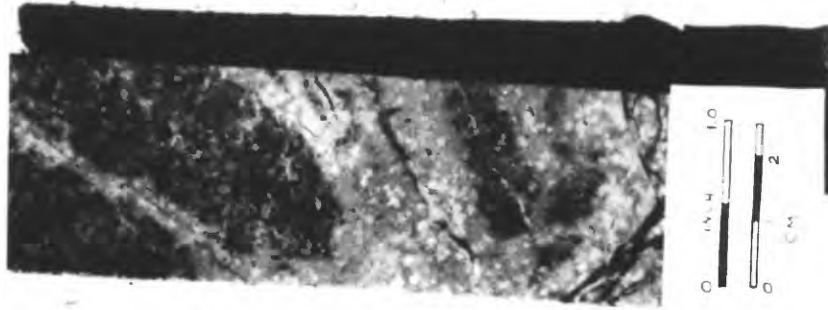
Alteration produced in the hornblende gneiss reflects the mineralogical and textural diversity of the fresh gneiss. Extremely fine-grained carbonate and sericite pseudomorphically replace primary mafic silicates, oxides, and sulfides. Alteration commenced along cleavage planes and then invaded the intervening areas. As a result, cleavage and mineral shapes are preserved, and altered rocks retain foliation and all other primary metamorphic textures. Amphiboles were more susceptible to alteration than biotite or andesine. This is apparent near the periphery of alteration zones where fresh biotite or feldspar coexists with completely altered amphibole (Figure 11a). Sericite is an alteration product of biotite and hornblende, but not of the low-aluminum amphiboles such as actinolite. Compositions of the carbonates, based upon X-ray diffractometer patterns and semiquantitative microprobe analyses, are intermediate between dolomite and ankerite, and approximate the iron-magnesium ratio of the host mineral.

Felsic minerals in the altered hornblende gneiss are relatively fresh, and none are completely altered. Quartz grains in the gneiss, as well as intercalated quartzite layers, are preserved regardless of the intensity of alteration. Finely disseminated sericite and minor paragonite replace andesine, initially along twin planes and subsequently throughout the mineral. Andesine is also locally albitized around grain boundaries, but the albite is not altered to white mica. Finely disseminated sericite is ubiquitous in orthoclase and microcline. Although fine-grained secondary carbonates locally replace calcite, many altered samples retain the relatively coarse primary carbonate. Tourmaline, apatite, and zircon are fresh in altered rocks. Leucoxene replaces sphene, locally with transitional ilmenite, and siderite replaces pyrrhotite.

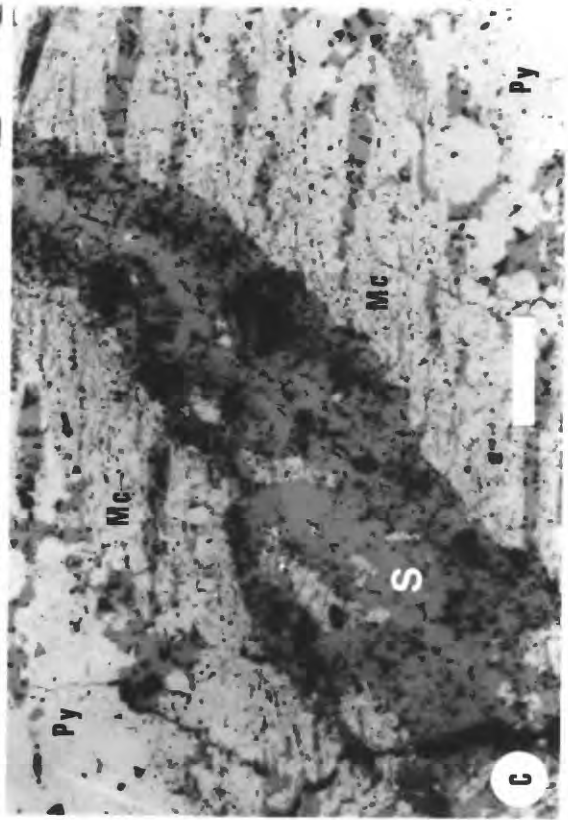
Alteration haloes in the hornblende gneiss vary from a few centimeters to two meters in width, depending upon the compo-

Figure 11. Carbonate-sericite alteration.

- a. Pseudomorphic alteration of amphibole (a) to ankerite and sericite. Biotite remains unaltered. Bar is 0.20 mm long.
- b. Alteration of garnet-biotite gneiss adjacent to small veinlets. Note pseudomorphic alteration of garnet (white spheres in altered zone).
- c. Alteration of Proterozoic pyrite (Py) to siderite (S) and marcasite (Mc). Bar is 0.10 mm long.



B



sition of the host rock. Alteration preferentially influenced those layers with modally abundant amphibole and, to a lesser extent, biotite. Alteration fronts migrated along foliation away from the veins owing to the oblique angle between layering and fault planes. Faults juxtaposed contrasting lithologies, and, as a result, subsequent alteration generated asymmetrical haloes. Hairline fractures parallel the veins in both the hangingwall and footwall. There is little or no apparent offset along the fractures, and they are commonly filled with carbonate. Alteration which extends up or down to these fractures typically diminishes in intensity across or terminates abruptly against the fractures. The minimal offset precludes post-alteration truncation of the altered layers, and suggests that the fractures served as partial to complete barriers to alteration fronts.

Alteration of Garnet-biotite Gneiss

The garnet-biotite gneiss is texturally and mineralogically more uniform than the hornblende gneiss. As a result, carbonate-sericite alteration migrated more evenly into the wall rocks from both major veins and minor fractures (Figure 11b). Fine-grained carbonate and sericite pseudomorphically replace biotite. In peripheral zones of alteration, only carbonate replaces biotite, and the amount of sericite increases towards the vein. Early alteration of garnet produced carbonate, epidote, and sericite along cracks in the garnets. With continued alteration, carbonate, paragonite, chlorite, and kaolinite replaced the remainder of the grain. Garnet was replaced either at the same time or after alteration of the biotite. In the latter instance, inclusions of biotite in garnets are unaltered despite complete destruction of groundmass biotite; these inclusions are replaced only where the host garnet is replaced. Fine-grained sericite locally replaces muscovite, but muscovite is otherwise fresh.

The felsic minerals are much less altered than the mafic minerals, and alteration is very similar to that in the hornblende gneiss. Quartz is fresh, and sericite and paragonite slightly dust all feldspars. Secondary albite is fresh.

Pyrite, marcasite, and siderite replace pyrrhotite. Pyrite and siderite form lamellar intergrowths with a thin intervening zone of marcasite. Inclusions of chalcopyrite in pyrrhotite are replaced as well. Lamellar intergrowths of siderite and marcasite replace pyrite of both metamorphic and alteration origin (Figure 11c). Siderite lamellae in these intergrowths are fine-grained and granular adjacent to marcasite, but are relatively coarse near the center of the lamellae. Microprobe analyses of both textural varieties show that both are pure siderite. Alteration of pyrite was incomplete, so equal volume replacement could not be established.

Pyrite is also replaced by a black, massive substance which is also present in some microveinlets in the altered wall rocks. The substance is opaque, and, in polished section, has a brownish gray color. It takes a good polish, but is much softer than pyrite. Internal reflections, bireflectance, and anisotropism were not observed. Replacement is pseudomorphic, and islands of unreplaced pyrite are usually abundant. Semiquantitative microprobe analyses indicate major Fe and S. Patterns from X-ray diffraction analyses have a very weak pyrite pattern, but these may reflect inclusions of pyrite. Downs and Bird (1965) described "black pyrite" with similar physical and chemical characteristics. Although it is not colloform, the substance bears some resemblance to melnicovite, an amorphous iron sulfide described by Ramdohr (1980).

Alteration of the pyrite-mica schist member is similar to that in the garnet-biotite gneiss. Carbonate and sericite replace biotite, and siderite replaces pyrite. Quartz, muscovite, and most feldspars are relatively fresh. Muscovite-rich layers are less altered than biotite-rich zones.

Alteration of Quartzite

Carbonate-sericite alteration of the quartzite is minor, although abundant carbonate-filled fractures lace the rock. Iron-rich dolomite invades the rock along grain boundaries and from the fractures. Minor minerals in the rock are completely altered, indicating that, although the quartz was relatively unreactive, the altering fluids were able to reach and replace the accessory minerals. Green chlorite is the principal alteration product other than carbonate, and it pseudomorphically replaces amphibole and biotite. Siderite locally replaces iron sulfides. Muscovite and magnetite are fresh.

Alteration of Mica Schist

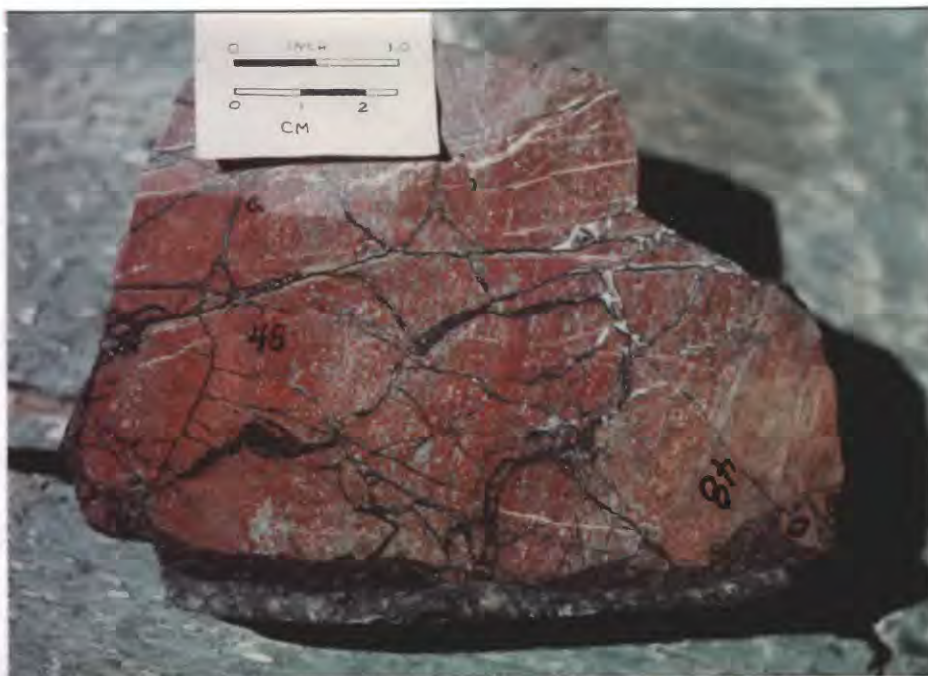
Because faults in the mica schist and similar lithologies did not generate an open breccia, these rocks rarely came into contact with altering hydrothermal fluids. Where altered, the fluids produced a carbonate-sericite assemblage similar to that formed in the garnet-biotite gneiss and pyrite-mica schist.

Hematite-adularia Alteration

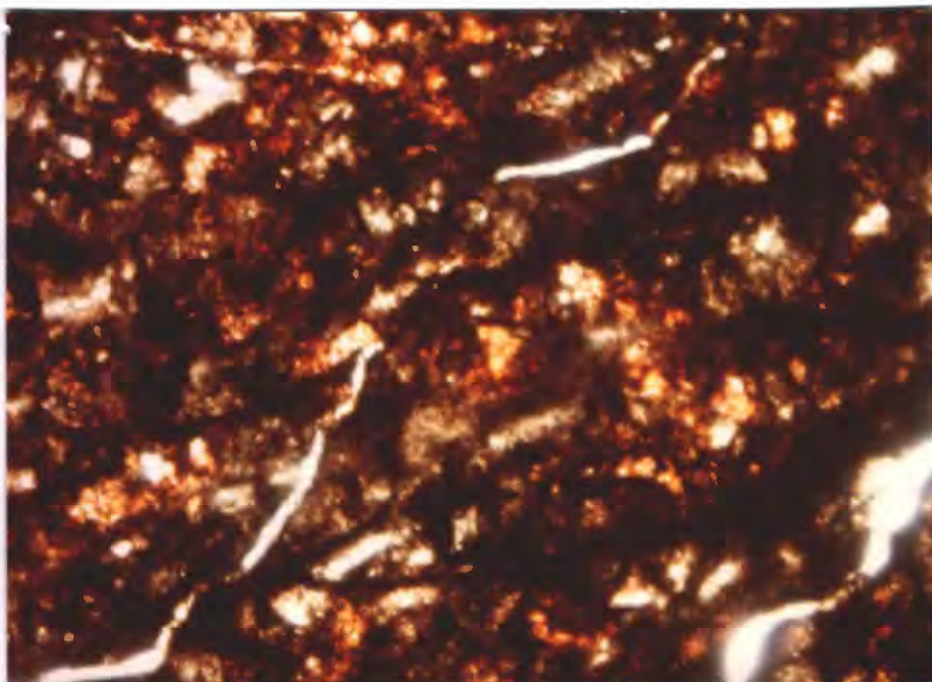
The hematite-adularia alteration zone forms a thin, asymmetric halo around many of the veins. Hematite and adularia replace the products of the earlier carbonate-sericite alteration as well as relict feldspars of metamorphic origin, as noted originally by Heyse (1972). It does not directly replace mafic minerals in the metamorphic rocks, a phenomenon reported by Adams and Stugard (1956) in the Golden Gate Canyon District to the south. Rocks altered to hematite and adularia are red to reddish orange (Figure 12a), in contrast to the pale green carbonate-sericite alteration and the black veins. Alteration of this type surrounds most veins, but is absent around numerous vein segments. In contrast,

Figure 12. Hematite - adularia alteration.

- a. Brecciated hornblende gneiss altered to hematite and adularia. Foliation and mineral textures are generally preserved. Veinlets of pitchblende and dolomite cut altered rock.
- b. Hematite replacing pre-existing carbonate-sericite alteration in massive amphibolite. Width of field of view is 6 mm.



a.



b.

Figure 12.

a thin reddish halo envelopes many non-uranium-bearing microfractures near the veins.

Hematite and adularia were the only minerals produced in this alteration zone, and adularia is locally absent. Hematite replaces iron-bearing carbonates in the carbonate-sericite zone, creating an earthy red stain in the carbonate (Figure 12b). In samples containing siderite and relict pyrite, the hematite visibly replaces only the siderite. Disseminated hematite imparts a pink coloration to relict metamorphic alkali and plagioclase feldspars. In such cases, the textures of the original feldspars are clearly identifiable. In many samples, the feldspars are altered to hematite, whereas the carbonates are either unaltered or only peripherally altered adjacent to the feldspars. All pre-hematite sericite in the feldspars was destroyed.

Adularia varies texturally from pseudomorphic replacement of feldspars to obliteration of all pre-existing minerals. However, it is also absent in many rocks containing hematite. Where present, adularia always contains abundant disseminated hematite, and many rocks derive their red hue predominantly or entirely from hematitic adularia. Where adularia pseudomorphically replaces both alkali and plagioclase feldspars, quartz and carbonate pseudomorphs after mafic minerals are preserved. With increased intensity of alteration, adularia replaces the sericite in the carbonate-sericite pseudomorphs, but the carbonate is unaffected and retains the pseudomorphic form of the original mineral. As a result, primary foliation is preserved despite the destruction of all primary minerals except quartz. The most intense alteration along parts of Illinois and Rogers faults destroyed most quartz and all primary textures, creating a hard, microcrystalline intergrowth of hematized adularia and irregular patches of carbonate. This texture grades imperceptibly into microgranular breccias composed of pulverized fragments of the same minerals.

Alteration of the quartzite during this episode differed somewhat from that in the other lithologies. Only minor amounts

of carbonate replaced the quartzite in the earlier episode, thereby minimizing the amount of hematite that could form from the iron-bearing varieties. In addition, very little adularia formed in the quartzite as an alteration product. Instead, patches of hematitic, spherulitic chalcedony replace the quartzite. The chalcedony fills solution voids in the quartzite, and consumes quartzite adjacent to chalcedony-filled microveinlets. Contemporaneous reddish-orange iron oxide is disseminated through the chalcedony. Deposition of the iron oxide ceased before most voids were filled, and clear chalcedony fills the remaining spaces and microfractures. Deposition of the iron oxide was rhythmic in some areas of the Titan vein: concentric red and colorless bands overlap the radiating needles of chalcedony in spherules. Much of the chalcedony in both the wallrocks and veinlets is replaced by euhedral iron dolomite.

The distribution of hematite-adularia alteration adjacent to veins is erratic and asymmetric. The zones rarely exceed 20 cm in width on both sides of the vein, and most haloes are only several centimeters wide. The alteration may be present on only one side of a vein, or it may be entirely absent. The hematite-adularia alteration shifts from the hangingwall to the footwall along strike of several horsetail veins, with an intermediate section where it is present on both sides of the vein.

Pre-ore faulting generated fault breccias composed of fragments of altered wallrock. Most fragments are of local derivation, and both hematized and non-hematized fragments coexist in the same breccia. However, most pre-ore breccia fragments are hematitic or have rims of hematite, indicating hematitization during or after brecciation. Post-ore faulting locally juxtaposed massive uranium ores against fresh or altered wallrock, obscuring the original vein-wallrock contact.

Chemical Effects of Alteration

Samples of fresh metamorphic rocks and their altered equivalents were analyzed for major and minor elements. An attempt was made to collect both fresh and altered samples from the same lithologic layer to maximize chemical comparisons, but this was not feasible at all sample sites. Numerous microveinlets in the hematite-adularia zone rendered most samples unsuitable for chemical comparisons. As a result, most samples used for chemical comparisons in this study are from the relatively more extensive and less-fractured carbonate-adularia zone. The garnet-biotite gneiss and hornblende gneiss units, juxtaposed by faulting prior to alteration, are the predominant altered wall rocks, and were sampled accordingly. An adequate comparison of fresh and altered rocks could not be made for the quartzite and mica schist. The relative absence of veins through the mica schist precluded sampling in that unit. Samples of "altered" quartzite proved to contain volumetrically more carbonate in numerous small fractures than as an alteration product.

Volume Relations

Based upon the observed textures, alteration in the carbonate-sericite zone progressed with little or no change in volume. Alteration preserved all primary textures, and neither void space nor mineral swelling, both suggestive of a volume change, were observed.

Alteration in the hematite-adularia zone destroyed most primary textures. Despite wholesale alteration by adularia, the carbonate in the carbonate-sericite pseudomorphs remains texturally intact, suggesting little or no change in volume. In other samples, however, all textures were destroyed. In addition, fault-related microfractures obscure overall volume relations.

Therefore, equal volume replacement could not be presumed for this zone except where textures locally indicate otherwise.

Chemical Gains and Losses

The gains and losses of major and minor elements during alteration of the garnet-biotite gneiss and hornblende gneiss can be estimated from the analyses of fresh rocks and altered equivalents. The average composition of each unaltered rock unit was calculated from analyses listed in Tables 1, 4, 5, and 7. The average compositions of the altered equivalents were derived from the analyses given in Appendix A.

Carbonate-sericite zone

Chemical gains and losses during carbonate-sericite alteration are summarized in Table 13, and shown graphically in Figure 13. Alteration of all rocks produced a decrease in total mass. Alumina and magnesia remained relatively stable during alteration. Concentrations of SiO_2 , FeO , and Fe_2O_3 decreased in all rocks, whereas that of CO_2 increased universally. Sulfur was removed as carbonates replaced primary iron sulfides.

The changes in several major oxides indicate that the original rock composition influenced hydrothermal alteration. The $\text{Fe}^{+2}/\text{Fe}^{+3}$ ratio remained constant during alteration of the garnet-biotite gneiss, but increased in the altered hornblende gneiss. CaO was added to the CaO -deficient garnet gneiss to form carbonates, but was removed from the CaO -rich hornblende gneiss; Na_2O behaved similarly. Potassium remained stable in the K_2O -rich garnet gneiss, but increased in the less potassic hornblende gneiss.

Alteration did not noticeably influence the distribution of most trace elements. Concentrations of As, Be, Hg, Mo, Pb, Sb, and especially U increased in altered rocks. As will be described

Table 13. Average compositions of unaltered garnet-biotite gneiss (GBG) and hornblende gneiss, (HG), and of altered equivalents in carbonate-sericite zone.

	Fresh	±	Alt	±	Fresh	±	Alt	±
	GBG		GBG		HG		HG	
SiO ₂ (%)	53.90	6.00	45.70	7.60	43.30	6.10	37.00	4.40
Al ₂ O ₃	12.40	1.50	11.00	1.80	14.00	3.20	13.80	1.90
Fe (total)	18.80	2.80	15.60	5.60	10.80	2.10	9.60	1.40
FeO	15.80	3	11.40	2.50	8.60	1.70	8.20	1.00
Fe ₂ O ₃	3.50	1.10	2.40	1.00	2.30	.64	1.32	.61
MgO	3.30	.90	3.67	1.00	4.30	1.00	4.62	.52
CaO	1.50	1.00	4.09	2.76	12.10	6.10	9.10	2.50
Na ₂ O	.36	.23	.87	.94	2.03	1.70	1.96	1.40
K ₂ O	3.40	.83	3.64	1.60	2.59	1.80	4.85	2.40
TiO ₂	.78	.99	1.03	1.10	1.37	.50	1.84	1.00
P ₂ O ₅	.25	.16	.30	.20	.29	.14	.30	.17
MnO	.66	.33	.76	.80	.50	.05	.23	.06
LOI	4.80	2.80	12.40	3.20	7.88	5.30	16.20	2.50
C (total)	1.31	.91	3.87	1.00	2.02	1.40	4.30	.60
C (org.)	.60	.50	.75	.76	.22	.18	.45	.44
C (carb.)	.77	.68	3.12	1.00	1.80	1.30	4.10	.96
S	1.40	1.60	.88	1.10	0.50	0.40	0.60	.10
Hg (ppm)	0.02	.02	.12	.24	.01	0	.08	.16
Ag	<5	0	<5	—	<5	—	<5.10	.40
As	14.40	14.90	28.30	18.70	18	30	38.80	28
B	66	92	59	84	N	—	L	—
Ba	363	192	133	99	341	391	221	138
Be	1.90	1	6.90	3.20	N	—	20.10	38
Bi	<.70	.60	<.60	.64	<.20	—	<.87	1.70
Cd	1.90	2.90	1.40	2.00	.49	.53	.63	.60
Co	18.70	6.60	16.10	9.10	31	17	27.30	5.50
Cr	57	17	63	35	173	73	184	84
Cu	92	95	75	73	69	52	60	101
F	1150	303	1518	606	1008	774	1163	809
Ga	20	4	26	16	19	5	21	5.80
La	<50	—	<50	—	<50	—	<50	—
Mo	15.20	24	136	263	10.70	12	53.50	88
Ni	40	13	32	13	58	27	53.10	32
Pb	63	34	914	2101	<10	—	38.10	47
Sb	2.80	3	16.80	29	<7	14	9.75	10.70
Sc	12	4	12	7	25	7	24.40	12.40
Sr	68	45	155	88	270	409	253	166
Th	<11.50	<4.20	<69	<131	<4.40	<4.13	<13.50	<20
Tl	<1	—	<1	—	<1	—	<1	—
U	18.30	24	326	660	9.32	17	71.40	106
V	191	165	176	52	199	96	209	90
Y	21.70	12	17.30	6.50	22	6.50	21	6.70
Yb	2.40	.50	2.44	.62	2.30	.70	2.10	.60
Zn	144	54	225	208	84	51	75	39
Zr	96	29	74	14.30	66	26	76.30	35.80
density (g/cm ³)	3.02	—	2.87	—	2.79	—	2.75	—

Analyzed for but not detected in any sample: Au, Ca, Eu, Ge, Hf, In, Li, Nb, Nd, Pd, Pr, Pt, Re, Se, Sm, Sn, Ta, Te, W. N: not detected; L: detected but below accurate detection limit; (—): not analyzed for.

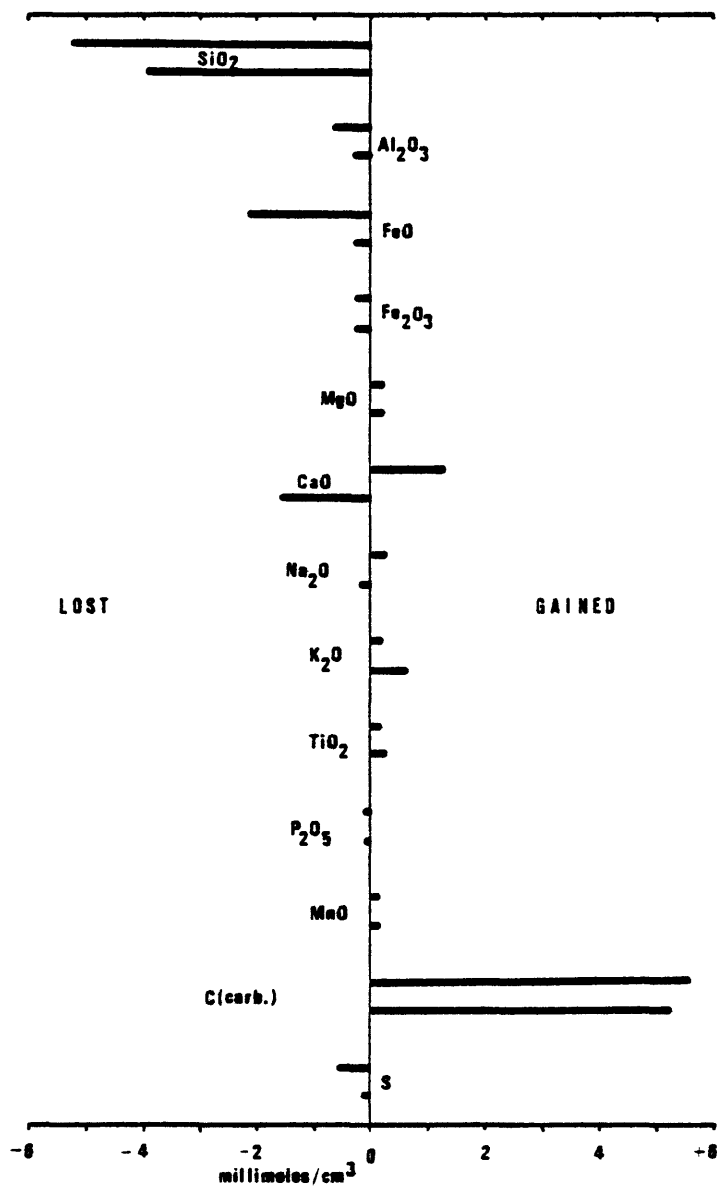


Figure 13. Graph showing the relative gains and losses of major oxides during carbonate-sericite alteration of the garnet-biotite gneiss (upper bar) and hornblende gneiss (lower bar). Gains and losses are relative to the compositions of the unaltered equivalents.

in the next chapter, this suite of elements is prevalent in the veins as well. Only Ba is consistently depleted in altered zones.

Hematite-adularia zone

An unfractured sample of hematite-adularia alteration was collected at only one location along with samples of fresh rock and carbonate-sericite alteration. Hematite was dominantly associated with reddened feldspars, including adularia and plagioclase, and alteration was incomplete. Chemical gains and losses for the alteration sequence are shown in Figure 14. The contents of SiO_2 and K_2O were enriched, whereas those of Al_2O_3 , MgO , CaO , Na_2O , and CO_2 were depleted. Surprisingly, the $\text{Fe}^{+2}/\text{Fe}^{+3}$ ratio decreased only slightly. Because the evidence for equal-volume replacement was equivocal, the chemical analyses may not be representative.

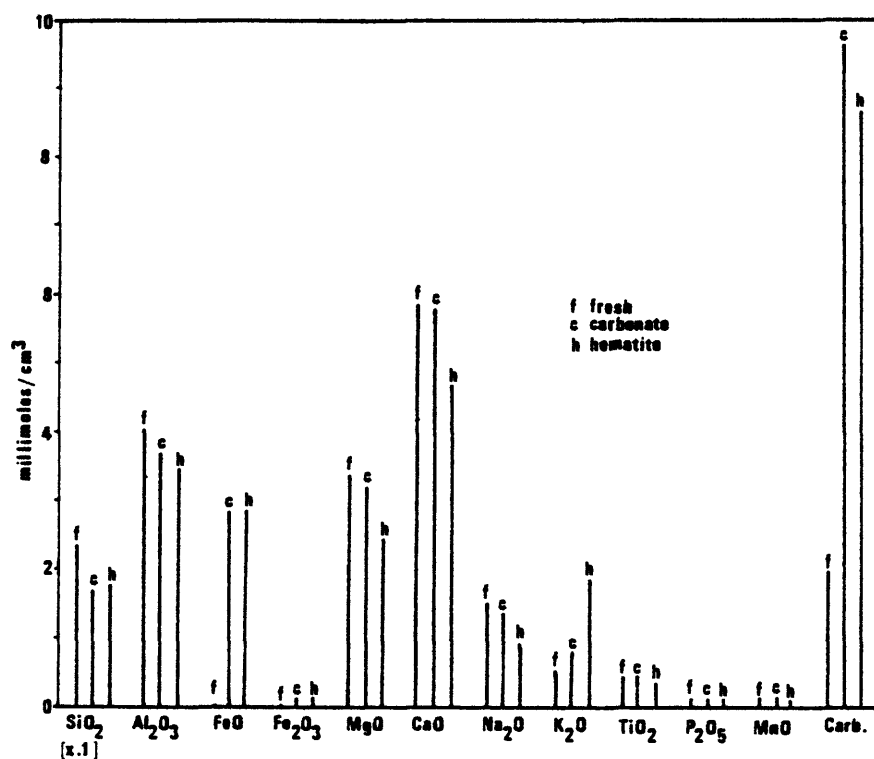


Figure 14. Major oxide composition of unaltered hornblende gneiss, and of equivalent samples in carbonate-sericite (c) and hematite-adularia (h) zones. FeO and Fe₂O₃ were not analyzed for in unaltered sample.

CHAPTER 5. VEIN MINERALOGY AND PARAGENESIS

Multistage uranium and gangue minerals fill virtually all faults and related fractures in the Rogers, Illinois, and horse-tail fracture systems. The post-ore Illinois fault is the only major fracture devoid of uranium ores, although it is partially to completely filled with late-stage gangue minerals. Hypogene vein mineralization spanned three successive stages. In addition, clastic dikes of various compositions were emplaced both before and during hydrothermal mineralization. Contemporaneous fault movement modified existing vein minerals and textures, and generated new conduits and open spaces for ensuing hydrothermal activity. Hypogene uranium minerals did not form below the present 16th level in the Illinois and horsetail veins, although subsequent movement along the post-ore Illinois fault displaced uranium veins in several horsetail fractures to lower levels.

The Rogers, Illinois, and horsetail fracture systems are the hosts for the uranium ores and associated gangue. The most significant structural control of the deposit was the presence of continuous open fractures. Discontinuous openings and impermeable gouge zones in the mica schist and hornblende gneiss units concentrated hydrothermal fluids into fault zones in the relatively brittle garnet-biotite gneiss and quartzite units. The faults pinch and swell dramatically along strike, and the widths of the veins vary accordingly. Abrupt changes in the dips of many horse-tail fractures, such as the RB and Titan veins, cause pronounced differences in the widths of mineralized structures (Downs and Bird, 1965). Intersections of the major vein systems, typically a favorable site for ore deposition (McMinistry, 1955), are either not exposed or have been obscured by major post-ore movement along the faults. Branching of veins in the uppermost levels of the deposit apparently generated structures favorable for ore deposition (Downs and Bird, 1965).

Descriptive Mineralogy

Uranium and gangue minerals filled the fracture system during three stages of vein mineralization and the invasion of clastic dikes. Evidence for all episodes could not be seen at any one location, and the general paragenetic diagram shown in Figure 15 therefore applies to the deposit as a whole.

Based upon samples collected above the 7th level, two previous reports (Heyse, 1972; Honea and Ferris, unpub. report) described the mineralogy of the veins. Both reported major pitchblende and sulfide stages but in opposing paragenetic sequences. Stark (1979) demonstrated that two sulfide stages bounded the uranium stage at the nearby Mena mine (Figure 1), and the present investigation found evidence for two sulfide stages at the Schwartzwalder mine (Figure 15). Supergene processes complicated the mineralogy of the uranium veins in the upper levels, and, as noted by Honea and Ferris (unpub. report), produced contradictory paragenetic sequences.

Stage I Mineralogy

Scattered evidence throughout the deposit indicates at least one pre-uranium stage of vein mineralization. In a few isolated locations, the uranium veins truncate oblique fractures filled with base-metal sulfides, chalcedony, and carbonates. Fragments of pre-uranium sulfides are also relatively common in most uranium veins, implying at least local early sulfide mineralization in those fractures. Furthermore, a pre-carbonate silica-hematite assemblage indurates early breccias in several pegmatites.

Two distinct assemblages fill the oblique fractures in the wall rocks: hematite-chalcedony-carbonate and base-metal sulfides-carbonate. The hematite-chalcedony-carbonate veinlets are adjacent to the Titan, RB, and 9x1 veins. Much of the hematite-chalcedony alteration in quartzites adjacent to the RB vein grades into veinlets lined with hematitized chalcedony and cored by dolo-

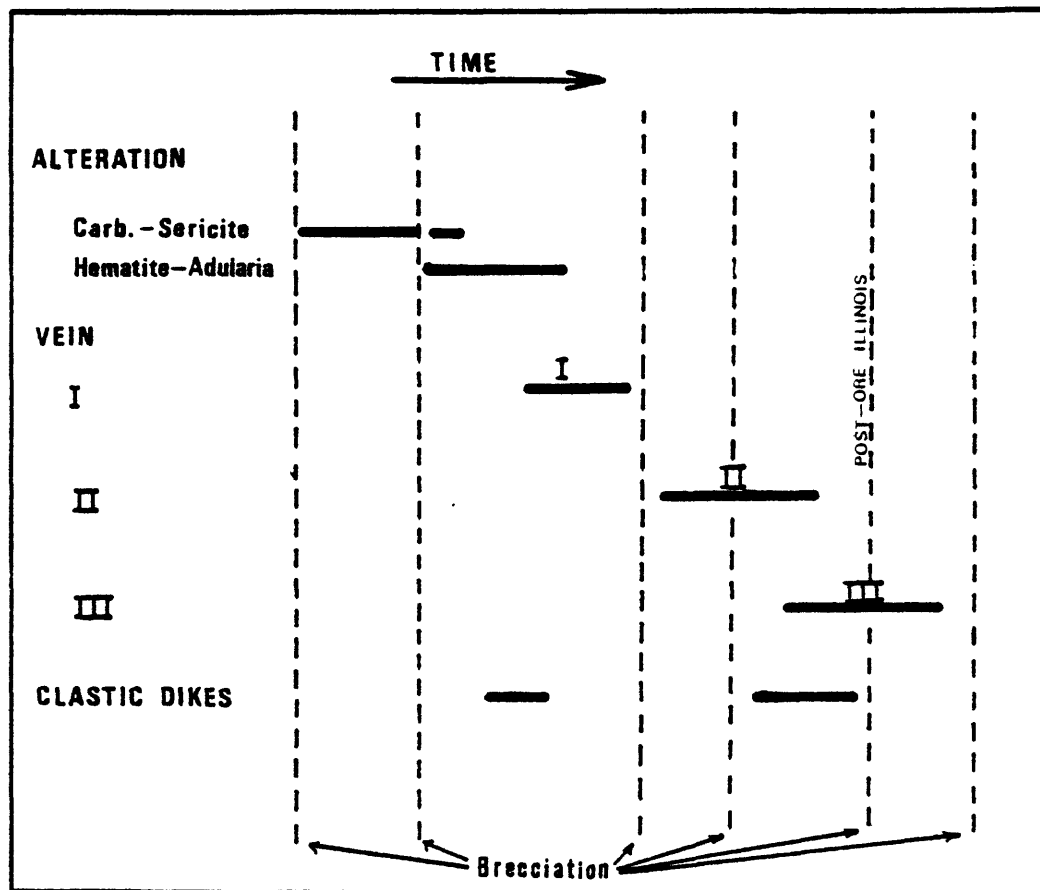


Figure 15. Paragenetic diagram of the major episodes of alteration, vein mineralization, and injection of clastic dikes. Also shown are the major periods of fault movement and brecciation.

mite. As such, these veinlets are contemporaneous with the second stage of alteration. Elsewhere, thin veinlets transect unaltered hornblende gneiss, and produce minor pyrite flooding in the adjacent rocks.

Veinlets containing the carbonate-base metal sulfide assemblage are adjacent to the 17-1 and RB veins. In addition, fragments of base-metal sulfides, especially pyrite, galena, and chalcopyrite, are ubiquitous in all veins, and are enveloped by pitchblende. Zoned yellow sphalerite is the predominant sulfide in the veinlets; the other three sulfides are locally abundant. Much of the sphalerite is broken and cemented by relatively coarse dolomite. The veinlet on the 17-1 vein is parallel to foliation, and follows the intrusive contact of an aplite dike. Reverse movement along the 17-1 fault offset the veinlet approximately one meter. Veinlets of pyrite and chalcopyrite along the 9x1 vein weave through garnet-biotite gneiss that has been altered to carbonate and sericite.

Breccia fragments in part of the RB vein are composed of fine-grained banded sulfides. The source of the fragments could not be determined because mining at that location exposed only the vein and not the wall rocks. Thin layers of massive pyrite, chalcopyrite, and chalcocite alternate with bands containing adularia, carbonate, and sulfides. The felsic bands are texturally conformable with and gradational into the massive sulfide layers, and do not appear to have developed as post-sulfide veinlets parallel to layering. Instead, the syngenetic formation of adularia with the sulfides in complex bands suggests a hydrothermal origin, possibly as a complexly zoned vein. Some of the adularia is slightly hematized, and is at least partly synchronous with the second stage of alteration. A major episode of brecciation intervened between sulfide-adularia and subsequent uranium mineralization (Figure 15).

A microcrystalline quartz-specular hematite cement fills early breccias in several pegmatites which were subsequently re-

brecciated and healed with carbonate and adularia. The quartz-hematite cement is identical to that in the Rogers and other major faults where they traverse the granitic terrane to the northwest (Wallace, in press). The assemblage is rare in the metasedimentary terrane, and is usually associated with pegmatite hosts in that region.

Stage II Mineralogy

Stage II encompasses the major ore-forming period during which roughly 80 percent of the vein minerals were deposited. It clearly followed both hematite-adularia alteration and Stage I mineralization. Two major episodes of fracturing and brecciation, one immediately before and the other during mineralization, played major roles in the development of the veins.

Stage II includes three substages, two producing uranium ores and one forming a sulfide-carbonate assemblage. This subdivision is a modification of an earlier paragenetic scheme (Wallace and Karlson, 1982). The first episode of pitchblende deposition corresponds to Stage II of the earlier report; the second pitchblende and the carbonate-sulfide substages comprise stage IV of Wallace and Karlson. Other reports (Heyse, 1972; Honea and Ferris, unpub. report; Rich and Barabas, 1976) describe only one major episode of pitchblende deposition. Although two pitchblende substages are evident, they combined, in one complex paragenetic interval, to form the observed uranium veins.

Although the early pitchblende comprises the bulk of the ores, the distinction between the two substages of uranium is usually impossible mesoscopically and difficult microscopically unless both stages are clearly represented. Both share many similar textures, and both are black in hand sample. Polished sections show that the sulfide-carbonate substage always directly follows the deposition of the second pitchblende, and that a major episode of brecciation separated the two substages of uranium deposition.

Therefore, the first pitchblende substage is very arbitrarily defined as that which is crosscut by either the second pitchblende or carbonate-sulfide substages. In practice, this distinction usually proves very satisfactory, but fails in samples containing only one substage of pitchblende without subsequent carbonate-sulfide mineralization.

The mineralogy and paragenesis for Stage II are illustrated in Figure 16. Pitchblende and coffinite are the only uranium minerals. Of particular importance is the Fe-Mo-As sulfide. All previous studies mention this phase, and refer to it as jordisite or molybdenite. The phase is very closely associated with pitchblende in the horsetail veins, but is notably rare in the battered ores along the Rogers and Illinois faults. The mineral commonly forms colloform coatings on top of the pitchblende, but is also disseminated through the massive ores. The color is silver with a reflectivity greater than that of galena. The mineral is usually isotropic, but locally has pink to purple polarization colors. Semiquantitative analyses with the scanning electron microscope indicate major Fe, Mo, and S, with variable amounts of As and very minor Cu. The phase is locally zoned, with alternating bands of variable reflectivity and hardness. Slightly softer, darker bands contain a higher Mo/As ratio than harder, lighter bands. The As-rich phase may represent Mo-bearing arsenopyrite. The Mo-rich phase, which is the most common of the two in the deposit, has no published equivalent (Ramdohr, 1980), but has many optical properties similar to those of molybdenite.

A major episode of brecciation preceded early pitchblende deposition along all existing faults. The fault movement shattered adjacent rocks and existing vein materials, producing a heterolithic and poorly sorted breccia in the fault zones. In addition, thin, continuous veinlets parallel the horsetail veins. Numerous anastomosing fractures splay into the adjacent rocks, especially in the hangingwalls of the horsetail fractures. The actual contact between veins and host rock is locally a narrow zone of shat-

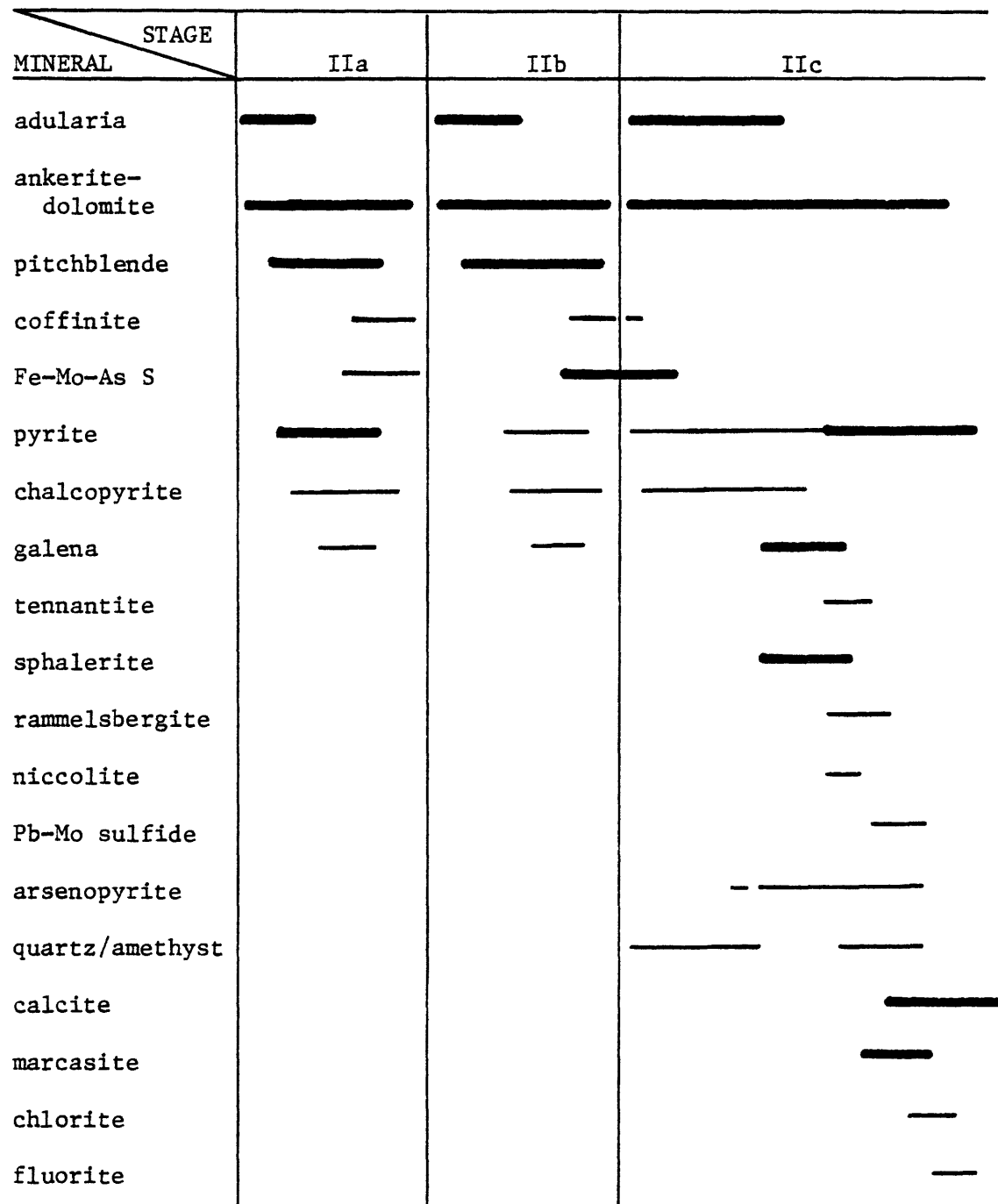


Figure 16. Paragenetic diagram of Stage II vein mineralization. Width of lines is estimate of relative abundances of minerals.

tered wall rock. The abundance and size of the breccia fragments in the vein increases towards these zones, giving the appearance of stoping or spalling during mineralization. In other wide, inclined veins, a layer of relatively coarse breccia appears to have accumulated along the basal contact of the vein.

The breccia fragments vary unpredictably in size, abundance, and lithology. Many faults are choked with poorly sorted rubble, whereas others are remarkably devoid of breccia, and must have been gaping dilations during mineralization. Clasts range in size from a fraction of a millimeter to more than 20 centimeters as space permits. Fragment lithologies include those of all pre-existing altered wall rocks and vein materials; lithologies exotic to that suite were not seen. The garnet-biotite gneiss, hornblende gneiss, and quartzite units are the predominant wall rocks, and consequently constitute the principal fragments of the breccias. Included also are small pieces of early clastic dikes. Most fragments are of local derivation, but many are exotic to the adjacent wallrock lithology. This is obvious where veins devoid of a hematite-adularia alteration halo contain fragments of hematitized wall rocks. Many clasts are subrounded to subangular, indicating possible abrasion during brecciation or possible subsequent fluid transport. Variable rotation of fragments is evident where foliation is preserved; the amount of rotation is minimal immediately adjacent to the walls of some veins.

Vein mineralization commenced with the deposition of carbonate and unhematized adularia in veinlets cutting the fractured wall rocks. Some veinlets, as seen in breccia fragments, stop at the edge of the fragment, whereas others clearly cut through the clasts from the vein. As such, the veinlets both accompanied and followed the major brecciation. Numerous veinlets of unhematized adularia cut the hematite alteration zone, indicating that the vein adularia is not related to the alteration adularia. The density of the fractures suggests that they formed as a result of hydrofracturing, similar to those in crackle breccia zones of por-

phyry copper and molybdenum systems (White et al., 1981).

Early pitchblende, along with several gangue minerals, fills the voids in the breccia zones and fractures in adjacent rocks. Pitchblende usually forms a black, very fine-grained mixture with ankerite, adularia, rock flour, and sulfides, which include pyrite, chalcopyrite, galena, and the Fe-Mo-As sulfide (Figure 17). Pitchblende forms tiny spherules or laths interstitial to or semi-colloform coatings around rock fragments. It is locally massive and completely fills voids. Coarse varieties are weakly to strongly replaced by coffinite. Coffinite replaces pitchblende outward from the center of the mass, and in places is more abundant than the host. Pitchblende invaded rock fragments, replacing muscovite and altered pyrite; the Fe-Mo-As sulfide is usually present as well. Both minerals pseudomorphically replace an unknown bladed vein mineral, perhaps calcite or barite. Quartz and ankerite produced a similar bladed texture in gangue at the Ladwig mine to the south.

Although the relative abundance of pitchblende is extremely small in some areas, the vein material remains very black because of the abundant submicroscopic sulfides and rock fragments. X-ray diffraction patterns of the optically amorphous, non-uraniferous black vein material have weak pyrite peaks that possibly indicate small amounts of or poorly crystallized iron sulfide. The black color and weak pyrite patterns resemble the descriptions by Downs and Bird (1965) of a ubiquitous "black pyrite."

A second major episode of brecciation followed deposition of the early pitchblende and associated minerals. Reactivation of the faults produced anastomosing breccia zones and fractures; many follow existing veins, but new, subparallel fractures cut the adjacent rocks. As with the earlier episode, fragments are angular to subrounded and of variable size. Lithologic mixing is prevalent, and virtually all pre-existing rock and vein types are represented in fragments.

Pitchblende and various gangue minerals filled the inter-



Figure 17. Photomicrograph of Stage IIa pitchblende (light gray), with minor amounts of chalcopyrite (yellow). Gangue (darker gray) includes ankerite and adularia, as well as minute rock fragments. Reflected light; bar is 0.04 mm long.

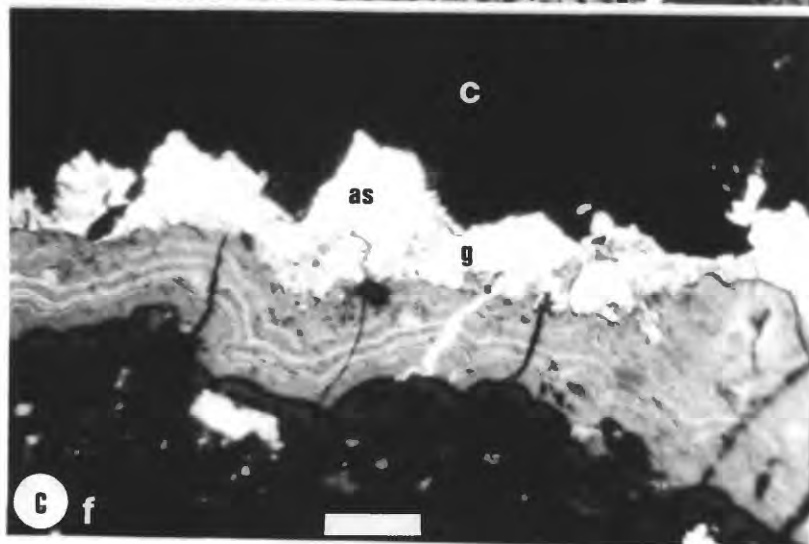
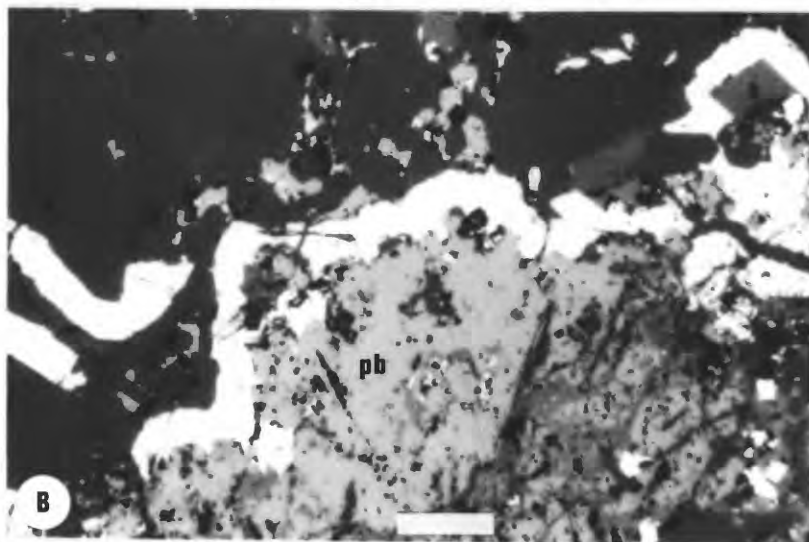
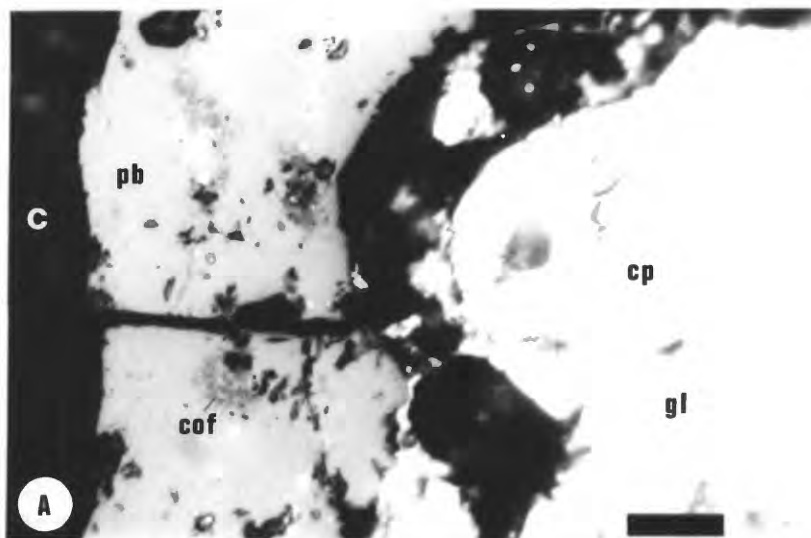
stices between breccia fragments in the reopened veins. Euhedral adularia encrusts many fragments, and was subsequently coated with pitchblende. Pitchblende, carbonates, and sulfides also precipitated directly on the fragments. Pitchblende did not form in many areas, and minerals of the subsequent sulfide-carbonate substage precipitated directly on breccia fragments. Mineralization in that episode filled the remaining voids in the veins.

Pitchblende is always colloform, regardless of whether it forms a thin encrustation or a more massive vein filling. Shrinkage cracks are usually common, although they are not ubiquitous and are of minor volume. Minor amounts of sulfides, including chalcopyrite, pyrite, galena, and the Fe-Mo-As sulfide, are disseminated throughout the pitchblende. The pitchblende may form alternating layers with the Fe-Mo-As sulfide (Figure 18a) and with dolomite. Coffinite replaces pitchblende, but is not as abundant as in the earlier substage. Pitchblende usually completely rims a fragment, but it locally coats only the upper surfaces of some fragments. Some thin veinlets have a continuous basal layer of pitchblende that is covered with dolomite.

The carbonate-sulfide assemblage filled the voids that remained after pitchblende deposition. The Fe-Mo-As sulfide, either as the homogeneous (Figure 18b) or banded phase (Figure 18c), forms a colloform coating that envelopes and fills shrinkage cracks in pitchblende. Veinlets also cut fragments and areas of the early massive pitchblende. Pyrite, chalcopyrite, galena, yellow sphalerite, and marcasite are the other major sulfide phases deposited during this substage. All are surrounded by dolomite or calcite. Tennantite replaces galena; both are replaced by minor amounts of niccolite and rammelsbergite. Arsenopyrite forms small grains in galena and carbonates. A Pb-Mo sulfide, containing Fe and minor Sb (based on semiquantitative microprobe analyses), fills microfractures and replaces galena and chalcopyrite of both Stage I and Stage II origin, thus creating thin veinlets and colloform masses. Replacement was pseudomorphic, preserving the

Figure 18. Stages IIb and IIc mineralization.

- a. Stage IIb pitchblende (pb) rimming fragment containing Stage I chalcopyrite (cp) and galena (gl). Coffinite (cof) partially replaces pitchblende. Pitchblende contains two diffuse layers of Fe-Mo-As sulfide. Carbonate (c) coats pitchblende. Dark area between fragment and pitchblende is a hole. Bar is 0.02 mm long.
- b. Fe-Mo-As sulfide (white) coating Stage IIb pitchblende and adularia (a). Pitchblende partially replaced by coffinite (darker gray). Pyrite forms bright grains in pitchblende. Pitchblende locally deposited after Fe-Mo-As sulfide. Carbonate is dark gangue coating sulfide. Bar is 0.04 mm long.
- c. Zoned FeAs(Mo) sulfide (light bands) and FeMo(As) sulfide (dark bands) coating Stage IIb pitchblende. Pitchblende forms thin layer on rock fragment (f). Galena (g) and arsenopyrite (as) coat and locally cut earlier sulfides. Major gangue is dolomite (c). Bar is 0.04 mm long.



original rim of pitchblende around the euhedral galena. Pyrite and marcasite coexist without any indication of the replacement of one by the other. They were generally the last sulfides to form in the voids.

Carbonates are volumetrically much more abundant than the associated sulfides. Textures range from fine-grained granular masses to zoned, sparry crystals protruding into the centers of the voids. Microprobe analyses of the zoned carbonates, listed in Table 14, indicate that the Fe/Mg ratio progressively decreases and the Ca/(Fe + Mg) ratio generally increases towards the center of the vein, creating a zonation of ankerite to dolomite to calcite. This trend was substantiated in several analyses of other veins. Granular varieties of carbonate consist of ankerite having Fe/Mg ratios near unity. Small grains of pyrite and chalcopyrite that formed in the troughs between euhedral dolomite crystals suggest relatively quiet, nonturbulent deposition. These sulfides, along with coarser varieties, were deposited after dolomite but prior to the final, vug-filling calcite stage.

Amethyst, chlorite, and fluorite fill fractures scattered throughout the deposit. Coarse-grained, zoned amethyst forms veins at several levels, and is cut by veinlets containing dolomite, pyrite, and galena. In addition, small euhedral crystals of quartz locally protrude into cavities from vein walls, or are intergrown with dolomite. As such, the amethyst probably formed during Stage II, but may be related to Stage I (see discussion of fluid inclusion data; Chapter 7). Chlorite, virtually absent as an alteration mineral, is present in veinlets with dolomite and adularia adjacent to the RB, Titan, and Illinois veins. The green chlorite is very fine grained, slightly granular, and is not pleochroic. Paragenetic relations with pitchblende could not be observed. Sparse crystals of purple fluorite are intergrown with late carbonates, and may belong to either Stage II or III.

Table 14. Microprobe analyses of zones carbonate in Stage II veinlet.

	<u>Vein wall</u>		<u>Vein center</u>	
	A	B	C	D
SiO ₂ %	0.00	0.00	0.00	0.06
Al ₂ O ₃	0.12	0.36	0.33	0.02
FeO	13.50	10.70	8.33	0.43
MgO	11.70	19.90	21.10	0.49
CaO	32.90	29.80	32.30	57.60
Na ₂ O	0.21	0.09	0.13	0.00
K ₂ O	0.03	0.00	0.00	0.01
TiO ₂	0.04	0.09	0.00	0.00
MnO	0.15	0.07	0.14	0.05
Total	58.64	61.03	62.28	58.64

Number of ions on basis of 6 O

Fe	1.05	0.75	0.57	0.03
Mg	1.62	2.49	2.55	0.07
Mn	0.01	0.00	0.00	0.00
Ca	3.28	2.68	2.81	5.80

Stage III Mineralogy

Stage III mineralization produced a coarse-grained calcite-sulfide assemblage that fills faults and fractures which post-date Stage II uranium mineralization. Calcite, pyrite, and marcasite comprise virtually all of the vein minerals. Chalcopyrite is present in small quantities, and silt-sized rock fragments are locally interlayered with calcite. Mineralization spanned, although not necessarily continuously, the time from the waning moments of Stage II through the development of the post-ore Illinois fault system.

Mineralization along the post-ore Illinois fault system produced two distinctive textures: (1) vuggy, coarse-grained calcite

and sulfides in dilational zones; and (2) multistage calcite and sulfides along shear zones. The two textures are locally gradational, and were controlled primarily by the local tightness of the fault opening. The multistage texture developed during repeated movement and dilation along the steeply dipping fractures, creating an anastomosing zone, several centimeters in width, of veinlets. Black, sooty pyrite lines the walls of each veinlet, and calcite fills the remaining space. Calcite and thin layers of rock dust form alternating bands in subhorizontal fractures.

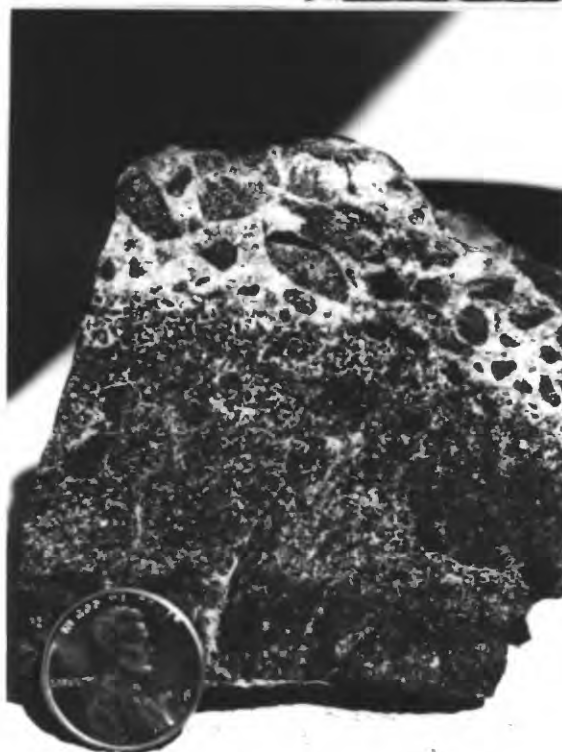
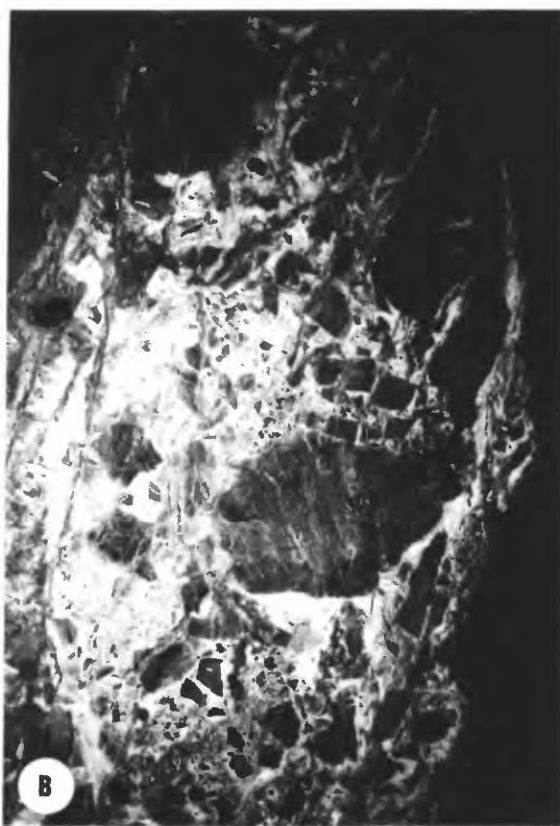
Many fractures and voids in the uranium veins and wallrocks are filled with vuggy calcite and iron sulfides that are texturally identical both to those that seal the Stage II voids and to vuggy minerals in the post-ore Illinois vein. However, fractures related to the latter fault clearly cut these veins, suggesting that there were at least two episodes of calcite-iron sulfide deposition after uranium mineralization. The earlier of the two may actually be a continuation of Stage II, but is distinguished by the absence of uranium or major sulfides other than pyrite and marcasite.

Several recurrent textures in the deposit suggest explosive brecciation and fluidized fragment transport during Stage III. The most obvious example, shown in Figure 19a, is reverse graded bedding of subrounded fragments of uranium ores in a calcite cement. Very narrow fault zones enlarge abruptly into broad zones of angular, unaltered breccia fragments (Figure 19b). Pressure release following explosive brecciation along many small fractures caused thin sheets of wallrock to spall into the vein, a feature typical of diatremes (Woolsey et al., 1975).

Pressure release and chemical corrosion combined to create diffuse areas within massive ore zones that resemble a fine-grained breccia composed of subrounded fragments of ore (Figure 19c). All such zones grade into true vein breccias, and both are cemented by calcite. The diffuse breccias gradually blend into massive ore away from the calcite vein. The fragments have two

Figure 19. Breccias produced by high-pressure fluids.

- a. Fragments of wallrocks and vein materials with a crude reverse grading. Note rounding of many fragments. Fragments cemented by calcite.
- b. Explosion breccia along Illinois fault. Fragments are rotated and unaltered. Calcite is major cement. Large fragment on right is about 60 cm in width.
- c. Pseudobreccia in ore zone created by a combination of implosion and corrosion of pitchblende by carbonate. Massive pitchblende at base; true breccia at top.



size distributions: (1) coarser fragments, up to a centimeter in width, with abundant interstitial, fine-grained fragments; and (2) a distinct gradation, usually upward, from very fine grained fragments to coarser material without any interstitial fines. Contacts of calcite with pitchblende are sharp to diffuse, whereas those with rock fragments are very distinct. Release of pressure in the vein may have caused adjacent areas to implode, thereby generating microfractures through the nearby rock. Carbonate-rich fluids possibly invaded and enlarged the cracks, dissolving some of the pitchblende and leaving intact the included wall rock fragments. Chemical corrosion may have preferentially attacked protuberances, eventually generating relatively smooth surfaces. The absence of such textures in altered and unaltered rocks may be attributable to the chemical inertness of the wallrocks and their tendency to implode as elongate sheets instead of as masses with orbicular, perlitic cracks. Dissolution of uranium is also evident where calcite, introduced along walls of uranium veins, preferentially invaded the uranium vein but not the altered wall rock.

Clastic Dikes

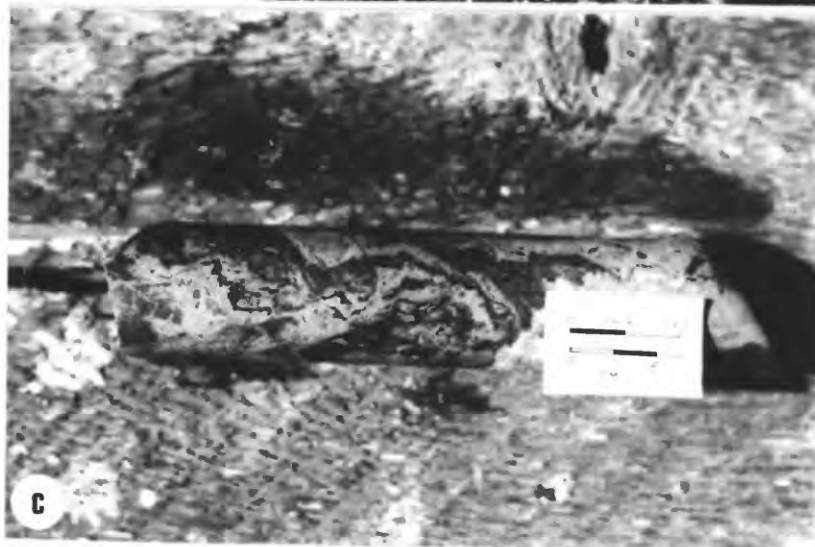
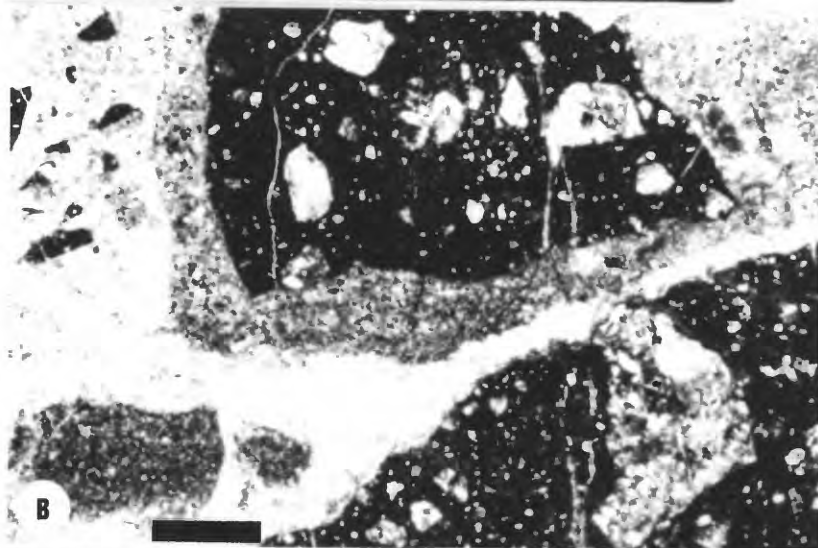
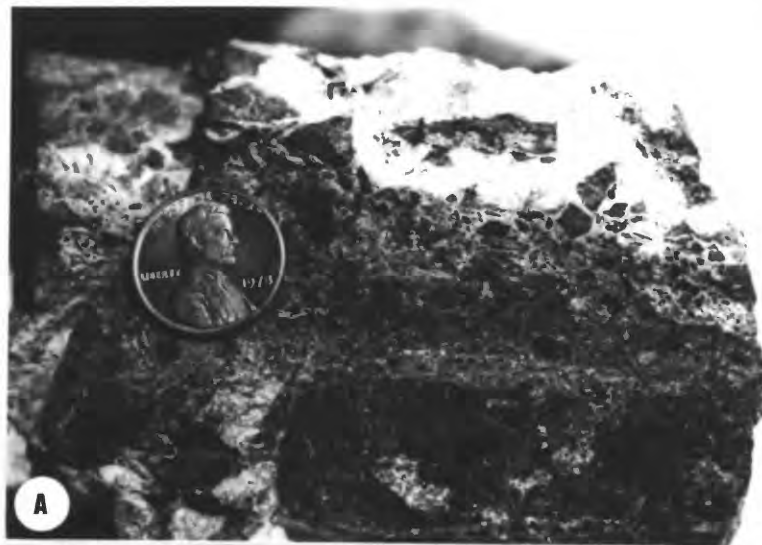
Clastic dikes invaded all veins in the deposit during two major intervals. The angular to rounded fragments are fine grained, and are composed of altered wallrocks and pre-existing vein materials. The clasts are set in a microcrystalline matrix of rock flour and are cemented by equally fine-grained carbonate and adularia. The resulting rocks are hard and brittle; some have a conchoidal fracture. The dikes vary in width from a few centimeters to a meter, and in places they may fill an entire fault zone. Contacts with adjacent rocks are distinct to diffuse. Injection was episodic, and commonly generated two or three dikes in the same zone. Some dikes are structureless, whereas others exhibit irregular layering with flowbanding of matrix and cement around the fragments.

The dikes developed during two major episodes: (1) contemporaneous with and subsequent to hematite-adularia alteration in the adjacent rocks; and (2) following uranium mineralization in Stage II. The early clastic dikes are prevalent along the footwall of the Rogers and Illinois veins but are less common along the horse-tail fractures. Extreme hematite-adularia alteration obliterated all primary textures in the adjacent rocks, generating a hard, pink- to flesh-colored aphanitic rock. This grades imperceptibly into a pink microbreccia composed of minute rounded fragments of the altered wallrock set in a microcrystalline ankerite-adularia cement. Multiple injections of microbreccia are evident, each deriving its fragments from the previous microbreccias and each being indurated by a progressively more cream-colored carbonate-adularia cement. The early pink slurries are more commonly associated with the intensely hematitized wall rocks, but subsequent clastic dikelets invade even the carbonate-sericite alteration zone. All of the identifiable rock fragments are composed of either altered wall rocks or antecedent clastic dikes; neither sulfide fragments nor lithologies exotic to the deposit and its wallrocks were observed. Many uranium veins contain breccia fragments of the pink dikes, and uranium veinlets locally transect those dikes. These features, and the association with hematite alteration, attest to a relatively early stage of dike emplacement.

Clastic dikes emplaced after Stage II uranium mineralization are polyphase and texturally similar to those formed earlier. The subrounded fragments and matrix carried in the initial phase of injection are composed predominantly of massive uranium ores. The resulting rocks, cemented by carbonate and lesser amounts of adularia, are dark gray (Figure 20a) and, depending upon the abundance of ore fragments and matrix, are locally of mineable grade. Compositions of other fragments include altered wall rocks, pyrite, and chalcopyrite. The contacts between the gray dikes grade imperceptibly, over the span of several centimeters, from distinct breccia into massive uranium ores, implying some re-

Figure 20. Clastic dikes.

- a. Dark clastic dike containing black fragments of massive pitchblende. Dike was rebrecciated and cemented by carbonate (white).
- b. Multiple clastic dikes. Early dark dikes contain more fragments and are cemented by finer-grained ankerite than the subsequent dike. Last episode produced dolomite cement. Bar is 0.40 mm long.
- c. Complexly banded dark and pink (light) fault gouge. The texture is in part a primary injection feature and in part a product of post-injection fault movement.



placement during intrusion.

Subsequent clastic dikes are pale green to cream-colored, and cut both the uranium ores and the antecedent dikes. The cream-colored dikes are texturally and mineralogically identical to the late dikes of the pre-ore episode, and the lack of cross-cutting relationships does not preclude contemporaneity. At least two cream-colored clastic dikes were emplaced after the gray uranium-bearing dikes. The cements of both are slightly more coarse-grained than in the preceding dike, and contain progressively fewer fragments (Figure 20b). Microprobe analyses of the cements in two successive dikes indicate that the ankerite becomes somewhat more calcic and magnesium-rich (Table 15). The last clastic dike was locally rebrecciated and cemented by relatively coarse dolomite, perhaps heralding carbonate deposition in Stage II or incipient Stage III mineralization. The contacts of most pale-colored dikes are well-defined. However, several pale green dikes cut and grade into intensely sheared wall rocks that have been altered to the carbonate-sericite assemblage. Proterozoic sphalerite, preserved in the altered rocks, is locally incorporated into adjacent clastic dikes. Most lithic fragments were derived from altered rocks, and fragments of uranium-bearing rocks are notably sparse or absent, even where the dikes cut those rocks. In addition, many dikes in veins devoid of associated hematite alteration can contain abundant fragments of hematized rock. In contrast to fragments in the uranium-bearing dikes, those in the light-colored dikes were apparently derived from sources other than adjacent rocks.

Clastic dikes containing fragments of uranium ore were noted along the Illinois vein below the 12th level and on horsetail veins as high as the 6th level. A gray dike is exposed along the distal ends of the Illinois vein on the 13th level, but increases in strike length with depth to the 15th level at the expense of the ore zone. Primary ore did not form below the 16th level along the Illinois vein, and the gray dikes are not present

Table 15. Microprobe analyses of carbonate cement in successive light clastic dikes.

	<u>Early clastic dike</u>		
	<u>1</u>	<u>2</u>	<u>3</u>
SiO ₂ %	0.17	1.19	0.25
Al ₂ O ₃	0.19	0.24	0.02
FeO	10.10	11.19	15.80
MgO	13.50	14.90	15.13
CaO	28.30	28.94	28.79
Na ₂ O	0.12	0.22	0.04
K ₂ O	0.16	0.29	0.08
TiO ₂	0.04	0.06	0.01
MnO	0.51	0.80	1.09
Total	53.15	57.83	61.19

Numbers of ions on basis of 6 0

Fe	0.84	0.84	1.16
Mg	2.01	2.00	1.98
Ca	0.04	0.06	0.08

* * * * *

	<u>Later clastic dike</u>	
	<u>1</u>	<u>2</u>
SiO ₂	0.18	0.23
Al ₂ O ₃	0.17	0.04
FeO	0.66	7.39
MgO	17.80	16.30
CaO	34.70	31.40
Na ₂ O	0.10	0.09
K ₂ O	0.08	0.08
TiO ₂	0.00	0.06
MnO	0.65	0.41
Total	63.35	56.04

Number of ions on basis of 6 0

Fe	0.66	0.57
Mg	2.18	2.24
Ca	3.05	3.09

below that level. This association indicates a close spatial, and probably genetic, relationship between the two. The cream-colored clastic dikes have a similar distribution, but continue below the 16th level, and comprise the entire vein filling in lower levels. The cream-colored breccia also fills the Rogers vein below the level of uranium mineralization in that system. The post-ore Illinois fault is notably devoid of any clastic dikes.

Effects of Fault Movement on Ores

Episodic movement along all of the faults in the deposit continually produced new conduits for invading hydrothermal fluids, as described in the previous pages. At the same time, fault movement destroyed or modified textures and minerals in existing veins. Furthermore, development of the post-ore Illinois fault system displaced several of the horsetail veins and disrupted mineralized sections of the pre-ore Illinois fault.

Post-ore movement along the Rogers and Illinois faults was much more destructive than that along the horsetail fractures. Most original vein materials were dragged and smeared, locally beyond recognition. Larger fragments in the clastic dikes apparently rolled as the matrix blended and flowed around them, and plastic deformation and flow of the matrix produced unusual banded textures (Figure 20c).

Movement along the horsetail fractures was generally brittle and non-destructive, and produced local breccias and planar shears parallel to and within the veins. As a result, the original vein textures remain relatively intact. Movement along the planar shears was episodic but usually of Stage III or later origin. They truncate the dark gray clastic dikes and the vertical multi-stage calcite veinlets of Stage III. The shears commonly define the upper surface of a vein, juxtaposing vein material and altered or unaltered wall rocks.

The anastomosing post-ore Illinois fault system sliced off

several horsetail veins, most notably the 17-1 vein, and displaced them down a hundred or so meters (Wright, 1980). In doing so, ore from the horesetail veins was dragged into the post-ore Illinois fault. The open fracture also serves as a free-flowing water-course, and uranium in veins truncated by the fault has been leached near the conduit.

Bottom of the Ore Deposit

The Illinois fault between the 15th and 17th levels changes from a five-meter-wide zone with good ore grades to a much narrower structure without any detectable uranium mineralization. The vein materials on the 15th and higher levels were disrupted by subsequent fault movement, but clearly formed in place and probably with textures similar to those along the horsetail fractures. In contrast, the dominant vein materials on the 17th and lower levels are light-colored clastic dikes. The footwall of the vein on the 16th level contains some structurally disturbed ore, but most of the meter-wide structure, including parts of the footwall, contains unmineralized breccia and light clastic dikes. As noted previously, the gray clastic dikes become more prevalent below the 13th level, but do not extend below the lowest level of hypogene uranium mineralization. Despite the downward demise of mineralization, a narrow but persistent carbonate-sericite alteration halo envelopes the vein to at least the 19th level.

The 17-1 vein intersects the Illinois between the 16th and 17th levels (Figure 2). On the 16th level above the intersection, the structure is less than a meter wide and contains light clastic dikes. The distribution of uranium mineralization in the vein is erratic; grades are usually subeconomic. However, mineralization at higher levels along the vein contains abundant primary ore. Regardless of the grade of ore, the surrounding rocks are altered to at least the carbonate-sericite assemblage.

Exploratory drilling into the Rogers vein system indicates

that uranium mineralization ceases somewhat below the 21st level. Some structures in the hangingwall region contain ore at slightly lower levels, but the drilling does not indicate if the ore is primary or was subsequently displaced by faulting to lower levels in the manner of the 17-1 vein. Textures and alteration along the vein closely resemble those seen in the equivalent zone along the Illinois vein. Drilling from the surface indicates that the Rogers vein is apparently unmineralized in the upper levels. Surface exposures of the vein are devoid of any mineralization, although thermoluminescence studies indicate that seemingly barren surface exposures of the Illinois fault were once mineralized and subsequently leached (Charles Spirakis, personal communication, 1980). Therefore, it is not possible at this point to determine if the Rogers vein has been leached of uranium that once extended to the present surface.

Supergene Processes

Inaccessible workings precluded access to most of the upper levels of the deposit, and the effects of supergene processes along uranium veins in those areas could not be studied. Derzay and Bird (1957), Sheridan et al. (1967), Heyse (1972), and Honea and Ferris (unpub. report) each provide a detailed description of the vein mineralogy of the upper levels, a brief summary of which follows.

Supergene processes along the uranium veins did not extend below the Steve (1st) level, and complete alteration of the pitchblende to secondary minerals was limited to within ten meters of the surface. Vein outcrops contain numerous secondary copper and uranium minerals. Copper, uranium, iron, and sulfur were transported down the veins, eventually producing sooty pitchblende, marcasite, bornite, chalcopyrite, covellite, and various minor minerals.

Sulfur isotope analyses of marcasite in the calcite-iron sul-

fide veins of the post-ore Illinois fault system indicate a supergene origin for the marcasite (Jensen et al., 1960; Heyse, 1972; J. Whelan, unpubl. data). Sulfur isotope ratios range from -18.0 to -40.5 per mil, typical for an iron sulfide precipitated from low-temperature, oxygenated water (Faure, 1977). The age of this supergene event is unknown. However, late movement along shears in the horsetail veins truncated fractures related to the post-ore Illinois fault system. As a result, the supergene event responsible for the calcite-marcasite assemblage is probably unrelated to modern, near-surface supergene processes, and may reflect Tertiary mineralization after Laramide ore deposition.

Trace Elements

Samples collected from underground exposures and diamond drill cores of the Rogers, Illinois, RB, 17-1, 18-1, and A-bed veins and the clastic dikes were analyzed for 47 trace elements. All analyzed vein materials are grab samples from the ore zone, as determined with calibrated scintillometers, regardless of the grade of ore. All vein materials sampled contained a heterolithic suite of rock fragments, as well as the products of one or more periods of mineralization. As a result, none of the samples represent a single episode of ore deposition. Mine access and the locations of drill hole intercepts dictated sample sites. The results of all analyses are listed in Appendix A and are summarized in Table 16.

A correlation matrix for each vein system was generated, using twelve elements, to determine which pairs of elements in each vein had good correlations. The elements included U, Mo, As, Ag, Cd, Co, Bi, F, Hg, Sb, Ni, and Tl, and were selected partly at random but largely for comparison with previous geochemical studies (Heyse, 1972; Young, 1979a). In addition, correlation coefficients were calculated for U versus Pb, Cu, Zr, S, and organic C. Correlation matrices are listed in Table 17. In the

Table 16. Summary of trace element concentrations for horsetail, Illinois, and Rogers veins. Complete data set in Appendix A, Tables A3-A5.

No. samples	Horsetail Veins		Illinois Vein		Rogers Vein	
	13		9		9	
	Mean	±	Mean	±	Mean	±
Ag (ppm)	26.30	30.60	*6.50	4.20	*12.70	8.90
As	124	102	61.40	43	44.40	34.30
B	N	—	N	—	N	—
Ba	116	53	147	70	259	294
Be	*1.80	1.40	1.94	1.16	*2.94	2.88
Bi	1.50	2.60	*3.22	3.36	0.29	0.13
Cd	2.54	2.20	*1.82	0.93	2.64	4.73
Co	45.50	58.90	20.20	5.60	22.20	14.90
Cr	40.00	29.90	67.20	41.00	33.30	21.10
Cu	494	855	432	967	147	76
F	215	99	267	235	378	466
Ga	*8.46	4.30	12.80	2.60	*9.44	5.27
Hg	4.43	6.00	0.30	0.29	0.82	0.56
La	N	—	N	—	N	—
Mo	3668	3043	583	739	1580	1337
Nb	L	—	*10.60	1.67	*11.70	3.50
Ni	64.60	53.60	42.60	17.20	42.30	29.30
Pb	4285	5383	629	971	1974	1666
Sb	166	166	*78.40	93.80	69.40	75.60
Sc	*7.77	3.68	15.20	4.50	8.56	2.24
Sr	149	79	149	71	223	177
Th	*4575	9030	*652	878	*1000	917
Tl	27.50	17.00	*5.33	5.12	*4.33	2.99
U	8664	8412	2154	2762	4547	4079
V	327	196	280	176	341	216
Y	*23.50	15.70	19.40	4.64	18.90	10
Yb	*1.65	0.85	2.00	0.66	N	—
Zn	239	543	237	226	367	620
Zr	83.80	72.60	72.20	47.40	80	37.70
W	N	—	N	—	N	—
SZ	1.14	1.03	0.42	0.36	NA	—
CZ inorg.	4.17	2.41	5.08	0.77	NA	—
CZ org.	0.66	0.70	0.47	0.21	NA	—

*Maximum value only: samples with concentrations below detection limits were calculated on basis of value of detection limit.

N: not detected

L: detected but at concentrations below accurate detection limit

NA: not analyzed for.

Table 17. Correlation matrices for trace elements from the horsetail, Illinois, and Rogers vein systems.

U	1.000											
Mo	0.873	1.000										
As	0.847	0.856	1.000									
Ag	0.516	0.766	0.816	1.000								
Co	0.463	0.739	0.767	0.970	1.000							
Ni	0.446	0.790	0.722	0.933	0.934	1.000						
F	0.466	0.271	0.413	0.083	0.110	0.032	1.000					
Bi	-0.138	-0.008	-0.123	-0.146	-0.017	0.062	-0.373	1.000				
Cd	0.188	-0.141	-0.160	-0.165	-0.234	-0.264	0.312	-0.203	1.000			
Sb	0.929	0.943	0.894	0.689	0.627	0.688	0.415	-0.128	0.124	1.000		
Tl	0.685	0.624	0.433	0.325	0.273	0.270	0.145	-0.120	-0.205	0.648	1.000	
Hg	0.761	0.790	0.820	0.755	0.772	0.606	0.346	-0.220	-0.129	0.699	0.474	1.000
	U	Mo	As	Ag	Co	Ni	F	Bi	Cd	Sb	Tl	Hg

Horsetail Veins

U	1.000											
Mo	0.574	1.000										
As	0.595	-0.023	1.000									
Ag	0.949	0.414	0.778	1.000								
Co	-0.304	-0.281	-0.310	-0.301	1.000							
Ni	-0.191	-0.079	-0.341	-0.156	0.836	1.000						
F	0.277	-0.266	0.208	0.243	0.310	0.207	1.000					
Bi	-0.367	-0.112	-0.140	-0.242	0.528	0.657	-0.227	1.000				
Cd	0.460	0.071	0.400	0.392	0.245	0.024	0.609	0.081	1.000			
Sb	0.809	0.151	0.865	0.914	-0.260	-0.227	0.346	-0.143	0.512	1.000		
Tl	0.446	0.806	-0.224	0.184	-0.030	0.014	0.085	-0.143	0.417	-0.042	1.000	
Hg	-0.128	0.435	-0.120	-0.193	-0.199	-0.345	-0.539	0.212	0.039	-0.102	0.287	1.000
	U	Mo	As	Ag	Co	Ni	F	Bi	Cd	Sb	Tl	Hg

Illinois Vein

U	1.000											
Mo	0.574	1.000										
As	0.167	0.510	1.000									
Ag	0.882	0.705	0.406	1.000								
Co	0.557	0.428	0.175	0.687	1.000							
Ni	0.663	0.816	0.573	0.896	0.675	1.000						
F	0.096	0.620	0.453	0.305	0.153	0.643	1.000					
Bi	-0.143	-0.089	0.085	-0.189	-0.274	-0.153	-0.108	1.000				
Cd	0.316	0.626	0.611	0.546	0.097	0.759	0.858	0.045	1.000			
Sb	0.279	0.909	0.690	0.488	0.228	0.730	0.772	-0.014	0.735	1.000		
Tl	0.666	0.857	0.331	0.665	0.356	0.604	0.166	0.074	0.287	0.662	1.000	
Hg	0.760	0.468	0.311	0.770	0.709	0.620	-0.080	0.241	0.147	0.251	0.650	1.000
	U	Mo	As	Ag	Co	Ni	F	Bi	Cd	Sb	Tl	Hg

Rogers Vein

horsetail veins, most pairs in the U-Mo-As-Hg-Sb and Ag-Co-Ni suites correlate well, as do those of U-Pb, U-S, and U-Zr. In contrast, relatively few pairs of elements have significant correlation coefficients in the Illinois and Rogers veins. Four pairs (U-Sb, As-Sb, Co-Ni, and U-Zr) are significant in both the horsetail and Illinois veins, and only two (U-Ag, Mo-Tl) are prevalent in both the Rogers and Illinois systems. None are common to all three vein systems. Correlation coefficients for U-organic C are -0.079 and 0.023 for the horsetail and Illinois veins, respectively. Based upon samples collected from the horsetail and Illinois veins above the 7th level, Heyse (1972) found significant correlations between U and Tl, Sb, and Mo, and between Co and Ni. Analyses reported by Young (1979a) indicate elevated concentrations of Mo, Sb, Ag, Pb, and W in high-grade samples of ore. Although only one sample collected for the present study contained detectable amounts of W, Young's analyses indicate up to 7000 parts per million (ppm) W in samples containing 500,000 ppm U. Furthermore, minor amounts of Sn appear in analyses of ore-grade samples reported by Heyse (1972).

Cluster analysis and R- and Q-mode factor analysis were performed on each vein to determine which, if any, elements characterized each vein. Cluster analyses graphically demonstrates which pairs and groups of elements are strongly correlated and therefore distinguish the population. R-mode analysis investigates the interrelationships between the elements. Q-mode analyzes those between samples, using the elements in each sample (Davis, 1973).

Cluster analysis for the horsetail veins (Figure 21a) indicate two suites of elements, Ag-Co-Ni and U-Mo-Sb-As-Hg, with significant correlations. All eight elements dominate Q- and R-mode analyses. Cluster analysis of the Illinois vein (Figure 21b) shows four significant pairs of elements: U-Ag, As-Sb, Mo-Tl, and Co-Ni. The suites U-As-Sb-Ag and Co-Ni control factor analysis, although variance is spread evenly over several factors.

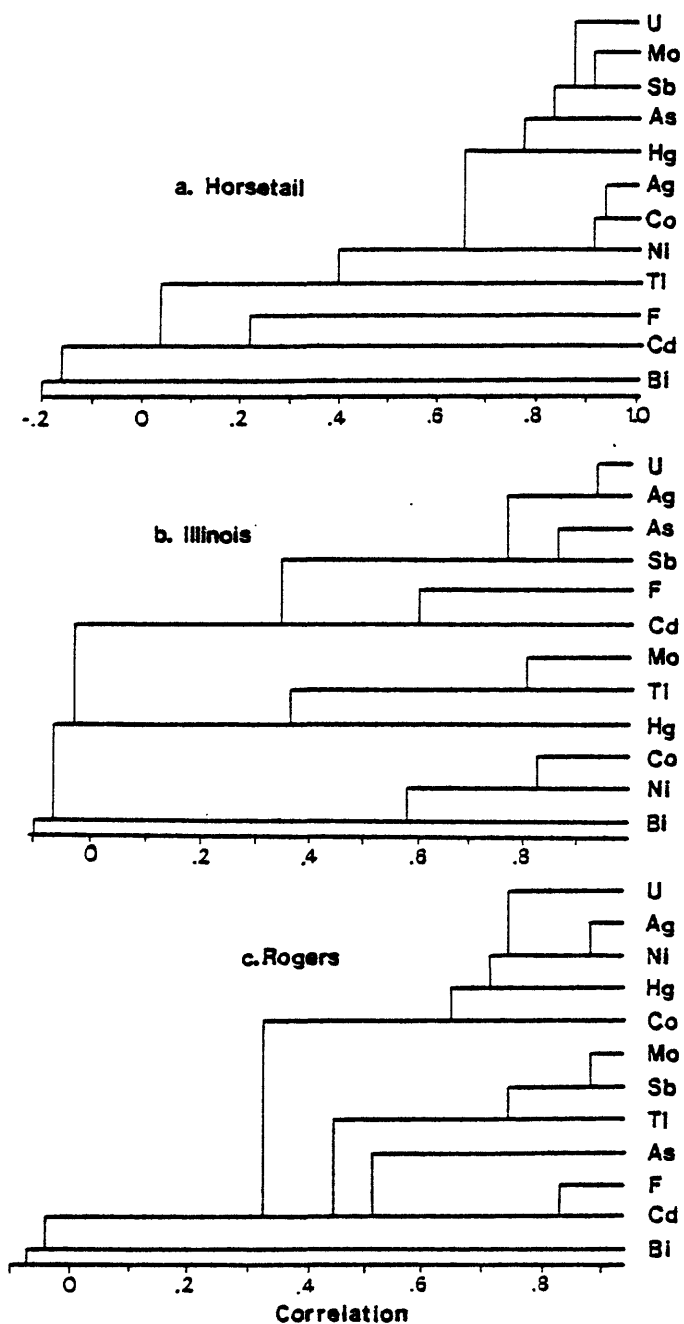


Figure 21. Cluster analyses of trace elements from the (a) horsetail, (b) Illinois, and (c) Rogers vein systems.

Cluster analysis for the Rogers vein (Figure 21c) has three pairs, Ag-Ni, Mo-Sb, and F-Cd, with significant correlations. Variance in Q- and R-mode factor analyses is distributed evenly over many factors, which are weakly influenced by the suites Co-Ni-F, Mo-Cd-Sb, As-Bi, and U-Ag.

Concentrations of Ag, As, Co, Hg, Mo, Pb, Sb, Th, Tl, and U are significantly greater in the horsetail fractures than in the Rogers and Illinois veins (Table 16). The latter two systems have a strikingly similar geochemical signature. In comparison with altered and unaltered wall rocks (Table 13), concentrations of Ag, As, inorganic C, Cu, Hg, Mo, Sb, Th, and U increased in all veins, whereas those of B, F, and Ga decreased. Organic C, Sc, Yb, and Zr have similar concentrations in all rocks and veins, and the values for vein Sr fall between those for altered garnet-biotite gneiss and hornblende gneiss, reflecting the preponderance of Ca associated with carbonates. With the exception of the horsetail veins, the Co/Ni ratio for all veins and altered and unaltered wall rocks is consistently between 0.47 and 0.53; a slight increase in Co in the horsetail veins raised the ratio in that system to 0.70.

Concentrations of the elements do not show any consistent change with elevation for the vertical interval sampled. When the 17-1 is reconstructed from its offset segments, U and several associated elements show a progressive increase upwards. However, ore grades for the vein as a whole do not increase upwards (R. C. Karlson, 1981, personal communication), so the observed trace element trend is instead an artifact of the U content of the particular samples. When normalized to constant U, none of the elements shows a consistent change with elevation. Thallium is the only element whose concentration increases upward in the 17-1 vein, but the trend is not repeated along any other vein. Heyse (1972) reported a similar lack of vertical change for element concentrations in the upper levels of the deposit.

A chemical analysis of one of the dark clastic dikes shows

some preservation of the U-Mo-volatile suite of the uranium veins (Table 18). Sample 80S21, collected from a cream-colored dike that cuts the gray dike (80S20), has very small concentrations of most trace elements, including U and volatile elements. Other light-colored clastic dikes have similar weak chemical signatures.

The results of the trace element and statistical analyses demonstrate that the horsetail vein system has a distinct chemical signature, whereas the Illinois and Rogers veins have different and less distinct chemical characteristics. Two suites of elements characterize the horsetail veins. One includes U, Mo, and the volatile elements As, Hg, and Sb; the other includes Ag, Co, and Ni. In addition, Pb, S, and Zr are closely associated with U. Many of the same elements weakly characterize the Illinois and Rogers veins, but the relationship between U and the volatile elements is much less distinct. Movement along the Rogers and Illinois faults destroyed many of the original ore textures, and undoubtedly influenced the primary correlations between elements. In contrast, ores along the horsetail veins survived fault movement relatively intact, as reflected by the strong correlations between many elements. The excellent correlation between U, Mo, and As clearly reflects the ubiquitous association of pitchblende and the Fe-Mo-As sulfide in the horsetail veins. The latter mineral is much less common in the disturbed Illinois and Rogers veins, and the relatively poor trace element correlations reflect its dissociation from pitchblende. The persistence of the Co/Ni ratio in wallrocks and veins may reflect the influence of brecciated wallrock in the veins, despite the presence of minor hydrothermal Ni minerals in the veins.

Table 18. Trace element data for gray, light-colored, and pink clastic dikes.

	Gray	Light				Pink	
	80S20	80S21	80S50	80S94	80S100	80S111	80S113
Ag (ppm)	2	<5	<5	<5	<5	<5	<5
As	30	7	70	10	20	<1	1
B	N	N	N	N	N	N	N
Ba	150	150	100	150	70	500	30
Be	N	N	L	L	N	L	L
Bi	0.70	5	<.20	<.20	<.20	<.20	<.20
Cd	1.50	1	.70	.20	.50	.50	.30
Co	14	8	20	16	13	7.90	12
Cr	15	50	70	50	70	30	70
Cu	50	10	10	5	100	20	7
F	100	100	200	200	100	100	<100
Ga	7	7	5	15	10	10	10
Hg	0.20	0.03	.02	.03	.06	.05	.03
La	N	N	L	N	N	N	N
Mo	384	35	6	<5	110	69	6.60
Nb	N	N	N	L	N	L	L
Ni	20	16	35	16	48	11	16
Pb	100	30	20	N	70	70	N
Sb	15	1.50	7	2	20	50	1
Sc	5	10	20	10	10	10	15
Sr	70	100	70	150	200	300	200
Th	<470	<4.80	<2.60	<6.40	<6.20	<26	<7.20
Tl	7	<1	<1	<1	<1	<1	<1
U	1560	6.50	3.40	5.31	22.20	114	21.20
V	100	100	150	150	300	150	200
Y	10	15	15	20	15	15	20
Yb	1.50	1.50	1.50	2	2	2	2
Zn	50	50	50	50	100	70	50
Zr	30	20	50	70	30	30	70
W	N	N	N	N	N	N	N
SZ	0.05	0.02	0.30	NA	NA	NA	NA
C inorg. %	6.25	7.46	5.07	NA	NA	NA	NA
C org. %	0.32	.18	.17	NA	NA	NA	NA

N: not detected

L: present but below detection limits

NA: not analyzed for

CHAPTER 6. AGE OF MINERALIZATION AND TECTONIC IMPLICATIONS

Uranium-lead, potassium-argon, and fission-track methods of dating were employed by several investigators in various attempts to determine the age of uranium deposition at the Schwartzwalder and related deposits. Although only the U-Pb method yielded accurate mineralization dates, the data from the fission-track dating provided information regarding Laramide uplift of the region. Attempts were made to date vein adularia, but all samples were contaminated by Proterozoic potassium feldspars and produced anomalous ages of 175 to 709 m.y. (Marvin and Dobson, 1979).

The results of the U-Pb age dating demonstrate that the Schwartzwalder and nearby Mena deposits formed 70-73 m.y. ago (Sheridan et al., 1967; K. R. Ludwig, written communication, 1982). Ludwig, using replicate ore samples collected from the Titan vein at the Schwarzwald mine, generated U-Pb isochrons corresponding to an age of 70.6 ± 3.2 m.y. A sample of pitchblende from the Mena mine produced an age of 73 ± 5 m.y. (Sheridan et al., 1967). Both suites used hydrothermal galena from the respective deposits for a common lead correction. Analyses of three samples collected from above the 5th level at the Schwartzwalder mine yielded ages ranging from 18-76 m.y. using galena for the common lead correction, and from 82-381 m.y. using average crustal common lead (Heyse, 1972). In comparison with this disparity of ages, the results of the other two suites are both internally consistent and reach a remarkably similar age for mineralization. Therefore, an age of 70-72 m.y. is the most reasonable time at which the uranium deposits formed.

Apatites from four samples of fresh and altered wall rock adjacent to the 9x1 vein were collected by Charles W. Naeser of the U.S. Geological Survey and dated using the fission track method (Naeser, 1978). Two other samples were collected for the present study, one from a Proterozoic pegmatite 2 km southeast of the Schwartzwalder mine, and the other from a Proterozoic felsic

gneiss in Golden Gate Canyon, 2 km west of the range front and 10 km southwest of the mine. Apatites from the Schwartzwalder mine yielded ages of 59.4 to 68.9 m.y., with an average age of 63.1 ± 2.2 m.y. (Marvin and Dobson, 1979). Ages from the other two samples were 63.9 and 109 m.y., respectively.

Fission tracks in apatite are completely annealed when heated to 105°C for millions of years, and provide ages indicative of subsequent cooling below that threshold temperature (Naeser, 1978). Because the apatites described above are from Proterozoic rocks, the Late Cretaceous and early Tertiary apparent ages indicate that they were subjected to elevated temperatures and then cooled approximately 63 m.y. ago. The somewhat older age of the Golden Gate Canyon apatites probably reflects incomplete annealing due to lower temperatures (Naeser, 1978).

Two thermal events could have caused the inferred annealing: (1) hydrothermal activity and concomitant district-wide increased heat flow, or (2) burial to below the 105°C isotherm during Mesozoic sedimentation, with exhumation during Laramide uplift. The uranium deposits formed 70-72 m.y. ago at temperatures in excess of 150°C (Chapter 7). Presuming that hydrothermal activity lasted for 1-3 m.y. (Silberman et al., 1979), all fission tracks in apatites next to the 9x1 vein should have annealed and produced ages indicative of subsequent cooling of the system (Naeser and Faul, 1969) or of later uplift if the isotherm was above the deposit. However, neither of the other two samples was in such close proximity to a hydrothermal system, and similar scenarios cannot explain their relatively young ages. Therefore, hydrothermal activity alone may not have been responsible for the annealing.

Although regional upwarping to the west caused the northeastward retreat of the Late Cretaceous sea approximately 67.5 m.y. ago (Tweto, 1975), the major uplift of the core of the Front Range took place 65 m.y. ago (Bryant and Naeser, 1980). Uranium mineralization clearly accompanied repeated major fault movement in the basement along the range front 70-72 m.y. ago. However, the ear-

liest stratigraphic evidence of uplift along the range front is an erosional unconformity in the Maastrichtian Arapahoe formation near Golden, where underlying sedimentary rocks were locally rotated 15-20° and eroded prior to subsequent deposition (Weimer and Tillman, 1980). Because most of the orogenic sedimentary units along the range front near Golden do not show evidence of early rotation or truncation, Tweto (1975) surmised that the early range front was several tens of kilometers west of its current position, and migrated eastward with further uplift of the Front Range.

It is therefore apparent that the site of uranium deposition 70-72 m.y. ago lay beneath the complete and uneroded cover of Mesozoic sedimentary rocks as well as the Cretaceous sea. The unconformable contact between the Proterozoic basement and overlying Pennsylvanian sedimentary rocks was no more than 100 m above the present top of the deposit (Sheridan et al., 1967), and the thickness of the sedimentary section from the unconformity to the top of the pre-uplift marine sedimentary rocks was about 3.1 km (Scott, 1972). Prior to uplift, apatite samples from the Schwartzwalder mine lay at a depth of about 3600 m, and the sample from the pegmatite at a depth of 3200 m. If burial alone caused annealing of the apatites in the pegmatite, the geothermal gradient must have been at least 33°C/km in order to produce the 105°C isotherm at a depth of 3200 m. A relatively high heat flow was necessary to heat the hydrothermal fluids to temperatures in excess of 200°C (Chapter 7), so this minimum geothermal gradient is probably not unreasonable. Furthermore, contemporaneous igneous activity in the Colorado mineral belt, some as close as 16 km to the west (Taylor, 1975), implies addition of heat to the upper crust as well as an increased thermal gradient in the lower crust to produce the magmas (Simmons and Hedge, 1978). A similar situation exists in northern Nevada, where a deep crustal magma is responsible for thermal gradients of up to 64.3°C/km over a relatively large surface area (Sass et al., 1971). As a result, the 63-64 m.y. anneal-

ing dates for samples from the pegmatite and the Schwartzwalder mine probably reflect the age of uplift past the 105°C isotherm, which is in agreement with other evidence of early Paleocene uplift of the range front (Hoblitt and Larson, 1975; Weimer and Tillman, 1980).

The slightly older age of the sample from Golden Gate Canyon is problematical because it supports neither hydrothermal annealing nor burial beneath the isotherm. If the Schwartzwalder deposit was produced as a result of a large thermal anomaly beneath the deposit, the apatites in the Golden Gate Canyon area might not have been affected by it. However, numerous uranium deposits surround the latter sample and, to be consistent, these also should have formed as the result of a local thermal anomaly which would have annealed the apatite. Additional work clearly needs to be done to resolve the problem, both in the Golden Gate Canyon area and the region in general.

CHAPTER 7. GEOCHEMISTRY OF ALTERATION AND VEIN MINERALIZATION

The mineral assemblages in the veins and alteration zones, together with fluid inclusion and stable isotope data, define the general chemical environment during hydrothermal mineralization. The extremely fine-grained size of all materials and the destructive effects of synchronous and subsequent tectonic activity have precluded detailed stable isotope and fluid inclusion studies. As a result, the estimates of some temperatures and of the concentrations of several components were necessarily subjective. However, the results of these independent studies are reasonably consistent, and provide a general estimate of the existent processes.

Estimates of Pressure and Temperature

An important, but unknown factor is the temperature during alteration. Alteration is uniform throughout the 900 vertical meters of exposed workings, which suggests that the temperature did not vary substantially throughout that interval. Studies of modern geothermal systems (Browne and Ellis, 1970; Ellis, 1979) indicate that, with increased depth, the temperature increases rapidly to above 200°C and then remains relatively constant in the deeper portions of the system. A uniform temperature would be expected because the present top of the deposit was at least 3 km below the paleosurface. Carbonate is a common alteration product at temperatures from below 100°C (Barnes et al., 1973) to above 280°C (Coveney, 1981). Siderite is very stable at low temperatures, but geologically unreasonable CO₂ fugacities are required to form that mineral above 250°C (Figure 22). Adularia is usually deposited at temperatures exceeding 200°C (Browne and Ellis, 1970; Hoagland and Elders, 1978) but it may also form between 100° and 150°C (Weissberg, 1969). Therefore, the mineralogy suggests that a temperature range of 175°-225°C is probably a

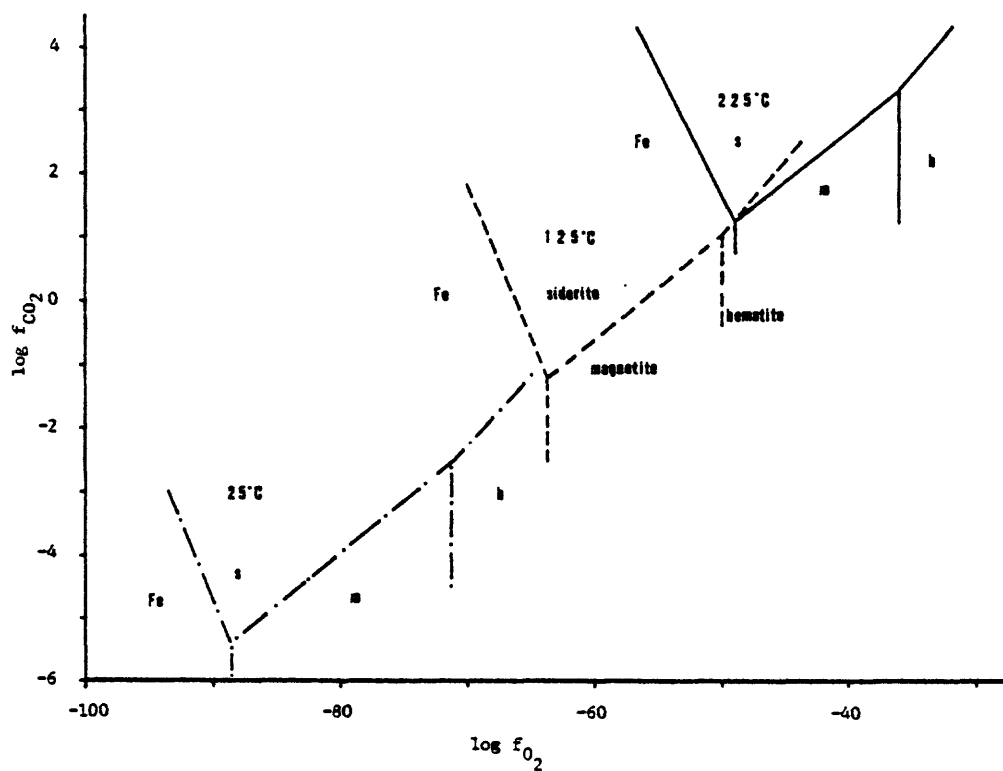


Figure 22. $\log f(\text{CO}_2)$ - $\log f(\text{O}_2)$ diagram showing the stabilities of iron-bearing minerals at 225°, 125°, and 25°C. Calculated from data in Robie et al. (1978) and Helgeson et al. (1978).

reasonable estimate for the temperature during alteration.

Standard and doubly polished thin sections of vein minerals from all paragenetic stages were examined for fluid inclusions. However, very few inclusions were found due to the fine-grained textures and to the relative scarcity of non-opaque minerals in some stages. Inclusions suitable for study were detected in Stage I sphalerite, Stage IIc(?) dolomite, and amethyst. Rich and Barabas (1976) observed extremely small inclusions in adularia associated with pitchblende, but none were seen during the course of this study.

Fluid inclusions in all samples are small (1-5 microns), and contain either one (liquid) or two (liquid and vapor) aqueous phases at room temperature. Vapor bubbles occupy 10-20 percent of the inclusions. Daughter minerals or evidence of boiling (coexisting liquid- and vapor-rich inclusions; Roedder, 1972) were not observed. Crushing stage tests did not indicate any CO_2 under pressure in the inclusions.

Uncorrected filling temperatures for inclusions in Stage I sphalerite range from 155°-210°C, and those in dolomite and amethyst from 98°-152°C, as listed in Table 19. Fluid inclusions in ore-stage adularia did not homogenize by heating to 160°C (Rich and Barabas, 1976). The salinity of the fluids in amethyst and dolomite was approximately 9.1 equivalent weight percent NaCl, based upon the conversion of freezing-point depression to salinity of Potter et al. (1978).

Reconstruction of the stratigraphic section indicates that the top and bottom of the present orebody were at depths of approximately 3200 to 4200 m, respectively, at the time of mineralization. These correspond to lithostatic pressures of 770-1000 bars ($d=2.4 \text{ g/cm}^3$), and hydrostatic pressures of 320-420 bars. Many of the fractures were open, and pressures may have been intermediate between lithostatic and hydrostatic (Robinson and Ohmoto, 1973). The pressure correction on filling temperatures for inclusions containing 10 percent NaCl is approximately 50°C in the

Table 19. Composite Fluid Inclusion Data, Schwartzwalder Mine.

Stage	Mineral	Level	Filling Temperatures (°C)			Salinity (wt. % NaCl)		
			No. inclusions	Range	Median	No. inclusions	Range	Median
I	Sphalerite	16	4	155-210	175	-	-	-
(?)	Amethyst	4	2	98-137	118	2	9.1	9.1
(?)	Amethyst	7	3	116-122	120	2	9.2-9.5	9.4
(?)	Amethyst	10	4	111-125	118	3	8.3-9.8	9.1
(?)	Dolomite	7	1	152	152	1	10.1	10.1

pressure range of 500–750 bars (Lemmllein and Klevtsov, 1961). Therefore, the true trapping temperature was 225°C during Stage I and 168–205°C for inclusions in amethyst and dolomite. If the pressure became progressively more hydrostatic as the fault system developed, the pressure correction would decrease for the later stages.

Independent estimates of the temperature during Stage IIc mineralization were derived from measurements of sulfur isotope fractionation between coexisting sphalerite and galena. Two pairs were used, one from the Illinois vein on the 12th level and the other from a horsetail vein on the 4th level. Temperatures were calculated from the $\delta^{34}\text{S}$ values for the two minerals (given in Table 21 of the next section), using the fractionation curve of Czamanske and Rye (1974). The temperatures, 86° and 120°C, respectively, are somewhat lower than those indicated by fluid inclusions. The disparity suggests that the amethyst-carbonate assemblage may actually be from an earlier stage (Stage I?) rather than Stage IIc; paragenetic relations are equivocal. Therefore, based upon estimates from the alteration mineralogy, fluid inclusion filling temperatures, and isotope fractionation, the temperatures of mineral deposition apparently decreased from approximately 225°C during alteration and Stage I to 100°–125°C in Stage IIc.

Stable Isotopes

Analyses of the isotopic composition of oxygen, carbon, and sulfur in Proterozoic, alteration, and vein minerals were made by Joseph F. Whelan of the U.S. Geological Survey. Analyzed minerals and rocks included those collected for the present mineralogical study, and by Whelan and K. R. Ludwig as part of their investigations. The fine-grained and tectonically mixed character of most minerals precluded a more thorough study of the uranium-stage mineralization. The relatively coarse, late-stage minerals were

easier to separate for analyses, but provided little direct data regarding the antecedent stages.

The C, O, and S isotopic compositions are reported in conventional per mil deviations from standards. The standards include Standard Mean Ocean Water (SMOW) for oxygen, PDB (PeeDee belemnite) for carbon, and troilite in the Cañon Diablo meteorite for sulfur (Faure, 1977).

Oxygen Isotope Data

Materials analyzed for oxygen isotopic compositions include dolomite and silicates from unaltered and altered wall rocks, and calcite and dolomite from hydrothermal veins. Silicate analyses represent whole-rock values after removal of carbonate minerals by acid leaching.

Unaltered and altered wall rocks

Three unaltered-altered pairs of garnet-biotite gneiss and one of hornblende gneiss were analyzed to determine isotopic changes during carbonate-sericite alteration. In addition, analyses were made on single samples of altered garnet-biotite gneiss and unaltered hornblende gneiss. All values are listed in Table 20.

The garnet-biotite gneiss is virtually devoid of metamorphic carbonates, and all carbonates in altered equivalents are presumably of hydrothermal origin. The $\delta^{18}\text{O}$ values for the secondary carbonates range from 16.0–19.2 per mil. Presuming an alteration temperature of 225°C, and using the dolomite-water fractionation curve of Northrop and Clayton (1966), the $\delta^{18}\text{O}$ values of the altering fluid varied between +4.6 and +7.8 per mil. The $\delta^{18}\text{O}$ values from two samples collected immediately adjacent to and 10 cm from the 18-1 vein demonstrate an increase in the $\delta^{18}\text{O}$ value of the altering fluid away from the vein as it reacted with the

Table 20. Summary of $\delta^{18}O$ and $\delta^{13}C$ values of carbonates and silicates in unaltered and altered wallrocks.¹

Sample	Rock type	Dolomite		Whole-rock silicate		w/r ratio
		$\delta^{18}O/_{\infty}$	$\delta^{13}C/_{\infty}$	$\delta^{18}O/_{\infty}$	Fluid $\delta^{18}O/_{\infty}$	
80S25	Garnet-biot. gneiss	19.90	-3.71	14.79		0.06
80S24	Alt. Gar.-biot. gneiss	19.22	-3.41	15.09	7.80	
80S67	Gar.-biot. gneiss	15.54	-5.51	11.95		0.56
80S66	Alt. gar.-biot. gneiss	16.94	-3.69	13.94	5.52	
80S97	Gar.-biot. gneiss	17.51	-	13.29		0.85
80S99	Alt. gar.-biot. gneiss	16.48	-3.54	16.21	5.06	
80S108	Alt. gar.-biot. gneiss	16.03	-11.71	-	4.61	
80S40	Hornblende gneiss	10.88	-3.26	10.64		
80S41	Alt. hornblende gneiss	20.05	-3.22	18.31		
80UW5B-1	Alt. gar.-biot. gneiss (18-1 vein, adj. to vein)	17.42	-3.98	17.62	6.00	12.6
80UW5B-2	Alt. gar.-biot. gneiss (18-1 vein, 10 cm. from vein)	21.67	-4.28	14.27	10.25	0.18
80UW5B-3	Gar.-biot. gneiss (18-1 vein)	-	-	12.85		

1. J. F. Whelan, Analyst.

metamorphic rocks. Using the method described by Taylor (1979), the water-rock ratio during alteration was calculated, using the fractionation curve for quartz and water (Clayton et al., 1972), from the isotopic values for the water and the rock silicates. The calculated ratio varied between 0.06 and 0.85 during alteration of the garnet-biotite gneiss (Table 20). The persistence of primary calcite in the altered hornblende gneiss contaminated the isotopic value for hydrothermal carbonate, thereby preventing the calculation of the water-rock ratio in that lithology.

Vein carbonates

Figure 23 shows the $\delta^{18}\text{O}$ values for vein carbonates from all three hydrothermal stages. Also shown are the calculated $\delta^{18}\text{O}$ values for the depositing fluids, presuming temperatures of 225°C for Stage I and 125°C for stages IIc and III. The calculations used the dolomite- and calcite-water fractionation curves of Northrup and Clayton (1966) and O'Neil et al. (1969), respectively.

The $\delta^{18}\text{O}$ values for Stage I dolomite range from +17.4 to +20.0 per mil. Both agree with the values for carbonate-sericite alteration. The $\delta^{18}\text{O}$ values for Stage IIc dolomites range from +15-20.1 per mil, with a mean of +18.6 per mil; the calculated fluid values have a mean of -1.78 per mil. The $\delta^{18}\text{O}$ values range from +8.0-14.0 per mil for Stage III calcite, and -9.5 to -3.5 for the depositing fluids.

Carbon Isotope Data

Analyses were made of the carbon isotopic composition of all carbonates used in the oxygen isotope study. Isotopic compositions for primary and secondary carbonates in wall rocks are listed in Table 20; those for vein carbonates are shown in Figure 23.

With one exception, the $\delta^{13}\text{C}$ values for carbonates in un-

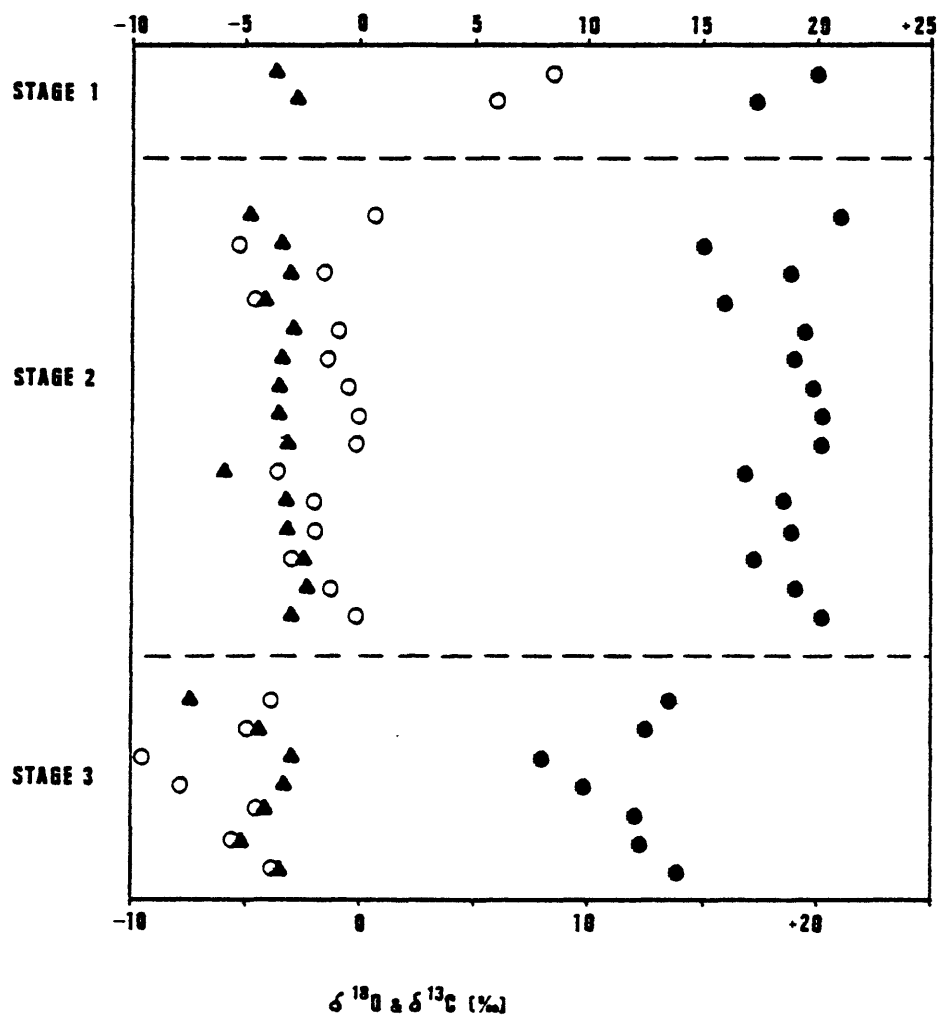


Figure 23. The $\delta^{18}\text{O}$ (solid circles) and $\delta^{13}\text{C}$ (triangles) values for vein carbonates from Stages I, II, III. Also shown are calculated $\delta^{18}\text{O}$ values for the depositing fluids (open circles).

altered and altered rocks are between -3.2 and -5.5 per mil. Most of the carbonate in altered garnet-biotite gneiss was derived from the hydrothermal fluid, and H_2CO_3 was the dominant aqueous carbon species (see following section). Using the fractionation curve of Bottinga (1968) and a mean $\delta^{13}\text{C}$ value of -3.6 per mil, the calculated $\delta^{13}\text{C}$ value of the altering fluid at 225°C was approximately -3.6 per mil. The $\delta^{13}\text{C}$ value for one sample of altered garnet-biotite gneiss is -11.71 (sample 80S108; Table 20), perhaps indicating local contamination by relict metamorphic graphite or CO_2 derived from graphite.

The $\delta^{13}\text{C}$ values for vein carbonates deposited during all three stages range from -2.39 to -7.3 per mil, with a mean value of -3.19 per mil for Stage I, -3.48 for Stage II, and -4.46 for Stage III. The similarity between values for all stages, including alteration, indicates that the $\delta^{13}\text{C}$ composition of the fluids in Stages II and III, at the lower temperature of 125°C and with HCO_3^- as the dominant aqueous carbon species (see following section), had shifted to a slightly lighter composition. The lighter carbon values in Stage III reflect the formation of calcite instead of dolomite (Sheppard and Schwarcz, 1970).

Sulfur Isotope Data

The physical limitations imposed by the rocks precluded a detailed study of the composition of the hydrothermal sulfides. Analyses, listed in Table 21, were made on metamorphic pyrite, Stage IIc sphalerite and galena, and Stage III marcasite. Additional data are available from Jensen et al. (1960) and Heyse (1972).

One analysis of metamorphic pyrite indicates a $\delta^{34}\text{S}$ value of +2.1 per mil. Analyses of pyrrhotite (Heyse, 1972) give compositions of -1.3 to -2.4 per mil. These values fall within the range of magmatic sulfur (Ohmoto and Rye, 1979), suggesting a genetic relationship with the mafic volcanic rocks of the hornblende

gneiss unit. Pre-metamorphic sphalerite and other nonferrous sulfides suggest a polymetallic environment. However, the abundant graphite and the associated pelitic rocks imply an anoxic restricted basin in which organic reduction of Proterozoic seawater sulfate (+25 per mil; Eichman and Schidlowski, 1975) could have produced the same isotopic values (Goodwin et al., 1976). Some sulfur may have been leached from the volcanic rocks, but, if deposited by bacterial action, would be much lighter than normal magmatic sulfur (Ohmoto and Rye, 1974).

Isotopic compositions of sphalerite from Stage IIc range from +1.6 to -0.6 per mil, and those for coexisting galena vary from -4.0 to -5.3 per mil (Table 21). Calculated sphalerite-galena equilibrium temperatures are 86° and 120°C, using the curves of Czamanske and Rye (1974). Analyses of Stage III marcasite and pyrite indicate a range from -18.0 to -40.5 per mil (Jensen et al., 1960; Heyse, 1972; J. F. Whelan, unpubl. data, 1982). As outlined in more detail in the following section, the fluid during Stage IIc mineralization overlapped the $\text{SO}_4^{=}$ - and HS^- -dominant fields. As a result, the $\delta^{34}\text{S}$ composition of the fluid, in order to deposit sulfides with the measured values, could have ranged from about -5 per mil in the sulfide-dominant field to +20 per mil in the sulfate-dominant field (Ohmoto, 1972). Furthermore, the neutral pH would have enhanced the stability of the intermediate sulfur species (Giggenbach, 1974), and may have produced unpredictable fractionation effects on the precipitating sulfides (Ohmoto and Rye, 1979). Estimation of the isotopic composition of the fluid during Stage III is a little more straightforward. Leaching of either metamorphic or hypogene sulfides would have produced a fluid composition near 0 per mil, and subsequent deposition of iron sulfides from the sulfate-rich solutions could have generated the isotopically light sulfides (Field, 1966).

Table 21. The $\delta^{34}\text{S}$ values of metamorphic and hydrothermal sulfides, and calculated isotopic temperatures.

Mineral	Stage	$\delta^{34}\text{S}$ ‰	T°C	Source
Pyrite	metamorphic	+2.1	-	1
Pyrrhotite	metamorphic	-2.41	-	2
Pyrrhotite	metamorphic	-1.30	-	2
Sphalerite	IIc	+1.6	86	1
Galena	IIc	-4.0		
Sphalerite	IIc	-0.6	120	1
Galena	IIc	-5.3		
Marcasite	III	-37.7	-	1
Marcasite	III	-33.8 → -36.98	-	2

Sources: (1) J. F. Whelan, unpubl. data, 1982.
(2) Heyse (1972)

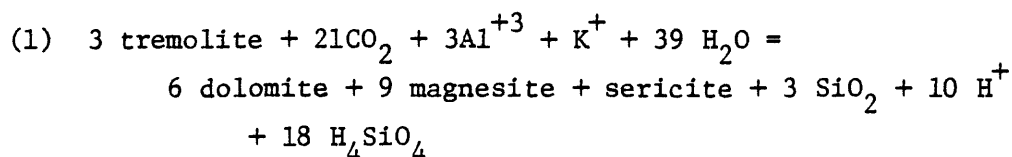
Processes of Alteration and Vein Mineralization

Hydrothermal activity progressed from early alteration at 225°C to late vein mineralization at 125°C. The mineralogy of the various stages was used to approximate the general chemical environment of alteration and vein mineralization. The methods of Barnes and Kullerud (1961), Garrels and Naeser (1958), and Holland (1959, 1965) have been employed to estimate the chemical parameters such as pH, $f(\text{CO}_2)$, $f(\text{O}_2)$, and $f(\text{S}_2)$. This information was then used to construct mineral stability diagrams for alteration, for the transition from alteration to vein mineralization, and for the cooler environment of Stage IIc. The chemical conditions during the episodes of uranium deposition may be approximated from these diagrams. Thermochemical data for all calculations were taken from Helgeson (1969), Usdowski and Barnes (1972),

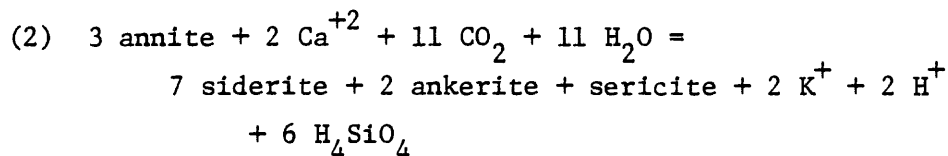
Helgeson et al. (1978), and Robie et al. (1978), except where otherwise noted.

Minerals created or destroyed during alteration reflect the chemical and physical environment of alteration. Of major importance are: (1) the introduction of large amounts of carbonate into the rocks; (2) the stability of iron-bearing minerals; (3) the sequential formation of sericite and adularia; and (4) the role of equal-volume replacement in determining the alteration mineralogy.

Biotite and amphibole were the two major minerals destroyed during carbonate-sericite alteration. Pseudomorphic replacement of amphibole by ankerite and sericite at 225°C is represented by reaction (1):



This requires a CO_2 fugacity of at least 1.0 bar. Equal-volume replacement of biotite by carbonate requires the formation of considerably more siderite than ankerite, due to the relative smaller molar volume of siderite (29 cm^3 vs. 64 for ankerite; Robie et al., 1978). The process, shown in reaction (2), requires an enormous CO_2 fugacity at 225°C.

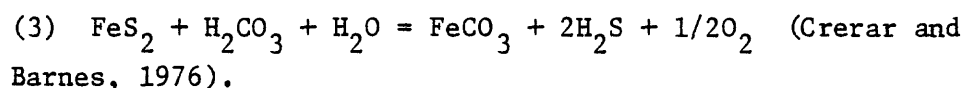


The CO_2 fugacity decreased with increased distance from the vein, and reached a point where biotite coexisted with altered hornblende. If one presumes a similar fugacity gradient in both amphibolitic and micaceous layers, the relatively large CO_2 fugacity required to alter biotite would restrict the width of alteration haloes in the micaceous layers. Indeed, micaceous layers in the

hornblende gneiss are generally less altered than adjoining amphibolitic layers.

Alteration produced virtually the same mineralogy in both the garnet-biotite and hornblende gneiss units, despite dissimilar metamorphic mineral assemblages. As noted in Chapter 4, the relative gains and losses of CaO, K₂O, Na₂O, and the Fe⁺²/Fe⁺³ ratio indicate different chemical potential gradients for these components in the two units. For example, the gradient for CaO decreased towards the vein in the hornblende gneiss but increased in the garnet-biotite gneiss, producing a loss of CaO in the former and a gain in the latter. The gradients of K₂O were just the opposite. The similarity of the resultant assemblages indicates that equilibrium was approached for the system.

Alteration of pyrite or pyrrhotite to siderite requires anionic substitution of carbonate for sulfur:

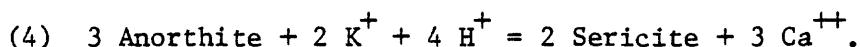


Marcasite, which is present at the interface between pyrite and siderite, is relatively more stable than pyrite with a decrease in pH (Gronvold and Westrum, 1976). As such, it may reflect the reaction of pyrite, prior to its destruction by siderite, to a slightly acidic fluid.

Carbonates are deposited to the exclusion of calcic silicates, such as zoisite and Ca-zeolites, at elevated CO₂ fugacities (Browne and Ellis, 1970). The observed abundance of carbonates and the absence of any other calcic alteration minerals corroborates other evidence for a large CO₂ fugacity during early carbonate-sericite alteration.

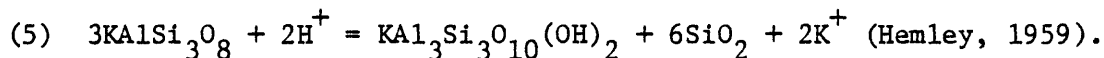
Early alteration preserved primary muscovite and generated sericite during replacement of primary feldspars and mafic silicates. Rare albite coincidentally replaced some plagioclase feldspars, but was itself not sericitized. At 225°C, contemporaneous formation of sericite and albite requires a Na/K ratio

between 15 and 50 (Figure 24), well within the range of thermal waters associated with epithermal mineralization (White et al., 1963). The alteration of plagioclase in the presence of albite requires the addition of potassium and hydrogen and the removal of calcium, according to the reaction:



The plagioclase-rich hornblende gneiss gained K_2O and lost CaO during alteration, while Na_2O remained constant (Table 13), supporting the predicted chemical changes.

The stabilities of muscovite and potassium feldspar are related by the reaction:



The K/H ratio must have been sufficiently low to generate sericite instead of adularia (Figure 24). The release of H^+ during alteration of both hornblende and biotite (reactions 1 and 2) might have locally enhanced sericite alteration in the rocks.

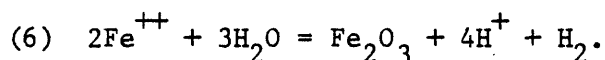
The concentrations of H^+ , K^+ , and aqueous SiO_2 control the pH of the sericite-adularia phase boundary at a particular temperature. Silica minerals were neither formed in nor removed from the host rocks during early alteration, and thus the activity of aqueous silica was likely near unity (Hemley, 1959). The altering fluids had a relatively high $a\text{K}^+$, as indicated by the influx of K_2O into the rocks. However, an equally large $a\text{H}^+$ was required to maintain the stability of sericite and prevent the formation of adularia in the early stage of alteration. The concentration of K^+ in vein-type hydrothermal fluids ranges from 0.1-0.001 molar (Roedder, 1972). At 225°C and 0.1 m K^+ , sericite and adularia are in equilibrium at a pH of 5.65 (Uzdowski and Barnes, 1972).

Kaolinite is a minor alteration product of garnet where the host mineral has been completely replaced. Its restricted occur-

rence clearly reflects a low K/H ratio at the site of garnet alteration (Figure 24). Its smaller molar volume, compared to that of muscovite (100 vs. 141 cm³), may have enhanced its stability during pseudomorphic alteration, presuming constant alumina.

Continued hydrothermal activity produced the hematite-adularia alteration assemblage at the expense of many of the pre-existing minerals. The concentration of K₂O in the rocks increased as adularia formed. Na₂O was removed and albite was destroyed as a result. The primary feldspars and secondary adularia are dusted with hematite, and all muscovite is absent.

Hematite replaced iron-bearing carbonates and is disseminated in all feldspars. Hematitization of siderite is relatively temperature-independent, and is largely dependent upon changes in the fugacities of CO₂ and O₂ (Figure 22). At elevated temperatures, a large $f(\text{CO}_2)$ is required to alter siderite to hematite without forming an intermediate magnetite phase. The hematitization of feldspars is controlled primarily by pH (Boone, 1970), according to the reaction



This reaction proceeded during or after the dissolution of sericite in the feldspars, as feldspars do not contain both hematite and sericite. Because the stabilities of both hematite and sericite may be pH-dependent, an increase in the pH could remove sericite and precipitate hematite. Adularia would form with an increase in pH (Hemley, 1959), and the codeposition of hematite and adularia would be expected under such conditions. Continued deposition of hematite with adularia in the altered wall rocks indicates that the pH continued to increase within the stability field of adularia. However, subsequent vein adularia is not hematitized. Hematite associated with chalcedony in the quartzite ceased to form before the end of alteration, perhaps indicating that the pH eventually stabilized or the $f(\text{O}_2)$ of the fluid moved

out of the hematite stability field. Concentric bands of hematite that overlap radiating chalcedony suggest repeated changes in the chemistry of the altering environment rather than alternating influxes of fluids of different compositions.

Detailed studies of alteration at Yellowstone (Keith et al., 1978) and Broadlands (Browne and Ellis, 1970) demonstrate that albite and sericite dominate zones of low permeability and slow rates of fluid flow, and that adularia is prevalent in permeable zones and fissures. In fissures, rapid flow increases the water/rock ratio and minimizes the buffering effect between rock and fluid. The fast-flowing fluids are generally hotter and consequently have a relatively greater K/Na ratio (Fournier and Truesdell, 1973). The alteration mineralogy in the adjacent rocks is therefore controlled by the composition of the fluid (Ellis, 1970), and adularia is produced.

The entire pre-ore fracture system must have been relatively open and interconnected at a very early stage to allow invading fluids to produce the ubiquitous carbonate-sericite alteration assemblage. However, both the presence of sericite and albite instead of adularia, and the relatively large width of the alteration halo suggest that the wall rocks were able to buffer the early fluids. Therefore, although the fracture system was readily accessible to invading fluids, the rate of flow through the fractures must have been sufficiently small to permit more extensive water-rock interaction. This is supported by the small water/rock ratios calculated from oxygen isotope data.

The hematite-adularia alteration accompanied a major episode of brecciation which, by virtue of the enhanced permeability, increased the rate of flow. The reduction in confining pressure could have also induced CO₂ effervescence. The resultant increase in pH and decrease in $f(\text{CO}_2)$ of the fluid would have enhanced the destruction of sericite, the hematitization of iron-bearing carbonates, and the precipitation of hematite in feldspars. The increased permeability and flow rate in the fissures reduced fluid-wallrock interaction, restricting alteration to a

very narrow zone adjacent to the veins and producing an assemblage dominated by the composition of the fluid. New fluids, invading the system from hotter source regions at depth and with a larger K/Na ratio (Ellis, 1970), would have enhanced the formation of adularia.

The second episode of alteration may have taken place at somewhat higher temperatures than the earlier stage. Carbonates form readily at lower temperatures (Holland and Malinin, 1979), and siderite is stable with much smaller CO_2 fugacities (Figure 22). With increased temperature, the stability field for adularia invades that of sericite (Figure 24). Although all observed assemblages and predicted reactions are feasible under isothermal conditions, all are enhanced by an increase in fluid temperatures during alteration. Early fluids may have progressively heated the adjacent rocks, thereby minimizing the amount of thermal loss by subsequent fluids. Increased flow rates in the later stages would have also reduced the loss of heat from fluids to wall rocks (Norton and Cathles, 1979).

The chemical environment during the hotter early vein mineralization and the cooler events of Stage IIc can be discussed with the aid of $\text{pH-f}(\text{O}_2)$ and $\text{f}(\text{O}_2)\text{-f}(\text{S}_2)$ diagrams for the two episodes. The concentrations and fugacities of several components were estimated in order to construct the diagrams. The total concentration of sulfur in most hydrothermal fluids is between 0.001 and 0.1 molar (Ohmoto, 1972), and an average of 0.01 m was used for this study. Early alteration required a large CO_2 fugacity of perhaps more than 100 bars, but the $\text{f}(\text{CO}_2)$ may have dropped to 1 bar as the faults became more open and total pressure declined. At the prevailing pressure and temperature, these correspond to a drop in dissolved CO_2 from perhaps 10 to 4 percent (Takenouchi and Kennedy, 1964).

The trend from hematite-adularia alteration into an early vein assemblage of pyrite-adularia-ankerite follows a distinct path shown in Figure 25. The absence of graphite requires a mini-

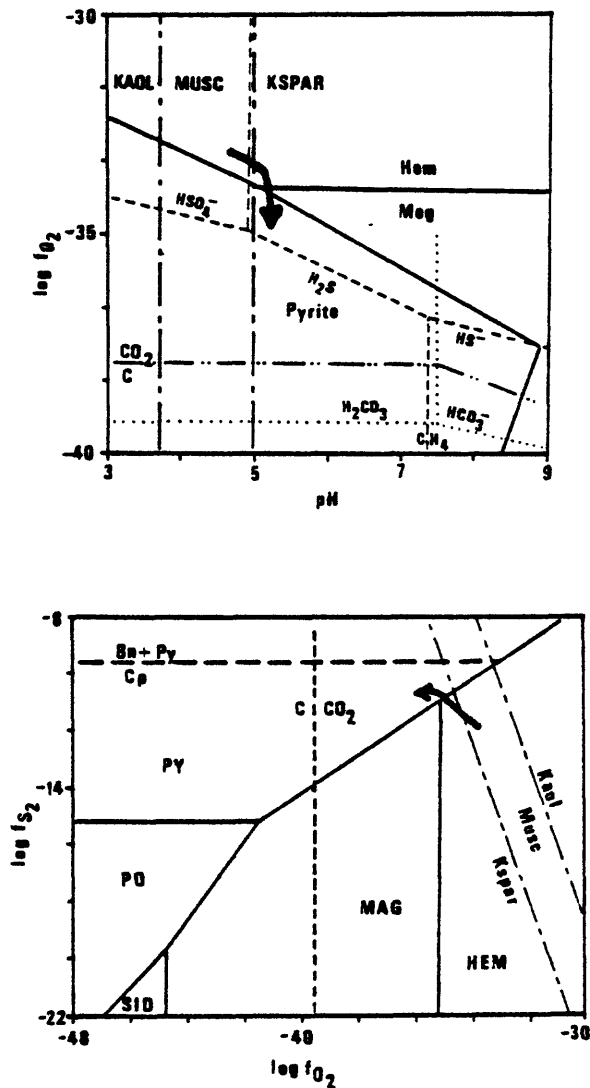


Figure 25. The (a) $f(O_2)$ -pH and (b) $f(S_2)$ - $f(O_2)$ stability fields for minerals formed during alteration and early vein mineralization at 225°C. Activities are: total S = 0.01 m; $[K^+] = 0.2$ m; $f(CO_2) = 100$ bars. Arrows show general trend from alteration into early vein mineralization.

mum $f(\text{O}_2)$ of 10^{-39} bars. Similarly, the presence of chalcopyrite and the absence of bornite limits the $f(\text{S}_2)$ to a maximum of 10^{-10} bars. A shift in stability from hematite to pyrite in the presence of adularia requires a decrease in $f(\text{O}_2)$. If the pH is 5 or greater, magnetite or chlorite form as intermediate phases. Their absence indicates a lower pH and a concentration of K^+ greater than 0.2 m (Usdowski and Barnes, 1972) to ensure the stability of adularia. A lower pH also requires more total $[\text{Ca} + \text{Mg} + \text{Fe}]$ to stabilize dolomite and a minimum total $[\text{Fe} + \text{Mg}]$ of 10^{-4} m to precipitate iron-rich dolomite instead of calcite. As shown in Figure 25a, both the presence of adularia and the absence of magnetite and bornite require that the shift from the hematite to pyrite stability fields was accomplished at relatively constant $f(\text{S}_2)$ with an increase in pH and slight decrease in $f(\text{O}_2)$. The dominant aqueous carbon species was H_2CO_3 throughout alteration and early vein mineralization; CH_4 was virtually absent (Figure 25b). Although HSO_4^- was the major sulfur species during alteration, $\text{SO}_4^{=}$ became dominant as the pH increased. The proximity to the sulfate-sulfide boundary and the neutral pH would have enhanced the stability and abundance of thiosulfate species along the boundary (Giggenbach, 1974). The concentration of H_2S may also have increased, depending upon the kinetics of sulfate reduction at this temperature.

By the beginning of Stage IIc the fluids had cooled to 125°C . Graphite and bornite are absent from the assemblage, thereby limiting the oxygen and sulfur fugacities to 10^{-51} and 10^{-15} bars, respectively (Figure 26). Adularia, chalcopyrite, and pyrite are common; a minimum pH of 6 is required for the coexistence of all three (Figure 26a). Depending upon the pH, HCO_3^- and possibly H_2CO_3 were the major aqueous carbon species (Figure 26b). Although sulfate was theoretically abundant during Stage IIc, thiosulfate and bisulfide may have been present in significant quantities.

The compositions of the carbonate minerals changed progres-

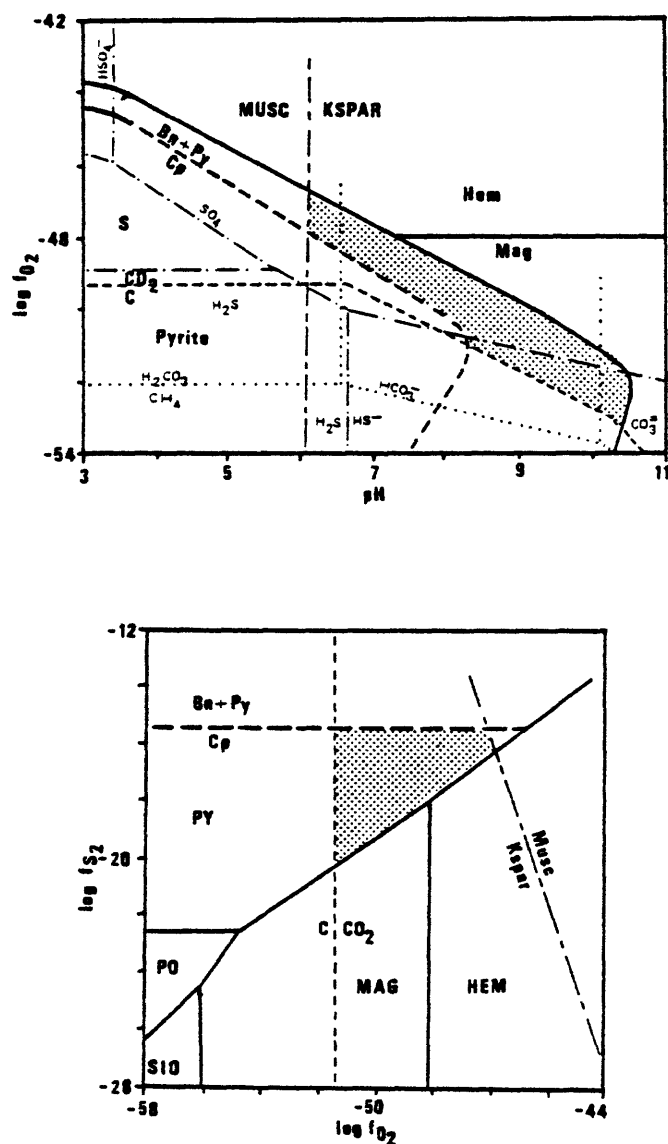


Figure 26. The (a) $f(O_2)$ -pH and (b) $f(S_2)$ - $f(O_2)$ stability fields for minerals formed during Stage IIc vein mineralization at 125°C. Activities are: total S = 0.01 m; $[K^+] = 0.2$ m; $f(CO_2) = 1.0$ bar.

sively from ankerite through dolomite to calcite, a trend common to the deposit as a whole and to Stage II veins in particular. An increase in the $\text{Ca}/(\text{Fe} + \text{Mg})$ ratio produces calcite instead of dolomite (Rosenberg et al., 1967), and an increase in pH has the same effect. A gradual decrease in the CO_2 fugacity may have produced the observed sequence if the cations were derived directly from the wallrocks (Naumov et al., 1971). However, none of the cations were released in appreciable quantities during alteration.

Pitchblende was deposited in massive quantities between Stages I and IIc. The temperatures of deposition were between 225° and 125°C , and the associated vein minerals included pyrite, chalcopyrite, adularia, ankerite, and the Fe-Mo-As sulfide; note that graphite, bornite, iron oxides, and sericite are absent from the assemblage. The pH was generally between 5 and 8, based upon estimates from the bounding stages and the mineralogy. Both H_2CO_3 and HCO_3^- were abundant. Under such conditions and a dissolved CO_2 concentration of 4 to 10 percent, uranium was likely carried as either a uranium carbonate (UO_2CO_3) or dicarbonate ($\text{UO}_2(\text{CO}_3)_2^{-2}$) complex (Figure 27). Thermodynamic calculations indicate that SO_4^{-2} initially was the dominant aqueous sulfur species, presuming a total sulfur concentration of 0.01 m, and that, with the onset of vein mineralization, the fluid composition approached and probably entered the sulfide-dominant field (Figure 25b).

Iron, molybdenum, arsenic, lead, and copper were transported and deposited with the uranium. If the solutions were relatively sulfate-rich, sulfide complexes were probably of minimal importance (Barnes, 1979). Thiosulfate complexes may have been important because the conditions of pH and $f(\text{O}_2)$ in the solutions favored their stabilities (Giggenbach, 1974). Chloride may have been the most effective complexing agent for all metals in the sulfate-dominated solution (Crerar and Barnes, 1976; Giordano and Barnes, 1981). Large concentrations of carbonate enhance the stability of lead-carbonate complexes (Giordano and Barnes, 1981),

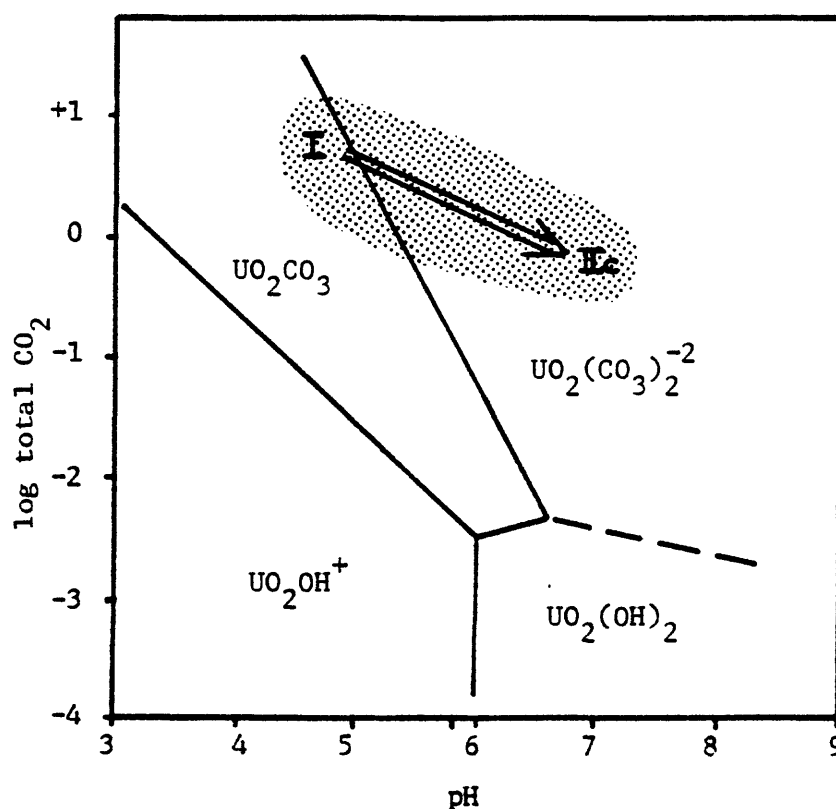


Figure 27. Total CO_2 -pH diagram showing the stability fields for uranyl carbonate complexes at 150°C . Boundaries are from Cuney (1978), based upon data in Sergeyeva et al. (1972). Stippled area corresponds to conditions during mineralization, based upon total CO_2 calculated from Takenouchi and Kenney (1964). Arrow shows general trend from Stage I to Stage IIc.

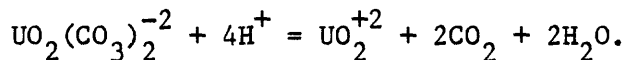
and the abundance of non-radiogenic lead in the ores (K. Ludwig, personal communication, 1982) suggests a similar mode of transport for both lead and uranium.

Deposition of uranium from a carbonate complex is a two-step process: the complex must first be destroyed and the uranyl ion (U^{+6}) then reduced to a tetravalent state (U^{+4}) in pitchblende. Several mechanisms have been proposed, but none adequately explain the destruction of this complex. Although the temperature dropped by 100°C during Stages IIa and IIb, cooling of the fluids could not have released the uranyl ion because uranyl carbonate complexes become more stable with decreasing temperatures (Romberger, 1978). Similarly, cooling increases the solubility of dolomite (Holland and Malinin, 1979). Hydrogen metasomatism of wall rocks also reduces the stability of carbonate complexes (Holland and Malinin, 1979), but the observed hydrogen-consuming alteration was not extensive and was paragenetically earlier than both stages of pitchblende deposition. Fluid mixing and consequent dilution of the carbonate-rich solutions is a viable scenario for the major Illinois and Rogers faults, where mixing of ascending and descending fluids is possible, but it is improbable along the discontinuous high-grade horsetail veins.

A major episode of brecciation preceded both stages of pitchblende deposition, and served to open new conduits and enlarge existing ones. The resultant increase in void space simultaneously decreased the total pressure on the fluids everywhere in the fracture system. Although the amount of pressure decrease is unknown, the gaping dilations on the horsetail veins and the probable propagation of the Illinois and Rogers faults upwards into the permeable Phanerozoic sedimentary rocks suggest that the decrease may have been considerable and was clearly sudden. Furthermore, the extremely fine-grained texture of the vein materials indicates rapid deposition.

Estimates from mineral stabilities indicate that the CO_2 fugacity was very large during alteration, and evidence from the

clastic dikes, imploded breccias, and graded breccia fragments demonstrate that high-pressure, CO_2 -dominated fluids were prevalent during the development of the deposit. The drop in total pressure during brecciation undoubtedly caused the evolution of CO_2 gas, thereby reducing the stability of the uranyl carbonate complexes:



Loss of CO_2 produces both an increase in pH and a decrease of the $f(\text{O}_2)$ (Rich et al., 1977). The fluids may not have boiled, as a dilute solution at 225°C with a total pressure of at least 300 bars (the hydrostatic minimum) should not boil (Haas, 1971). However, large concentrations of CO_2 reduce the density of the solution and severely depress the boiling point (Mahon et al., 1980). Even with one percent steam loss, 50 percent of the CO_2 and 30 percent of any H_2S would be lost (Ellis, 1963). Loss of CH_4 was minimal owing to its originally low concentration (Figure 25b), and it therefore could not adequately balance the reducing effect of CO_2 effervescence.

Large quantities of adularia and ankerite were deposited with pitchblende. A pronounced increase in the permeability of a conduit enhances the formation of adularia, both by the metastability of high K/Na ratios and by the increased pH due to CO_2 evolution (Grindley and Browne, 1976). Loss of CO_2 , either through effervescence or boiling, causes the deposition of ankerite (Holland and Malinin, 1979). Both mechanisms would have been initiated by a major episode of brecciation and related decrease in total pressure.

The second step in the deposition of uranium is the reduction of the uranyl ion. Again, several previously proposed mechanisms are not consistent with observed relations. Iron-rich metamorphic

rock units host all of the uranium deposits in the foothills region, and hematite alteration is common to all (Sims and Sheridan, 1964). This led to the conclusion that oxidation of iron to produce hematite caused reduction of the uranyl ion (Adams and Stugard, 1956; Rich et al., 1977). However, at the Schwartzwalder and other deposits studied during this project, this was not an important mechanism for reduction because (1) hematite is not always present; (2) uranium was also precipitated in fractures hosted by iron-deficient quartzites; (3) hematite is an alteration product that preceded uranium deposition, and was separated from it by unhematized adularia; and (4) iron sulfides and ankerite, not hematite, were the iron-bearing minerals that precipitated with pitchblende. Instead, the hematite reflects the more alkaline conditions produced in the wall rocks after brecciation.

Rich and Barabas (1976, 1979) reported carbonaceous material associated with pitchblende, based upon semi-opaque materials observed in thin sections and upon chemical analyses. Reanalysis of the samples by J. S. Leventhal of the U.S. Geological Survey was made after leaching with 4 N HCl at 60°C with successive additions of acid to dissolve all carbonate. The resultant values, 0.06-0.13 weight percent (J. Leventhal, written communication, 1979), are considerably smaller than the "one to several weight percent" reported by Rich and Barabas (1979), which perhaps suggests incomplete leaching of carbonate prior to the original analyses. Furthermore, regression analysis demonstrates that uranium and organic carbon in the veins are noncorrelative. Therefore, organic carbon was apparently not responsible for reduction.

Lacking an external reductant, the pitchblende must have been precipitated by a reducing agent in the fluid. Methane, an excellent reductant, was virtually absent (Figure 25b). The sulfur species in solution probably exerted a strong influence, but the mechanisms were clearly complex. Sulfate theoretically predominated in the solution, but significant amounts of reduced sulfur

may have been present if the total sulfur concentration was less than 0.01 m. The pH-f(O_2) conditions during mineralization partially overlapped the sulfide-sulfate boundary (Figures 25 and 26), and intermediate thiosulfate and sulfite species could have been abundant (Giggenbach, 1974). Any sudden loss of H_2S during pressure release would have destabilized any thiosulfate species, leading to the deposition of metal sulfides (Ewers and Keays, 1977) and the possible reduction of uranium (Spirakis, 1981). The sluggish reduction of sulfate at temperatures below $250^{\circ}C$ produces a progressively more reducing fluid as the temperature decreases, allowing H_2S or HS^- to reduce the uranium (Spirakis, 1981). Loss of H_2S would have further upset the sulfate-sulfide equilibrium, and may have enhanced uranium deposition. Sulfide deposition with pitchblende indicates that reduced sulfur was precipitated in significant amounts, in accord with Spirakis's model. Decreases in both temperature and pressure reduce the stability of chloride, carbonate, and sulfur complexes; a decrease in oxygen fugacity and increase in pH further destabilizes chloride complexes and enhances the formation of sulfides (Barnes, 1979). Therefore, pressure release due to brecciation conceivably led to the deposition, either directly or indirectly, of all the observed vein minerals.

Deposition in Stage IIa was rapid, as reflected by the extremely fine-grained and chaotic textures. Those in Stages IIb and IIc are also fine-grained, but the delicate "colloform" textures of pitchblende and the Fe-Mo-As sulfide resemble those deposited from a colloid. However, evidence against a colloidal origin include the elevated temperature, the absence or relatively small volume of shrinkage cracks, and synchronous or cyclic deposition with crystalline substances (Roedder, 1968). The textures are more likely the product of deposition from a supersaturated fluid. Cyclic precipitation of pitchblende with sulfides and carbonates indicate that both sulfur and carbonate were related to uranium deposition. The local dissolution of pitchblende by carbonate attests to a reversible complexing reaction (Sverjensky,

1981), and implies cyclic fluctuations in the CO_2 fugacity or the oxidation state of sulfur near the point of uranium supersaturation.

Uranium deposition took place at temperatures between 225° and 125°C. A large decrease in temperature, from adiabatic cooling and loss of volatiles, probably accompanied each major period of brecciation (Barton and Toulmin, 1961). Heat loss by conduction may have been important depending upon the rate of flow through the conduits (Browne and Ellis, 1970). If a long interval of time separated stages IIa and IIb, the fluids responsible for the later period may have been somewhat cooler than earlier solutions as the hydrothermal system began to wane. Mineral deposition in Stage IIb may not have been so rapid due to the enhanced solubilities of carbonate minerals and uranyl carbonate complexes at lower temperatures (Romberger, 1978).

The trend of increasing pH and decreasing oxygen fugacity is similar to that observed for uranium deposits at Echo Bay, Canada, (Robinson and Ohmoto, 1973) and the Mena mine (Stark, 1979). The sequential deposition of native bismuth, native silver, and acanthite within the hematite stability field reflected a pronounced increase in the sulfur fugacity at relatively constant pH prior to the end of hematite deposition at Echo Bay (Robinson and Ohmoto, 1973). However, uranium and hematite formed contemporaneously as vein minerals, and prior to the noted increase in sulfur fugacity. This contrasts with the paragenetic sequence at the Schwartzwalder deposit, where pitchblende was deposited with pyrite and ankerite after hematite alteration.

CHAPTER 8. PROPOSED GENESIS OF THE URANIUM DEPOSITS

Three components are required to form a hydrothermal ore deposit: (1) a hydrodynamic plumbing system; (2) sources for the heat, dissolved constituents, and water; and (3) a mechanism for mineral deposition. Based upon geologic and isotopic evidence, the following discussion will propose that the components of the uranium deposits along the foothills of the Front Range were derived almost entirely from the metamorphic rocks, and were transported to and deposited in the fracture systems during the very earliest stages of Laramide uplift.

Structural Development

The range front on the eastern side of the Front Range has two structural styles. North of Boulder, differential uplift and rotation of basement blocks produced drape folds that dominate the frontal zone (Matthews and Work, 1978). South of Boulder, the northwest-trending fault system and the major frontal reverse faults combined to produce the observed deformation (Warner, 1980). Interaction between the reverse and northwest-trending faults generated complex movements and produced numerous subsidiary fractures along the northwest-trending faults, which are in the upthrown block of the reverse faults. The steeply inclined Pennsylvanian unconformity along the range front indicates rigid rotation of the basement. The influence of the reverse fault decreased sharply away from the range front, and the movement along the northwest-trending faults was probably much less complex as a result. Analogous structural situations include the shattered frontal lobes of the Owl Creek and Wind River ranges of Wyoming (Couples and Stearns, 1978). Therefore, extensive basement faulting during the early stages of Laramide uplift was extremely pronounced along the frontal zone south of Boulder.

The Front Range continued to rise until Eocene time. Thereafter, peneplanation produced a widespread erosion surface (Epis and Chapin, 1975), a remnant of which is preserved near Golden (Scott, 1972). Similar areas of low relief, immediately above and near the Schwartzwalder mine, have the same elevation as and may be relicts of the Eocene surface. If so, by late Eocene time more than 3.1 km of sedimentary rocks and 100 m of metamorphic rocks had been eroded from this terrane to leave the top of the deposit exposed. Renewed uplift in Miocene time may have reopened some fractures and created fractures such as the post-ore Illinois fault.

Origin of Clastic Dikes

The clastic dikes represent fault gouge, breccia, and ore fragments that were locally remobilized and injected into fractures. As such, they demonstrate (1) intense faulting during mineralization, and (2) extremely high fluid and tectonic pressure. Cataclasis along the Rogers and, to a lesser extent, Illinois faults generated the finely milled breccia during major movement. The development of the gouge is evident where clastic zones grade imperceptibly into severely altered wall rock. Displacement must have been considerable to produce such fine-grained materials (Engelder, 1974), although high fluid pressures also would have enhanced the formation of gouge (Engelder et al., 1975). Similar tectonic breccia is typical of major faults, including the Heart Mountain thrust of Wyoming (Pierce, 1979) and Muddy Mountain thrust of Nevada (Engelder, 1974).

Injection of the breccia into new and existing fractures took place in response to high fluid and tectonic pressures (Voight, 1973). Some breccia, such as that derived from the ores, was injected only locally. However, other breccias, such as that in the light-colored dikes, commonly do not have a local source, and must have been injected from a considerable distance. The up-

ward decrease in clastic material along the Illinois fault suggests an upward propagation of the injected breccia. Although emplacement of the dikes may have temporarily released pressure, it may have also served to reseal the faults and consequently generate another cycle of pressure build-up. Carbonate gouge initially increases the strength of shear surfaces (Logan and Shimamoto, 1976), and the intensities of subsequent fault movements may have been much greater as a result. However, Irwin and Barnes (1975, 1980) have demonstrated that protracted CO_2 evolution during metamorphic decarbonation maintains high fluid pressures in active fault zones, which thereby may produce numerous small earthquakes. High-pressure, CO_2 -dominated fluids persisted at the Schwartzwald deposit after the formation of the clastic dikes to locally generate graded and winnowed breccias.

Source of Fluid and Mineral Components

Geologic and isotopic constraints demonstrate that the uranium and associated carbonate and metals were derived largely from the metamorphic rocks. Fluids involved in alteration and early mineralization were in isotopic equilibrium with the metamorphic rocks, but were mixed with some meteoric water by Stage IIc.

Carbon

Regional geologic evidence precludes a non-metamorphic source rock. All of the uranium deposits in the northwest-trending faults are confined exclusively to the metamorphic terrane, even though the fractures transect the granitic terrane as well (Figure 3). Carbonate-adularia cement, similar to the gangue in the uranium deposits, fills the faults only in the metamorphic terrane, whereas quartz and hematite are prevalent along the same structures in the granitic terrane (Wallace, in press). The Mesozoic sedimentary rocks that flank both terranes to the east include

large volumes of calcareous shales. If these units, by whatever means, were the source of the carbonate (Young, 1979b), then the distribution of carbonate would not be constrained by host rock lithology, and carbonate would instead be concentrated along faults in all crystalline rocks of the range front. Similarly, any genetic models requiring descent of carbonate-rich fluids through the open fractures cannot be limited to the metamorphic terrane unless the carbonate was derived from the metamorphic rocks. Emanation of carbonate from magmas is equally improbable because it would imply that the intrusions were limited to the metamorphic terrane. However, the regional distribution of plutons disproves any such rigid restriction (Tweto, 1979), although deep Laramide intrusions along the range front could have induced decarbonation reactions in carbonate-bearing metamorphic rocks.

Calcite and graphite are the major carbon-bearing minerals in the metamorphic rocks. The $\delta^{13}\text{C}$ value of Proterozoic graphite is generally between -20 and -30 per mil (Barker and Friedman, 1969; Eichman and Schidlowski, 1975), and the $\delta^{13}\text{C}$ value of any CO_2 derived from the graphite would be less than -10 per mil. As a result, dolomite precipitated from fluids containing this CO_2 would have very negative per mil values. In contrast, the isotopic composition of calcite in the metamorphic rocks is between -3.2 and -5.5 per mil (Table 20). Aqueous carbonate derived from the calcite would produce hydrothermal dolomite with a similar isotopic composition (Bottinga, 1968). The measured compositions of dolomite in the uranium deposit range from -2.4 to -7.3 per mil, in close agreement with the predicted values for the carbonate source. These values are also within the range of magmatic carbon (Ohmoto and Rye, 1979), but geologic evidence does not totally favor a magmatic source. Therefore, it appears that the carbon in the hydrothermal carbonates was derived from metamorphic carbonates, of which virtually all is from the calc-silicate and hornblende gneiss units (Sheridan et al., 1967).

Sulfur

The isotopic compositions of sulfides from Stage IIc range from +1.6 to -0.6 per mil, and are similar to those for the metamorphic sulfides (Table 21). In order for the metamorphic sulfides to have been the source of sulfur for the hypogene sulfides, the fluids would have had to have been sulfide-dominated to produce the necessary fractionation (Ohmoto, 1972). Based upon mineral stabilities for the ore-forming stages, however, the fluids were relatively sulfate-rich as they entered the environment of ore deposition. Even if H_2S and sulfate were present in equal amounts, the sulfur composition of the fluid must have been at least 10 per mil to produce sulfides with $\delta^{34}S$ values near 0 per mil (Sakai, 1968; Ohmoto, 1972). On this basis, it is unlikely that the sulfur in the fluids was derived directly from sulfides in the metamorphic rocks. This conclusion, however, is based upon admittedly scanty data. Furthermore, the neutral pH and decreasing temperatures would have simultaneously stabilized intermediate sulfur species (Giggenbach, 1974) and upset sulfide-sulfate equilibria (Spirakis, 1981), and may have produced unpredictable fractionation effects on the precipitating sulfides (Ohmoto and Rye, 1979). A sedimentary sulfate source for the heavy sulfur, such as that described by Casadevall and Ohmoto (1977), is not likely because sulfates have not been noted in the overlying Phanerozoic rocks (Scott, 1972; Van Horn, 1976).

The sulfides in Stage III are isotopically very light (-18 to -41 per mil). Leaching of the metamorphic or hypogene sulfides would have produced a fluid composition near 0 per mil. Subsequent deposition of the iron sulfides from the sulfate-rich solutions might have generated the isotopically light sulfides (Field, 1966).

Oxygen

The relatively heavy composition (4.6 to 8.6 per mil) of oxygen in the hydrothermal fluids during early alteration and Stage I vein mineralization suggests two possible sources: (1) magmatic water, or (2) water in equilibrium with the metamorphic rocks (Taylor, 1979). The absence of any evidence of spatially associated magmatic activity requires that any magmatic water source was considerably removed from the vicinity of ore deposition, thereby increasing the chance for isotopic interaction with metamorphic rocks and non-magmatic fluids. The $\delta^{18}\text{O}$ values for metamorphic silicates range from 10 to 15 per mil (Table 20). Regardless of its origin, water in small volumes and with a long residence time in the metamorphic rocks would acquire an isotopic composition similar to that of the rocks (Taylor, 1979). Therefore, the oxygen isotope values do not suggest a unique source. However, because the carbon and oxygen in the carbonates were probably derived from the same source, and because the carbon is from the metamorphic terrane, the oxygen more than likely had a history of interaction with, or origin from, the metamorphic terrane rather than a magmatic source.

The $\delta^{18}\text{O}$ value of the water during Stage IIc was substantially lighter than that during the early stages, ranging largely from 0 to -5 per mil (Figure 23). This implies contamination of the original fluids by meteoric water or less-evolved connate water from the overlying sedimentary rocks. The $\delta^{18}\text{O}$ values in Stage III water were even lighter, and had an average of -5.6 per mil (Figure 23). These fluids may have been composed entirely of meteoric water, as supported by the apparent supergene origin of coexisting sulfides.

Uranium and Lead

Analyses of the isotopic compositions of hydrothermal uranium and lead by Kenneth R. Ludwig of the U.S. Geological Survey indicate that both elements were derived from a mid-Proterozoic source and that the source was not a pre-existing uranium deposit. Based upon the $^{207}\text{Pb}/^{206}\text{Pb}$ ratio in hydrothermal galena, the age of the source is 1.6-1.9 b.y. old. This age is identical to that of the metamorphic rocks, and is older than all plutonic rocks in the region (Hedge and Peterman, 1968). Furthermore, the concentration of uranium in the source was very small, and the Th/U ratio was approximately 1.7 (K. Ludwig, oral commun., 1982). The low concentration of uranium in the source conflicts with previous models (Fisher, 1976; DeVoto and Paschis, 1979; Nelson and Gallagher, 1981) that propose mobilization and preconcentration of uranium in fold axes and faults during Proterozoic metamorphism. The arkosic Pennsylvanian Fountain formation is composed entirely of clasts of Proterozoic metamorphic and igneous rocks, and originally overlay the basement above the deposit. Intrastratal alteration of the uranium-bearing minerals, such as augite, hornblende, and biotite, probably introduced abundant uranium into subsurface waters (Walker, 1975), and the lead in any consequent uranium deposit would have a Proterozoic source age. The alteration took place shortly after diagenesis (Walker, 1967), and little uranium was available for leaching by Laramide time. However, some of the uranium-rich groundwater may have migrated into underlying regolith above the crystalline basement.

Possible Source Rocks

With the exception of the Bonzo deposit, all of the uranium deposits along the range front are hosted by or are in close proximity to major hornblende gneiss units similar to that at the Schwartzwalder mine. These units contain a large component of

volcanic materials, and associated sediments include chert, fine-grained pelites, and carbonate. The Bonzo deposit is hosted by garnet and felsic gneisses (Scott, 1963).

Reconnaissance studies of Proterozoic stratabound sulfide deposits in Colorado demonstrate that the sulfides are intimately associated with amphibolite, garnet and felsic gneisses, and related marble and metachert layers (Sheridan and Raymond, 1977). In areas of lower metamorphic grade, the hornblende and felsic gneisses clearly represent metamorphosed mafic and felsic volcanic and volcanoclastic rocks, respectively, and most of the quartzite layers are metamorphosed chert (Sheridan and Raymond, 1977). Associated metals in the rocks include zinc, copper, lead, silver, and gold. In addition, many of the deposits are anomalously radioactive, and several contain uranium minerals (Sims and Sheridan, 1964).

The association of uranium with submarine volcanism has been shown in other areas as well. Uranium was precipitated at the seawater-sediment interface during the waning stages of volcanism and sulfide deposition at Camp Smith, New York (Grauch, 1978). In the Kaipokok Bay-Big River area of Labrador, uranium and titanium were deposited in the distal reducing environment related to submarine volcanism (Gandhi, 1978). In both areas, uranium deposition was associated with both the volcanic rocks and related chemical precipitates.

Based upon geologic and isotopic evidence at the Schwartzwalder and other deposits, and upon the association of uranium with stratiform volcanogenic sulfide deposits in other areas, the hornblende gneiss units were probably the major sources for uranium and carbonate in the district. Not only are the lithologies and sequences of these metamorphic units similar to those described elsewhere, but Proterozoic sulfides, including those of iron, zinc, lead, and copper, are disseminated or locally abundant throughout the rocks. The garnet-biotite gneiss unit is the host lithology at the Bonzo, Ladwig, and parts of the Schwartzwalder

deposits. Its precursors clearly formed in a reducing environment in proximity to a volcanic center, and may have contained chemically precipitated uranium, such as that found in chemically-precipitated sediments in Labrador. As such, it also may have been a source rock, although its absence at most of the deposits suggests that it was not the major source. It is usually stratigraphically present between brittle and ductile rocks, and was probably more important as a conduit adjacent to the relatively impermeable schists. None of the metamorphic units contain anomalous amounts of uranium, in harmony with the results of the uranium-lead isotope studies that indicate a relatively low uranium concentration.

The isotopic data indicate that the hydrothermal fluids were in isotopic equilibrium with the metamorphic rocks. This suggests both a long residence time in the rocks and perhaps a relatively small water/rock ratio (Taylor, 1979). Three possible storage reservoirs in the metamorphic rocks were: (1) microfractures and intergranular pores in the rocks; (2) major fracture zones such as the Rogers fault; and (3) the regolith in the metamorphic rocks immediately below the overlying sedimentary rocks. Considering the depth of burial, it is unlikely that microfractures and pore spaces in unbroken crystalline rocks were sufficiently open and abundant to constitute a viable reservoir. Snow (1968) estimated a maximum porosity of less than 0.001 percent for this setting.

The major fracture systems, which have a Proterozoic ancestry and were possibly reactivated during Pennsylvanian uplift, may have been a deep reservoir. The individual faults, such as the west strand of the Rogers fault, are relatively wide zones composed of abundant anastomosing fractures. As such, they provide a large surface area for leaching relatively to the volume of rock within the zones. The close proximity to the overlying regolith indicates that the faults were exposed at the surface during the Pennsylvanian uplift, and that meteoric water probably permeated the system much as it does today. Entrapment of some of this

water during subsequent burial could have provided a reservoir for subsequent hydrothermal activity during Laramide uplift.

The regolith in the weathered metamorphic rocks beneath the Pennsylvanian Fountain Formation is 20-30 m thick, and grades downward from a reddish buried paleosoil to highly fractured metamorphic rocks. This zone was encountered at a depth of 3638 m in the Rocky Mountain Arsenal well, which was drilled about 3 km northeast of Denver (Pickett, 1968). Test pumping into the zone indicated that the effective reservoir area of the fracture-controlled regolith was about $50-150 \text{ km}^2$ (Pickett, 1968). An analysis of the water drawn from the existing reservoir prior to pumping showed a high concentration of radium (Wrucke and Sheridan, 1968). This modern reservoir, at a depth of 3.6 km, is probably identical to that which was present in the regolith above the range front prior to Laramide uplift.

Extraction of mineral components by the hydrothermal fluid from the rock could have been accomplished by several mechanisms. Interaction between rock and water at a low water/rock ratio appreciably changes the composition of the fluid but not so much that of the rock (Bischoff et al., 1981). As a result, the water acquires proportionately large quantities of K, Ca, CO_2 , and metals (Dickson et al., 1979; Bischoff et al., 1981). Uranium is removed from rocks as a carbonate complex during decarbonation reactions (Yermolayev, 1971), suggesting that the relation between carbonate and uranium, noted for the deposition of the uranium in the veins, may have persisted back to the original derivation of the components from the source rocks. Elevated temperatures, especially at depth, induce decarbonation reactions in metamorphic carbonates (Barnes et al., 1973), and high water pressures along fault zones and adjacent rocks may further lower the stability of the carbonates (Winkler, 1974). Springs rich in CO_2 are closely related to major zones of seismicity, and a significant amount of CO_2 may be released as a result of decarbonation reactions (Irwin and Barnes, 1982). Carbon dioxide-rich springs in central

Colorado are probably similarly related to decarbonation of Proterozoic marble layers at depth (Barnes et al., 1978).

The Hydrothermal System

A convective hydrothermal system requires a plumbing system, heat, and fluids. The plumbing systems for the Schwartzwalder and other deposits of the Front Range were the complexly faulted, northwest-trending fault systems near the emerging range front. The steep dips of both the metamorphic rock layering and the faults produced deep conduits, especially where the foliation and competency of the rocks facilitated brecciation. Subsidiary faults, such as those at the Schwartzwalder deposit, enhanced the ground preparation by providing additional closely spaced conduits within the major fault system. Elsewhere, such as in the nearby Golden Gate Canyon district, the abundance of subsidiary fractures over a large area may have diluted the effect of invading fluids. The presence of a relatively impermeable schist adjacent to the conduit undoubtedly enhanced deposition at the Schwartzwalder and Ladwig mines (Wallace, 1979); pegmatites may have served the same function at the Ladwig and Ascension deposits. The Phanerozoic sedimentary rocks blanketed the entire basement, and, until penetrated by the fault systems, may have served as a cap on the hydrothermal system.

Evidence of Late Cretaceous magmatic activity has not been documented along the range front, but contemporaneous activity was prevalent in the nearby Colorado mineral belt to the west (Marvin et al., 1974). Regional heat flow was therefore probably much greater than the present magmatic geothermal gradient of $22.2^{\circ}\text{C}/\text{km}$ (Decker, 1969), and temperatures at a depth of 4 km could have exceeded 250°C . Contributions of heat from the north-east-trending mineral belt probably decreased southward along the range front. Because all but one deposit is in the northern half of the potentially favorable, metamorphic-dominated range front,

the high heat flow near the mineral belt may have influenced the observed distribution.

At the inception of uplift, the faults and regolith were charged with evolved "connate" waters that contained large quantities of carbonate. Fault movement, especially in the developing frontal zone, created large areas of locally high permeability with relatively low fluid potential (Berry, 1973). Convective circulation, induced by the inferred deep magmas, directed fluids towards brittle conduits such as that in the transition zone rocks at the Schwartzwalder mine. Major fault movement, perhaps enhanced by high fluid pressures along the faults at depth (Hubbert and Rubey, 1958), produced sudden increases in permeability and decreases in confining pressure. Repeated fault movements and increased rates of flow may have diminished the stability of the carbonate complexes in the invading fluids, thereby leading to the deposition of uranium. Although the initial fluids were derived from rocks in the fault zones and regolith, the isotopic data suggest the introduction of meteoric water by Stage IIc. This indicates that the faults by that time had penetrated the overlying cover of sedimentary rocks and allowed the influx of the less evolved fluids. However, continued deposition of large quantities of carbonate suggests that decarbonation reactions may have continued in carbonate-rich zones at depth.

The bottom of the Schwartzwalder ore deposit, although somewhat masked by subsequent clastic dikes, may represent the depth at which the decrease in confining pressure due to faulting and to ascent of the fluids was sufficient to weaken the carbonate complexes. This depth may have been somewhat greater along the larger and more open faults, such as the Rogers system, where the confining pressure may not have been as great as along the smaller subsidiary fractures. It may have also descended as the fracturing continued to open the system and thereby reduce the overall confining pressure.

Supergene mineralization of Stage III may be a much younger

event than the Laramide hypogene uranium deposition. Exposure of the top of the deposit, combined with post-Laramide faulting, would have permitted descending fluids to generate the late calcite-iron sulfide assemblage.

CHAPTER 9. SUMMARY AND CONCLUSIONS

The geology of the Schwartzwalder deposit has three principal components: (1) a metamorphosed, iron-rich sequence of Proterozoic sedimentary and volcanic rocks; (2) a major, steeply plunging synform; and (3) a complex, steeply dipping fault system. The combination of these three components produced a structural setting that facilitated the subsequent formation of the uranium deposit.

The foliated and layered metamorphic rocks include major units of hornblende gneiss and mica schist, with a transition sequence of garnet-biotite gneiss and quartzite. The sequence reflects a heterolithologic assemblage of mafic volcanoclastic units and calcareous argillites overlain by a chemically precipitated chert and a thick sequence of iron-rich pelites. The sequence probably formed in a shallow restricted basin in close proximity to submarine volcanism.

Proterozoic folding produced a synform whose axis plunges steeply to the south. The mica schist comprises the core of the fold, and is bounded successively by garnet-biotite gneiss, quartzite, and hornblende gneiss. Due to the steep plunge of the fold axis, the dip of the rock layering is also steep.

The northwest-trending Rogers fault system dips steeply to the east, and cuts the synform. The Illinois fault system dips steeply to the west and forms a cymoid-type fault between the two major strands of the Rogers fault. A somewhat younger Illinois fault, subparallel to and intersecting the earlier Illinois fault, formed after uranium mineralization. A stacked series of east-dipping tension fractures are prevalent in the hangingwall of the pre-ore Illinois fault. They probably developed as a result of normal movement along the pre-ore Illinois fault. The later Illinois fault segmented several of the tension fractures.

When disturbed during fault movement, the mica schist and hornblende gneiss units were more ductile and formed diffuse zones

and fractures filled with fault gouge. Fault movement in the relatively brittle rocks of the transition sequence generated broad zones of angular fault breccia with relatively little gouge.

The structural combination of the steeply dipping layers of the brittle transition zone and their offset by the steeply dipping fault system generated a laterally narrow, but extremely deep, system of continuous fault breccia. Invading hydrothermal fluids were concentrated along the open conduit.

The hydrothermal fluids produced two successive assemblages of wall rock alteration. The early carbonate-sericite assemblage pseudomorphically replaced all mafic minerals in the metamorphic rocks, but did not severely alter the felsic minerals. The ensuing hematite-adularia stage replaced the pre-existing alteration minerals immediately adjacent to the veins, and commonly destroyed all relict textures. Chemical analyses of fresh and altered rocks indicate a large influx of CO_2 into the carbonate-sericite zone, with a concomitant loss of SiO_2 .

Hypogene vein mineralization spanned three successive stages, and filled virtually all existing faults and related fractures except for the younger, post-ore Illinois fault. All mineralization filled open spaces, and was accompanied by repeated fault movement. The first stage is sparsely represented, and produced base-metal sulfides, adularia, and carbonate. Stage II was the major ore-forming period, and had three substages. The first two produced the uranium ores, which are composed of pitchblende and coffinite with ankerite, adularia, and various base-metal sulfides and sulfosalts. The third substage immediately followed the second, and is characterized by relatively coarse sulfides and carbonate. Stage III is partly hypogene, with evidence of high-pressure fluids. The later part, however, is dominantly supergene. Carbonate, pyrite, and marcasite are typical of the entire stage. Several generations of clastic dikes, composed of fault-generated microbreccias, were injected into new and existing fractures. Uranium mineralization does not extend below the 16th

level on the Illinois and horsetail systems, or below the 21st level on the Rogers fault. Analytical data from vein samples indicate a strong correlation between uranium and volatile elements, but a complete absence of vertical or lateral elemental zoning.

Vein mineralization took place 70-72 m.y. ago. Tectonic reconstructions indicate that this age corresponds to the incipient stages of Laramide uplift of the range front. As a result, the present top of the deposit was buried beneath about 3 km of Phanerozoic sedimentary rocks at the time of mineralization. Evidence from fission track ages in apatite indicate a relatively high heat flow.

Alteration and early vein mineralization formed at 225°C and 750-1000 bars, but mineralization in Stage IIc took place at 125°C and somewhat lower pressures. Early alteration is the product of CO₂ metasomatism with relatively slow flow rates of the altering fluids. Major brecciation increased the permeability and thereby increased the flow rate and lowered the pressure. The pH increased and oxygen fugacity decreased as CO₂ was evolved from the fluid. The increased alkalinity of the fluid produced the hematite-adularia alteration. Loss of CO₂ reduced the solubilities of carbonate and adularia. Uranium, which was carried in a uranyl dicarbonate complex, was released as the complexes became unstable with CO₂ loss. Reduced and intermediate sulfur species in solution reduced the uranyl ion and induced the precipitation of pitchblende with sulfides, ankerite, and adularia.

Geologic and isotopic evidence indicate that the uranium, lead, carbonate, and some water were derived from the metamorphic terrane, especially the major hornblende gneiss units. The frontal zone of the developing range front was intensely faulted by the interaction of the northwest-trending faults and the range-bounding reverse faults. Fluids residing in the faults were drawn into the more permeable zones. Heat was supplied by the increased regional heat flow produced by igneous activity in the nearby Colorado mineral belt. Dilation in the frontal zone, combined

with the heat, caused the fluids to migrate into the most permeable segments of the fault zones.

In conclusion, the interaction of several essential factors led to the formation of the uranium deposits along the range front. These include:

- (1) A source terrane: uranium as well as the carbonate were provided by the hornblende gneiss, which represents submarine volcanic and volcanoclastic units with related clastic and chemical sediments.
- (2) A complex, interconnected fault system: the northwest-trending fault system served as a fluid reservoir, as the conduit for migrating hydrothermal fluids, and as the mechanism that generated sudden decreases in confining pressure.
- (3) Heat: magmatic activity in the nearby mineral belt profoundly increased the heat flow in the crystalline basement and induced convective circulation. Heat may have been provided by as yet unexposed intrusives along the range front, although this interpretation is purely speculative.
- (4) Depth of formation: the deep burial produced high fluid and gas pressures and increased the ambient temperature. Sudden reductions in confining pressures with fault movement lowered the stability of complexes in the high-pressure fluids.

Only in a restricted segment of the eastern range front did all factors combine to form the uranium deposits. Similar settings are present along the flanks of the other Laramide uplifts in the Rocky Mountain region.

REFERENCES

- Abbott, J. T., 1972, Rb-Sr study of isotopic redistribution in a Precambrian mylonite-bearing shear zone, northern Front Range, Colorado: Geol. Soc. Amer. Bull. v. 83, p. 487-494.
- Adams, J. W., and Stugard, Frederick, Jr., 1956, Wall-rock control of certain pitchblende deposits in Golden Gate Canyon, Jefferson County, Colorado: U.S. Geol. Survey Bulletin 1030-G, p. 187-209.
- Barker, Fred, and Friedman, Irving, 1969, Carbon isotopes in pelites of the Precambrian Uncompahgre formation, Needle Mountains, Colorado: Geol. Soc. America Bull., v. 80, p. 1403-1408.
- Barnes, H. L., and Kullerud, G., 1961, Equilibria in sulfur-containing aqueous solutions, in the system Fe-S-O, and their correlation during ore deposition: Econ. Geol., v. 56, p. 648-688.
- Barnes, Ivan, Irwin, W. P., and White, D. E., 1978, Global distribution of carbon dioxide discharges and major zones of seismicity: U.S. Geol. Survey Water Res. Invest. Open-file Report 78-39, 12 p.
- Barnes, Ivan, O'Neil, J. R., Rapp, J. B., and White, D. B., 1973, Silica-carbonate alteration of serpentine: wall rock alteration in mercury deposits of the California Coast Ranges: Econ. Geol., v. 68, p. 388-398.
- Barton, P. B., and Toulmin, Priestly, Jr., 1961, Some mechanisms for cooling hydrothermal fluids: U.S. Geol. Survey Prof. Paper 424-D, p. D348-D352.
- Berry, F. A. F., 1973, High fluid potentials in California Coast Ranges and their tectonic significance: American Assoc. Pet. Geol. Bull., v. 57, p. 1219-1249.
- Bird, A. G., 1958, The petrology and ore deposits of the Schwartzwalder uranium mine, Jefferson County, Colorado: unpubl. Master's thesis, Univ. of Colorado, Boulder.
- _____, 1979, An epigenetic model for the formation of the Schwartzwalder uranium deposit - a discussion: Econ. Geol., v. 74, p. 947-948.
- Bischoff, J. L., Radtke, A. S., and Rosenbauer, R. J., 1981, Hydrothermal alteration of graywacke by brine and seawater: roles of alteration and chloride complexing on metal solubilization at 200° and 350°C: Econ. Geol., v. 76, p. 659-676.

- Boone, G. M., 1969, Origin of clouded red feldspars: petrologic constraints in a granitic porphyry intrusion: *Amer. Jour. Sci.* v. 267, p. 633-668.
- Bottinga, Y., 1968, Calculation of fractionation factors for carbon and oxygen exchange in the system calcite-carbon dioxide-water: *Jour. Phys. Chemistry*, v. 72, p. 800-808.
- Browne, P. R. L., and Ellis, A. J., 1970, The Ohaki-Broadlands hydrothermal area, New Zealand: mineralogy and related geochemistry: *Amer. Jour. Sci.*, v. 269, p. 97-131.
- Bryant, Bruce, McGrew, L. W., and Wobus, R. A., 1981, Geologic map of the Denver 1° x 2° quadrangle, north-central Colorado: U.S. Geol. Survey Map I-1163.
- Bryant, B., and Naeser, C. W., 1980, The significance of fission-track ages of apatite in relation to the tectonic history of the Front and Sawatch Ranges, Colorado: *Geol. Soc. America Bull.*, v. 91, p. 156-164.
- Casadevall, Tom, and Ohmoto, Hiroshi, 1977, Sunnyside mine, Eureka mining district, San Juan County, Colorado: Geochemistry of gold and base metal ore deposition in a volcanic environment: *Econ. Geol.*, v. 72, p. 1285-1320.
- Chinner, G. A., 1960, Pelitic gneisses with varying ferrous/ferric ratios from Glen Clova, Angus, Scotland: *J. Petrol.*, v. 1, p. 178-217.
- Clayton, R. N., O'Neil, J. R., and Mayeda, T. K., 1972, Oxygen isotope exchange between quartz and water: *Jour. Geophys. Research*, v. 77, p. 3057-3067.
- Couples, Gary, and Stearns, D. W., 1978, Analytical solutions applied to structures of the Rocky Mountains foreland on local and regional scales; in Matthews, V., ed., Laramide folding associated with basement block faulting in the western United States: *Geol. Soc. America Memoir* 151, p. 313-335.
- Coveney, R. M., Jr., 1981, Gold quartz veins and auriferous granite at the Oriental Mine, Alleghany District, California: *Econ. Geol.*, v. 76, p. 2176-2199.
- Crerar, D. A., and Barnes, H. L., 1976, Ore solution chemistry V. Solubilities of chalcopyrite and chalcocite assemblages in hydrothermal solution at 200° to 350°C: *Econ. Geol.*, v. 71, p. 772-794.

- Cuney, Michel, 1978, Geologic environment, mineralogy, and fluid inclusions of the Bois Noirs-Limouzat uranium vein, Forez, France: *Econ. Geol.*, v. 73, p. 1567-1611.
- Czamanske, G. K., and Rye, R. O., 1974, Experimentally determined sulfur isotope fractionation between sphalerite and galena in the temperature range 600°C to 275°C: *Econ. Geol.*, v. 69, p. 17-25.
- Davis, J. C., 1973, *Statistics and Data Analysis in Geology*. John Wiley & Sons, New York, 550 p.
- Decker, E. R., 1969, Heat flow in Colorado and New Mexico: *Jour. Geophysical Research*, v. 74, p. 550-559.
- DeVoto, R. H., and Paschis, J. A., 1980, Geology of uranium vein deposits (including Schwartzwalder Mine) in Proterozoic metamorphic rocks, Front Range, Colorado: in *Proceedings of the Pine Creek Geosyncline Symposium*, p. 683-692.
- Dickson, F. W., Rye, R. O., and Radtke, A. S., 1979, The Carlin gold deposit as a product of rock-water interactions: Nevada Bureau of Mines and Geology, Report 33, p. 101-108.
- Downs, G. R., and Bird, A. G., 1965, The Schwartzwalder uranium mine, Jefferson County, Colorado: *Mountain Geologist*, v. 2, p. 183-191.
- Eichmann, R., and Schidlowski, M., 1975, Isotopic fractionation between coexisting organic carbonate-carbonate pairs in Precambrian sediments: *Geochim. Cosmochim. Acta*, v. 39, p. 585-595.
- Ellis, A. J., 1963, The solubility of calcite in carbon dioxide solutions: *Amer. Jour. Sci.*, v. 57, p. 354-365.
- _____, 1970, Quantitative interpretation of chemical characteristics of hydrothermal systems: *Geothermics*, Spec. Issue 2, p. 516-528.
- _____, 1979, Explored geothermal systems; in Barnes, H. L., ed., *Geochemistry of hydrothermal ore deposits*. John Wiley & Sons, New York, p. 632-683.
- Engelder, J. T., 1974, Cataclasis and the generation of fault gouge: *Geol. Soc. America Bull.*, v. 85, p. 1515-1522.
- Engelder, J. T., Logan, J. M., and Handin, J., 1975, The sliding characteristics of sandstone on quartz fault-gouge: *Pure and Applied Geophysics*, v. 113, p. 69-86.

- Epis, R. C., and Chapin, C. E., 1975, Geomorphic and tectonic implications of the post-Laramide, late Eocene erosion surface in the southern Rocky Mountains; in Curtis, B., ed., Cenozoic history of the southern Rocky Mountains: Geol. Soc. America Memoir 144, p. 45-74.
- Ewers, G. R., and Keays, R. R., 1977, Volatile and precious metal zoning in the Broadlands geothermal field, New Zealand: Econ. Geol., v. 72, p. 1337-1354.
- Faure, Gunter, 1977, Principles of Isotope Geology. John Wiley & Sons, New York, 464 p.
- Ferris, C. S., and Bennett, Norman, 1977, Geochemical prospecting at the Ladwig uranium mine, near Golden, Colorado; in Campbell, J. A., ed., Short Papers of the U.S. Geological Survey Uranium-Thorium Symposium, 1977: U.S. Geol. Survey Circular 753, p. 66-68.
- Field, C. W., 1966, Sulfur isotopic method for discriminating between sulfates of hypogene and supergene origin: Econ. Geol., v. 61, p. 1428-1435.
- Fisher, J. C., 1976, Remote sensing applied to exploration for vein-type uranium deposits, Front Range, Colorado: Colo. Sch. Mines Remote Sensing Report 76-2, 157 p.
- Flanigan, V. J., 1977, Surface geophysical methods applied to uranium exploration in crystalline terranes; in Campbell, J. A., ed., Short papers of the U.S. Geological Survey Uranium-Thorium Symposium, 1977: U.S. Geol. Survey Circular 753, p. 5-6.
- Fournier, R. O., and Truesdell, A. H., 1973, An empirical Na-K-Ca geothermometer for natural waters: Geochim. Cosmochim. Acta, v. 37, p. 1255-1275.
- Gandhi, S. S., 1978, Geologic setting and genetic aspects of uranium occurrence in the Kaipokok Bay-Big River area, Labrador: Econ. Geol., v. 73, p. 1492-1522.
- Garrels, R. M., and Naeser, C. R., 1958, Equilibrium distribution of dissolved sulphur species in water at 25°C and 1 atm total pressure: Geochim. Cosmochim. Acta, v. 15, p. 113-130.
- Giggenbach, W. F., 1974, Equilibria involving polysulfide ions in aqueous sulfide solutions up to 240°C: Inorg. Chem., v. 13, p. 1724-1730.
- Giordano, T. H., and Barnes, H. L., 1981, Lead transport in Mississippi Valley-type ore solutions: Econ. Geol., v. 76, p. 2200-2211.

- Goodwin, A. M., Monster, J., and Thode, H. G., 1976, Carbon and sulfur isotope abundances in Archean iron-formations and Early Precambrian life: *Econ. Geol.*, v. 71, p. 870-891.
- Grauch, R. I., 1978, Geology of the uranium prospect at Camp Smith, New York, with a model for the formation of uranium deposits in metamorphosed submarine volcanogenic rocks: U.S. Geol. Survey Open-file Report 78-949, 29 p.
- Grindley, G. W., and Browne, P. R. L., 1976, Structural and hydrological factors controlling the permeabilities of some hot-water geothermal fields: *Proceedings, 2nd U.N. Symp. on the Devel. and Use of Geothermal Resources*, v. 1, p. 377-386.
- Gronvold, F., and Westrum, E. F., Jr., 1976, Heat capacities of iron disulfides: Thermodynamics of marcasite from 5 to 700 K, pyrite from 300 to 780 K, and the transformation of marcasite to pyrite: *Jour. Chem. Thermodynamics*, v. 8, p. 1039-1048.
- Haas, J. L., Jr., 1971, The effect of salinity on the maximum thermal gradient of a hydrothermal system at hydrostatic pressure: *Econ. Geol.*, v. 66, p. 940-946.
- Helgeson, H. C., 1969, Thermodynamics of hydrothermal systems at elevated temperatures and pressures: *Amer. Jour. Sci.*, v. 267, p. 729-804.
- Helgeson, H. C., Delany, J. M., Nesbitt, H. W., and Bird, D. K., 1978, Summary and critique of the thermodynamic properties of rock-forming minerals: *Amer. Jour. Science*, v. 278A, p. 1-229.
- Hemley, J. J., 1959, Some mineralogical equilibria in the system $K_2O-Al_2O_3-SiO_2-H_2O$: *Amer. Jour. Sci.*, v. 257, p. 241-270.
- Heyse, J. V., 1972, Mineralogy and paragenesis of the Schwartzwalder Mine uranium ore, Jefferson County, Colorado: U.S. Atomic Energy Commission Report GJO-912-1, 87 p.
- Hills, F. A., and Houston, R. S., 1979, Early Proterozoic tectonics of the central Rocky Mountains, North America: *Contributions to Geology*, Univ. of Wyo., v. 17, p. 89-106.
- Hoagland, J. R., and Elders, W. A., 1978, Hydrothermal mineralogy and isotopic geochemistry in the Cerro Prieto geothermal field, Mexico. I. Hydrothermal Mineral Zonation: *Geoth. Resources Council, Transactions*, v. 2, p. 283-286.

- Hoblitt, R., and Larson, E., 1975, Paleomagnetic and geochronologic data bearing on the structural evolution of the north-eastern margin of the Front Range, Colorado: Geol. Soc. America Bull., v. 86, p. 237-242.
- Holland, H. D., 1959, Some applications of thermochemical data to problems of ore deposits: I. Stability relations among the oxides, sulfides, sulfates, and carbonates of ore and gangue minerals: Econ. Geol., v. 54, p. 184-233.
- _____, 1965, Some applications of thermochemical data to problems of ore deposits II. Mineral assemblages and the composition of ore-forming fluids: Econ. Geol., v. 60, p. 1101-1166.
- Holland, H. D., and Malinin, S. D., 1979, The solubility and occurrence of non-ore minerals; in Barnes, H., ed., Geochemistry of Hydrothermal Ore Deposits. John Wiley & Sons, N. Y., p. 461-508.
- Hollister, L. S., 1966, Garnet zoning: an interpretation based on the Rayleigh fractionation model: Science, v. 154, p. 1608-1622.
- Honea, R. M., and Ferris, C. S., unpub. report, Mineralogy and paragenesis of the Schwartzwalder Mine, Jefferson County, Colorado: Cotter Corp., 37 p.
- Hubbert, M. K., and Rubey, W. W., 1959, Role of fluid pressure in mechanics of overthrust faulting. I. Mechanics of fluid-filled porous solids and its application to overthrust faulting: Geol. Soc. America Bull., v. 70, p. 115-166.
- Immeys, I. P., and Klein, C., Jr., 1976, Mineralogy and petrology of some metamorphic Precambrian iron formations in southwestern Montana: Amer. Mineral., v. 61, p. 1117-1144.
- Irwin, W. P., and Barnes, Ivan, 1975, Effect of geologic structure and metamorphic fluids on the seismic behavior of the San Andreas fault system in central and northern California: Geology, v. 3, p. 714-716.
- _____, 1982, Map showing relation of carbon dioxide-rich springs and gas wells to the tectonic framework of the conterminous United States: U.S. Geol. Survey Map I-1301.
- James, H. L., 1954, Sedimentary facies of iron-formation: Econ. Geol., v. 49, p. 235-293.
- _____, 1966, Chemistry of the iron-rich sedimentary rocks: U.S. Geol. Survey Prof. Paper 440-W, 61 p.

- Jensen, M. L., Field, C. W., Nakai, Nobuyuki, 1960, Sulfur isotopes and the origin of sandstone-type uranium deposits: Biennial Progress Report for 1959-1960, U.S. Atomic Energy Commission Contract AT (30-1)-2261, 281 p.
- Keith, T. E. C., White D. E., and Beeson, M. H., 1978, Hydrothermal alteration and self-sealing in Y-7 and Y-8 drill holes in northern part of Upper Geyser Basin, Yellowstone National Park, Wyoming: U.S. Geol. Survey Prof. Paper 1054-A, 26 p.
- Kellogg, K. S., 1973, A paleomagnetic study of various Precambrian rocks in the northeastern Colorado Front Range and its bearing on Front Range rotations: unpubl. Ph.D. thesis, University of Colorado, Boulder, 177 p.
- Klein, Cornelius, Jr., 1966, Mineralogy and petrology of the metamorphosed Wabush iron-formation, southwestern Labrador: Jour. Petrology, v. 7, p. 246-305.
- _____, 1973, Changes in mineral assemblages with metamorphism of some banded Precambrian iron-formations: Econ. Geol., v. 68, p. 1075-1088.
- Kluth, C. F., and Coney, P. J., 1981, Plate tectonics of the Ancestral Rocky Mountains: Geology, v. 9, p. 10-15.
- Leake, B. E., 1978, Nomenclature of amphiboles: Amer. Mineral., v. 63, p. 1023-1052.
- LeMaitre, R. W., 1976, The chemical variability of some common igneous rocks: J. Petrol., v. 17, p. 589-637.
- Lemlein, G. G., and Klevtsov, P. V., 1961, Relations among the principal thermodynamic parameters in a part of the system H_2O-NCl : Geochemistry, no. 2, p. 148-158.
- Lickus, R. J., and LeRoy, L. W., 1968, Precambrian structure and stratigraphy along the mountain front west of Golden, Jefferson County, Colorado - a reconnaissance study: Colo. School Mines Quart., v. 63, p. 129-165.
- Logan, J. M., and Shimamoto, T., 1976, The influence of calcite gouge on the frictional sliding of Tennessee Sandstone: EOS, v. 57, p. 1011.
- Lovering, T. S., and Goddard, E. N., 1950, Geology and ore deposits of the Front Range, Colorado: U.S. Geol. Survey Professional Paper 223, 319 p.

- Mahon, W. A. J., McDowell, G. D., and Finlayson, J. B., 1980, Carbon dioxide: its role in geothermal systems: New Zeal. Jour. Sci., v. 23, p. 133-148.
- Marsh, S. P., and Sheridan, D. M., 1976, Rutile in Precambrian sillimanite-quartz gneiss and related rocks, east-central Front Range, Colorado: U.S. Geol. Survey Prof. Paper 959-G, 17 p.
- Marvin, R. F., and Dobson, S. W., 1979, Radiometric ages: compilation B: U.S. Geological Survey: Isochron West, no. 25.
- Marvin, R. F., Young, E. J., Mehnert, H. H., and Naeser, C. W., 1974, Summary of radiometric age determinations on Mesozoic and Cenozoic igneous rocks and uranium and base metal deposits in Colorado: Isochron West, no. 11, p. 1-41.
- Maslyn, R. M., 1978, An epigenetic model for the formation of the Schwartzwalder uranium deposit: Econ. Geol., v. 73, p. 552-557.
- Matthews, Vincent, III., and Work, D. F., 1978, Laramide folding associated with basement block faulting along the north-eastern flank of the Front Range, Colorado: Geol. Soc. America Memoir 151, p. 101-124.
- Moench, R. H., 1964, Geology of Precambrian rocks, Idaho Springs district, Colorado: U.S. Geol. Survey Bull. 1182-A, 70 p.
- Naeser, C. W., 1978, Fission track dating: U.S. Geol. Survey Open-file Report 76-190.
- Naeser, C. W., and Faul, H., 1969, Fission track annealing in apatite and sphene: Jour. Geophys. Res., v. 74, p. 705-710.
- Nash, J. T., Granger, H. C., and Adams, S. S., 1981, Geology and concepts of genesis of important types of uranium deposits: Econ. Geol., 75th Anniversary Volume, p. 63-116.
- Naumov, G. B., Motorina, Z. M., and Naumov, V. B., 1971, Conditions of formation of carbonates in veins of the lead-cobalt-nickel-silver-uranium type: Geochem. Int., v. 6, p. 590-598.
- Nelson, C. E., and Gallagher, J. R. L., 1981, Early Proterozoic origin for uranium mineralization in the Colorado Front Range: Geol. Soc. America Abst. Progs., v. 13, no. 4, p. 220.
- Nockolds, S. R., 1954, Average chemical composition of some igneous rocks: Geol. Soc. America Bull., v. 65, p. 1007-1032.

- Northrop, D. A., and Clayton, R. N., 1966, Oxygen-isotope fractionations in systems containing dolomite: Jour. Geology, v. 74, p. 174-196.
- Norton, Denis, and Cathles, L. M., 1979, Thermal aspects of ore deposition; in Barnes, H., ed., Geochemistry of Hydrothermal Ore Deposits (2nd ed.). John Wiley & Sons, New York, p. 611-631.
- Ohmoto, Hiroshi, 1972, Systematics of sulfur and carbon isotopes in hydrothermal ore deposits: Econ. Geol., v. 67, p. 551-578.
- Ohmoto, Hiroshi, and Rye, R. O., 1974, Hydrogen and oxygen isotopic compositions of fluid inclusions in the Kuroko deposits, Japan: Econ. Geol., v. 69, p. 947-953.
- _____, 1979, Isotopes of sulfur and carbon; in Barnes, H., ed., Geochemistry of Hydrothermal Ore Deposits. John Wiley & Sons, New York, p. 509-567.
- O'Neil, J. R., Clayton, R. N., and Mayeda, T. K., 1969, Oxygen isotope fractionation in divalent metal carbonates: Jour. Chem. Physics, v. 51, p. 5547-5558.
- Paschis, J. A., 1979, Mining and geologic developments at Cotter Corporations's Schwartzwalder uranium mine, Jefferson County, Colorado: Colo. Mining Assoc., 1979 Mining Yearbook, p. 123-129.
- Peterman, Z. E., and Hedge, C. E., 1968, Chronology of Precambrian events in the Front Range, Colorado: Can. Jour. Earth Sci., v. 5, p. 749-756.
- Pickett, G. R., 1968, Properties of the Rocky Mountain Arsenal disposal reservoir and their relation to Derby earthquakes: Colo. Sch. Mines Quarterly, v. 63, p. 73-100.
- Pierce, W. G., 1979, Clastic dikes of Heart Mountain fault breccia, northwestern Wyoming, and their significance: U.S. Geol. Survey Prof. Paper 1133, 25 p.
- Potter, R. W., Clynne, M. A., and Brown, D. L., 1978, Freezing point depression of aqueous chloride solutions: Econ. Geol., v. 73, p. 284-285.
- Ramdohr, Paul, 1980, The Ore Minerals and their Intergrowths, 2nd edition. Pergamon Press, Inc., New York, 1229 p.

- Rich, R. A., and Barabas, A. H., 1976, Mineralogy, paragenesis, fluid inclusions, and origin of the Schwartzwalder uranium mine, Jefferson County, Colorado: Geol. Soc. America Abst. Programs, v. 8, no. 6, p. 1068.
-
- _____, unpub., Genetic implications of preliminary mineralogic, paragenetic, and fluid inclusion data for the Schwartzwalder uranium mine, Colorado, U.S.A.: Int. Atomic Energy Agency, Lisbon, 1979.
- Rich, R. A., Holland, H. D., and Peterson U., 1977, Hydrothermal Uranium Deposits: Elsevier, New York, 264 p.
- Robie, R. A., Hemingway, B. S., Fisher, J. R., 1978, Thermodynamic properties of minerals and related substances at 298.15 K and 1 bar (10^5 pascals) pressure and at higher temperatures: U.S. Geol. Survey Bull. 1452, 456 p.
- Robinson, B. W., and Ohmoto, H., 1973, Mineralogy, fluid inclusions, and stable isotopes of the Echo Bay U-Ni-Ag-Cu deposits, Northwest Territories, Canada: Econ. Geol., v. 68, p. 635-656.
- Roedder, Edwin, 1968, The noncolloidal origin of "colloform" textures in spharelite ores: Econ. Geol., v. 63, p. 451-471.
-
- _____, 1972, Composition of fluid inclusions: U.S. Geol. Survey Prof. Paper 440JJ.
- Romberger, S. B., 1978, Hydrothermal transport and deposition of uranium, and the origin of vein uranium deposits: Geol. Soc. America Abst. Progs., v. 10, no. 7, p. 480.
- Rosenberg, P. E., Burt, D. M., and Holland, H. D., 1967, Calcite-dolomite-magnesite stability relations in solutions: the effect of ionic strength: Geochim. Cosmochim. Acta, v. 31, p. 391-396.
- Sakai, H., 1968, Isotopic properties of sulfur compounds in hydrothermal processes: Geochem. Jour., v. 2, p. 29-49.
- Sass, J. H., Lachenbruch, A. H., Munroe, R. J., Greene, G. W., and Moses, T. H., 1971, Heat flow in the western United States: Jour. Geophys. Res., v. 76, p. 6376-6413.
- Sassano, G. P., Fritz, P., and Morton, R. D., 1972, Paragenesis and isotopic composition of some gangue minerals from the uranium deposits of Eldorado, Saskatchewan: Can. Jour. Earth Sci., v. 9, p. 141-157.

- Scott, G. R., 1963, Bedrock geology of the Kassler quadrangle, Colorado: U.S. Geol. Survey Prof. Paper 421-B, 125 p.
- _____, 1972, Geologic map of the Morrison quadrangle, Jefferson County, Colorado: U.S. Geol. Survey Map I-790-A.
- Sergeyeva, E. I., Nikitin, A. A., Khodakovsky, I. L., and Naumov, G. B., 1972, Experimental investigation of equilibria in the system $\text{UO}_3\text{-CO}_2\text{-H}_2\text{O}$ in 25°-200°C temperature interval: *Geochem. Int.*, v. 9, p. 900-910.
- Sheppard, S. M. F., and Schwarcz, H. P., 1970, Fractionation of carbon and oxygen isotopes and magnesium between metamorphic calcite and dolomite: *Contr. Min. and Petrol.*, v. 26, p. 161-198.
- Sheridan, D. M., and Raymond, W. H., 1977, Preliminary data on some Precambrian deposits of zinc-copper-lead sulfides and zinc spinel (gahnite) in Colorado: U.S. Geol. Survey Open-file Report 77-607, 27 p.
- Sheridan, D. M., Maxwell, C. H., and Albee, A. L., 1967, Geology and uranium deposits of the Ralston Buttes District, Jefferson County, Colorado: U.S. Geological Survey Professional Paper 520, 121 p.
- Silberman, M. L., White, D. E., Keith, T. E. C., and Docktor, R. D., 1979, Duration of hydrothermal activity at Steamboat Springs, Nevada, from ages of spatially associated volcanic rocks: U.S. Geol. Survey Prof. Paper 458-D, 14 p.
- Simmons, E. C., and Hedge, C. E., 1978, Minor-element and Sr-isotope geochemistry of Tertiary stocks, Colorado Mineral Belt: *Contrib. Mineral. and Petrol.*, v. 67, p. 379-396.
- Sims, P. K., and Gabb, D. J., 1967, Petrology and structure of Precambrian rocks, Central City quadrangle, Colorado: U.S. Geol. Survey Prof. Paper 554-E, 56 p.
- Sims, P. K., and Sheridan, D. M., 1964, Geology of uranium deposits in the Front Range, Colorado: U.S. Geological Survey Bulletin, 1159, 116 p.
- Snow, D. T., 1968, Hydraulic character of fractured metamorphic rocks of the Front Range and implications to the Rocky Mountain Arsenal well: *Colo. Sch. Mines Quarterly*, v. 63, p. 167-199.
- Spirakis, C. S., 1981, The possible role of sulfate reduction kinetics in the formation of hydrothermal uranium deposits: *Econ. Geol.*, v. 76, p. 2236-2239.

- Stark, J. H., 1979, Geology of the Mena mine area with emphasis on the mineralogy and paragenesis of the Mena mine deposit, Jefferson County, Colorado: unpubl. Master's thesis, Colorado State Univ., Fort Collins, 164 p.
- Stearns, D. W., 1978, Faulting and forced folding in the Rocky Mountains foreland; in Matthews, V., ed., Laramide folding associated with basement block faulting in the western United States: Geol. Soc. America Memoir 151, p. 1-37.
- Takenouchi, S., and Kennedy, G. C., 1964, The binary system H_2O-CO_2 at high temperatures and pressures: Amer. Jour. Sci., v. 262, p. 1055-1074.
- Taylor, H. P., Jr., 1979, Oxygen and hydrogen isotope relationships in hydrothermal mineral deposits: in Barnes, H. L., ed., Geochemistry of Hydrothermal Ore Deposits, (2nd ed.). John Wiley & Sons, New York, p. 236-277.
- Taylor, R. B., 1975, Geologic map of the Black Hawk quadrangle, Gilpin, Jefferson, and Clear Creek Counties, Colorado: U.S. Geol. Survey Map GQ-1248.
- Turner, F.J., 1981, Metamorphic Petrology. McGraw-Hill, New York, 524 p.
- Tweto, Ogden, 1975, Laramide (Late Cretaceous-early Tertiary) orogeny in the Southern Rocky Mountains; in Curtis, B., ed., Cenozoic history of the Southern Rocky Mountains: Geol. Soc. America Memoir 144, p. 1-44.
- _____, 1977, Nomenclature of Precambrian rocks in Colorado: U.S. Geol. Survey Prof. Paper 1422-D, 22 p.
- _____, 1979, Geologic map of Colorado: U.S. Geological Survey.
- Tweto, Ogden, and Sims, P. K., 1963, Precambrian ancestry of the Colorado Mineral Belt: Geol. Soc. America Bull., v. 74, p. 991-1014.
- Usdowski, H. Z., and Barnes, H. C., 1972, Untersuchungen uber das Gleichgewicht zwischen K-Feldspat, Quarz and Muskovit und die Anwendung auf Fragen der Gesteinsbildung bei tieferen Temperaturen: Contr. Mineralogy Petrology, v. 36, p. 207-219.
- Van Horn, Richard, 1972, Surficial and bedrock geologic map of the Golden quadrangle, Jefferson County, Colorado: U.S. Geol. Survey Map I-761-A.

- Van Horn, Richard, 1976, Geology of the Golden quadrangle, Colorado: U.S. Geol. Survey Prof. Paper 872, 116 p.
- Voight, Barry, 1973, Clastic fluidization phenomena and the role of fluid pressure in mechanics of natural rock deformation: Geol. Soc. America Abst. Programs, v. 5, no. 2, p. 233.
- Walker, T. R., 1967, Formation of red beds in modern and ancient deserts: Geol. Soc. America Bull., v. 78, p. 353-368.
- _____, 1975, Intrastratal sources of uranium in first-cycle, nonmarine red beds: Amer. Assoc. Pet. Geol., v. 59, p. 925.
- Wallace, A. R., 1979, Alteration and vein mineralization, Ladwig uranium mine, Jefferson County, Colorado: U.S. Geol. Survey Open-file Report 79-1615, 34 p.
- Wallace, A. R., and Karlson, R. C., 1982, Alteration and vein mineralization, Schwartzwalder uranium mine, Jefferson County, Colorado: Geol. Soc. America Abst. with Programs, v. 14, no. 6, p. 353.
- Wallace, A. R., in press, Structural and mineralogical characteristics and distribution of carbonate-dominated fault breccia associated with uranium deposits, Front Range, Colorado: Economic Geology.
- Warner, L. A., 1980, The Colorado Lineament: Colorado Geology, p. 11-21.
- Weimer, R. J., and Tillman, R. W., 1980, Tectonic influence on deltaic shoreline facies, Fox Hills Sandstone, west-central Denver, Basin: Prof. Contrib., Colorado Sch. Mines, no. 10, 131 p.
- Weissberg, B. G., 1969, Gold-silver ore-grade precipitates from New Zealand thermal waters: Econ. Geol., v. 64, p. 95-108.
- White, D. E., Hem, J. D., and Waring, G. A., 1963, Chemical composition of sub-surface waters: U.S. Geol. Survey Prof. Paper 440-F, p. 1-67.
- White, W. H., Bookstrom, A. A., Kamilli, R. J., Ganster, M. W., Smith, R. P., Ranta, D. E., and Steininger, R. C., 1981, Character and origin of Climax-type molybdenum deposits: Econ. Geol., 75th Anniv. Volume, p. 270-316.
- Winkler, H. G. F., 1974, Petrogenesis of metamorphic rocks: (3rd ed.). Springer-Verlag, New York, 320 p.

- Woolsey, T. S., McCallum, M. E., and Schumm, S. A., 1975, Modeling of diatreme emplacement by fluidization: Phys. Chem. of the Earth, v. 9, p. 29-42.
- Wright, J. H., 1980, Economic geology of the Schwartzwalder Mine; in Uranium resource technology, v. III: Golden, Colo. Sch. Mines Press, p. 73-92.
- Wright, J. H., Wallace, A. R., and Karlson, R. C., 1981, New studies at the Schwartzwalder Mine, Jefferson County, Colorado: Can. Inst. Mining, Geol. Division, Uranium Symposium and Field Tours, 1981, p. 25-26.
- Wrucke, C. T., and Sheridan, D. M., 1968, Precambrian rocks penetrated by the deep disposal well at the Rocky Mountain Arsenal, Adams County, Colorado: U.S. Geol. Survey Prof. Paper 600-B, p. 852-859.
- Yermolayev, N. P., 1971, Processes of redistribution and extraction of uranium in progressive metamorphism: Geochem. Int., v. 6, p. 599-609.
- Young, E. J., 1977, Geologic, radiometric, and mineralogic maps and underground workings of the Schwartzwalder uranium mine and area, Jefferson County, Colorado: U.S. Geol. Survey Open-file Report 77-725, 38 p.
- _____, 1979a, Analytical data on the Schwartzwalder uranium deposit, Jefferson County, Colorado: U.S. Geol. Survey Open-file Report 79-968, 34 p.
- _____, 1979b, Genesis of the Schwartzwalder uranium deposit, Jefferson County, Colorado: Contributions to Geology, Univ. of Wyoming, v. 17, no. 2, p. 179-186.

APPENDIX

Table A1. Chemical analyses of altered hornblende gneiss.

	80S7	80S14	80S27	80S30	80S34	80S41	80S66	80S79	80S80*	80S65*
SiO ₂ (%)	30.90	39.40	42.50	40.90	37.50	39.60	35.80	30.70	35.40	39.30
Al ₂ O ₃	12.20	13.80	13.90	13.70	13.50	11.90	13.50	18.10	12.50	12.90
Fe (total)	9.76	12.30	8.14	9.97	8.96	8.68	7.99	10.80	7.42	8.04
FeO	8.59	10.20	7.07	8.32	7.74	7.87	7.56	—	—	7.52
Fe ₂ O ₃	1.17	2.33	1.19	1.83	1.35	0.90	0.48	—	—	0.58
MgO	5.39	4.00	5.36	4.30	4.20	4.70	4.60	4.40	4.90	3.60
CaO	13.00	5.97	6.53	8.12	10.50	7.82	11.90	8.81	11.00	9.64
Na ₂ O	<0.20	2.10	3.30	2.90	3.50	0.50	3.00	<0.20	0.40	2.10
K ₂ O	5.94	4.22	4.18	2.72	3.18	9.62	2.43	6.52	7.95	6.37
TiO ₂	0.80	3.78	0.82	1.72	1.42	0.79	1.14	1.85	1.31	1.08
P ₂ O ₅	0.20	0.57	0.20	0.50	0.20	0.10	0.20	0.40	0.30	0.20
MnO	0.22	0.38	0.20	0.19	0.19	0.21	0.21	0.20	0.22	0.16
LOI	21.36	14.58	14.25	13.65	16.38	14.98	17.46	16.89	16.34	14.58
C (total)	5.46	3.76	3.82	3.67	4.38	4.26	4.77	4.23	4.67	4.28
C (org.)	0.16	0.41	0.24	0.51	1.45	0.02	0.55	0.22	0.15	0.42
C (carb.)	5.30	3.35	5.58	3.16	2.93	4.21	4.22	4.01	4.52	3.86
S	0.03	0.03	0.02	0.32	<0.01	<0.01	<0.01	<0.01	0.03	0.06
Hg (ppm)	<0.01	<0.01	0.02	<0.01	0.02	0.01	0.04	0.48	0.12	0.03
Ag	<5	<5	<5	<5	<5	6	<5	6	6	6
As	15	50	15	20	30	30	30	100	100	50
B	L	L	N	N	L	N	N	50	N	N
Ba	500	150	150	300	150	300	70	150	300	300
Be	2	5	10	2	2	1.50	N	15	L	L
Bi	<0.20	0.70	5	<0.20	<0.20	<0.20	<0.20	<0.20	<0.20	0.70
Cd	0.50	0.30	<0.20	0.30	0.70	0.30	2	0.70	0.70	10
Co	26	31	23	26	22	27	24	39	26	16
Cr	100	200	200	300	150	150	70	300	150	70
Cu	15	5	5	70	300	10	7	70	20	70
F	1500	1000	1200	1000	800	100	800	2900	700	400
Ga	20	20	15	20	30	15	20	30	10	15
La	N	N	N	L	N	N	N	N	N	N
Mo	69	67	4	2	<5	<5	16	260	160	48
Ni	44	12	39	108	38	43	45	96	71	22
Pb	20	50	N	15	20	N	30	150	50	70
Sb	2	15	3	3	30	3	2	20	10	10
Sc	20	15	20	20	50	30	10	30	15	15
Sr	70	500	300	500	150	150	150	200	200	300
Th	<2.70	<5.50	<5.50	<4.40	<61	<3.50	<7.20	<18	<240	<230
Tl	<1	<1	2	<1	<1	<1	<1	3	7	2
U	1.59	7.38	9.52	4.96	298	6.38	18.40	67.20	936	906
V	100	300	200	200	300	200	70	300	300	150
Y	15	30	20	20	30	15	L	15	15	10
Yb	2	3	2	2	3	2	L	2	2	2
Zn	70	150	50	50	100	100	30	50	70	50
Zr	50	150	70	70	100	70	30	70	70	50
density (g/cm ³)	2.75	2.76	2.80	2.76	2.68	2.71	2.73	2.76	2.69	2.70

Analyzed for but not detected in any sample: Au, Ce, Eu, Ge, Hf, In, Li, Nb, Nd, Pd, Pt, Re, Se, Sm, Sn, Ta, Te, W. N: not detected; L: detected but below accurate detection limit; (-): not analyzed for

*Hematite adularia zone

Table A2. Chemical analyses of altered garnet-biotite gneiss.

	79S17	80S18	80S24	80S49	80S70	80S76	80S83	80S86	80S99	80S108	80S118
SiO ₂ (%)	53.90	48.10	37.80	36.60	37.80	45.80	34.70	51.60	51.60	50.10	55.20
Al ₂ O ₃	12.80	10.60	13.40	10.90	10.90	7.07	12.70	9.61	9.98	10.30	12.40
Fe (total)	11.10	17.20	8.44	15.00	14.90	18.40	30.10	13.50	14.80	16.60	11.30
FeO	9.85	13.20	7.37	13.20	—	—	—	10.60	12.90	14.50	9.23
Fe ₂ O ₃	1.39	4.44	1.19	2.00	—	—	—	3.22	2.11	2.33	2.30
MgO	3.10	3.50	4.80	5.55	4.50	4.50	2.60	3.10	3.00	3.20	2.60
CaO	1.59	1.93	10.20	4.78	6.09	2.04	7.13	3.25	2.70	3.92	1.38
Na ₂ O	<0.20	<0.20	2.20	2.50	2.00	<0.20	<0.20	<0.30	<0.20	<0.20	1.30
K ₂ O	5.86	3.18	4.49	3.14	4.19	2.56	0.11	4.02	5.13	2.36	5.05
TiO ₂	0.54	0.47	1.15	3.6	2.75	0.41	0.49	0.45	0.46	0.56	0.48
P ₂ O ₅	0.30	0.20	0.20	0.52	0.40	0.30	0.77	0.30	0.10	0.10	0.10
MnO	0.20	1.24	0.26	0.51	0.51	0.52	2.96	0.53	0.29	1.01	0.28
LOI	10.18	13.40	16.60	16.45	15.58	15.14	7.08	10.40	11.70	11.00	9.26
C (total)	2.61	3.87	4.38	4.49	4.69	4.76	2.32	—	—	—	—
C (org.)	0.20	1.49	0.51	0.17	0.38	2.13	0.37	—	—	—	—
C (carb.)	2.41	2.38	3.87	4.32	4.31	2.63	1.95	—	—	—	—
S	0.02	1.58	0.02	0.15	0.04	2.47	1.88	—	—	—	—
Hg (ppm)	<0.01	<0.01	0.01	0.02	0.01	0.81	0.03	0.28	0.08	0.02	0.02
Ag	<5	<5	<5	<5	<5	6	6	8	<5	<5	<5
As	30	30	30	70	30	50	20	20	<1	20	10
B	50	50	L	L	N	20	N	300	20	100	30
Ba	150	100	200	70	150	30	15	300	50	100	300
Be	15	7	7	5	5	7	N	10	7	5	3
Bi	0.20	1.50	<0.20	2	<0.20	1	<0.20	<0.20	<0.20	<0.20	<0.20
Cd	<0.20	2	0.50	2	0.50	7	1.50	0.50	0.70	0.70	<0.20
Co	11	25	26	31	15	22	5.20	18	6.40	4.60	13
Cr	70	50	150	10	70	30	50	70	70	50	70
Cu	3	100	3	70	3	200	100	200	3	70	70
F	2600	2500	1100	1200	1100	1900	700	1500	1600	1500	1000
Ga	30	15	20	20	20	20	—	20	70	20	20
La	N	N	N	N	N	N	N	L	N	N	50
Mo	4	28	12	<5	24	560	<5	760	25	71	<5
Ni	32	39	47	46	38	42	10	33	24	18	20
Pb	30	150	20	200	70	500	50	2000	20	7000	10
Sb	<1	15	1.50	15	7	100	2	20	2	20	<1
Sc	10	7	30	15	15	5	10	10	7	7	15
Sr	200	70	300	150	300	50	30	150	150	150	150
Th	<7.20	<27	<11	<2.20	<4.70	<370	<16	<290	<17.60	<7.10	<3.70
Tl	<1	<1	2	<1	<1	<1	<1	<1	<1	<1	<1
U	12.00	115	25.80	1.89	8.89	1550	67.80	1760	17.00	20.90	5.47
V	150	100	300	200	200	150	150	200	150	150	150
Y	20	20	20	30	20	10	20	10	10	L	20
Yb	2	2	3	3	3	1.50	3	—	—	—	2
Zn	70	20	100	500	30	700	150	200	300	200	200
Zr	70	70	70	100	70	70	70	70	50	70	100
density (g/cm ³)	2.83	2.87	2.76	2.80	2.81	2.86	3.47	2.80	2.81	2.75	2.80

Analyzed for but not detected in any sample: Au, Ce, Eu, Ge, Hf, In, Li, Nb, Nd, Pd, Prd, Pt, Re, Se, Sm, Sn, Ta, Te, W. N: not detected; L: detected but below accurate detection limit.

Table A3. Trace element data for samples from Illinois vein system.

	80S12	80S17	80S23	80S26	80S29	80S33	80S43	80S57	80S60
Ag (ppm)	<5	13	<5	<5	<5	14	<5	<5	<5
As	50	70	30	70	30	150	30	N	N
B	N	N	N	N	N	N	N	N	N
Ba	300	150	150	150	150	50	150	150	70
Be	L	2	1.50	1.50	1.50	1.50	5	1.50	1.50
Bi	5	1.50	1	7	10	2	1.50	N	N
Cd	1	2	1.50	3	1.50	3	3	N	N
Co	15	18	23	123	30	18	26	14	15
Cr	70	30	70	70	150	70	30	15	100
Cu	150	300	100	100	150	3000	30	50	7
F	100	200	100	100	200	500	800	200	200
Ga	15	10	10	10	15	15	15	10	15
Hg	0.64	0.33	0.59	0.75	0.04	0.09	0.07	0.16	0.04
La	N	N	N	N	N	N	N	N	N
Mo	707	2370	574	848	5	<5	260	440	38
Nb	L	15	N	N	L	10	L	N	N
Ni	30	44	31	36	83	26	52	43	38
Pb	1000	3000	200	1000	30	150	200	70	15
Sb	70	150	50	50	30	300	50	N	N
Sc	20	10	20	15	15	15	15	7	20
Sr	200	100	150	150	150	70	70	150	300
Th	<38	<2400	<450	<290	<5	<1600	<430	NA	<2.80
Tl	3	15	5	10	2	<1	10	N	N
U	169	7100	1440	880	7.40	5830	1800	NA	3.44
V	500	500	500	150	200	300	150	70	150
Y	20	30	15	15	20	20	15	20	20
Yb	3	N	2	1.50	2	3	1.50	2	2
Zn	70	500	70	70	70	150	200	700	N
Zr	30	150	30	50	70	150	70	70	30
SZ	0.11	0.87	0.14	0.97	0.23	.44	.15	NA	NA
C carb. %	5.41	4.73	5.75	5.89	4.14	5.62	4.05	NA	NA
C org. %	0.27	0.66	0.63	0.52	0.71	.29	.20	NA	NA
W	N	N	N	N	N	N	N	N	N

N: not detected

L: present but below detection limits

NA: not analyzed for

Table A4. Trace element data for sample from horsetail vein system.

	79S16	79S23	79S26	80S1	80S2	80S3	80S6	80S64	80S69	80S72	80S75	80S78	80S82
Ag(ppm)	<5	8	13	105	<5	21	15	27	12	18	6	79	27
As	50	50	100	300	50	70	70	100	50	100	70	300	300
B	N	N	N	N	N	N	N	N	N	L	N	N	N
Ba	150	150	30	150	30	50	150	100	100	100	150	200	150
Be	1.50	L	N	1.50	N	N	1.50	N	5	1.50	1.50	1.50	5
Bi	1	2	0.70	1	0.70	0.70	10	0.20	0.20	0.20	0.30	0.20	2
Cd	1.50	0.70	5	2	1.50	0.70	1	0.50	1	5	7	2	5
Co	14	17	18	188	6	14	49	43	33	6.5	9	160	34
Cr	50	15	30	10	15	20	50	20	100	30	50	100	30
Cu	50	150	100	3000	50	150	100	300	150	100	70	1500	700
F	200	200	<100	200	200	100	100	200	400	200	200	300	400
Ga	15	N	N	L	5	5	10	5	15	5	15	10	10
Hg	0.17	1.70	0.95	11	6.70	0.57	0.64	6	0.60	0.14	0.20	20	9
Ia	N	N	N	N	N	N	N	N	N	N	N	N	N
Mo	550	2710	2890	9810	5210	3210	2940	1800	1800	910	350	7500	8000
Nb	N	L	N	10	N	N	L	N	L	L	L	20	20
Ni	20	47	60	212	28	70	74	32	58	21	23	130	65
Pb	2000	1500	700	7000	5000	2000	500	1000	1500	7000	500	7000	20000
Sb	30	150	70	500	200	100	50	70	70	50	70	300	500
Sc	7	L	N	N	5	7	15	10	15	5	7	10	N
Sr	150	150	50	100	150	70	150	70	300	100	200	150	300
Th	<560	<3100	<1300	<5800	<4600	<780	<680	<1600	<160	<1200	<1000	<4700	<34000
Tl	20	30	30	50	50	15	15	50	10	7	10	20	50
U	1850	9380	4430	18000	14,400	2680	2300	5550	586	4090	3270	18100	28000
V	300	300	150	100	700	300	500	100	300	300	200	300	700
Y	10	20	L	30	20	L	20	30	30	15	20	20	70
Yb	N	N	N	N	N	1.50	2	3	3	N	2	3	N
Zn	70	30	50	100	70	70	50	15	30	2000	70	50	500
Zr	50	70	30	100	70	30	30	50	70	70	70	150	300
SZ	0.50	0.74	0.60	2.34	1.09	0.52	0.32	0.60	0.24	2.12	0.84	1.02	3.84
carb CZ	5.31	6.50	1.44	1.24	0.26	4.58	5.74	8.62	3.57	4.56	3.20	3.48	3.72
org CZ	0.36	0.34	2.55	0.23	0.08	0.26	0.23	0.04	1.19	1.17	1.24	0.49	0.34
W	N	N	N	N	N	N	N	N	N	N	N	N	200

N: not detected

L: present but below detection limits

NA: not analyzed for.

Table A5. Trace element data for samples from Rogers vein system.

	80S85	80S86	80S88	80S92	80S93	80S98	80S104	80S110	80S120
Ag (ppm)	24	8	14	<5	<5	16	29	8	<5
As	100	20	100	30	10	50	20	50	20
B	N	300	N	N	N	N	N	N	N
Ba	150	300	30	50	300	200	200	100	1000
Be	5	10	N	N	N	2	2	L	L
Bi	0.50	0.50	0.30	0.30	0.20	0.20	0.20	0.20	0.20
Cd	15	0.50	0.30	0.30	1.50	2	1	3	0.20
Co	26	18	36	13	8.90	16	55	17	10
Cr	30	70	5	5	50	50	30	30	30
Cu	300	200	100	100	50	150	150	150	20
F	700	1500	100	100	100	200	100	400	200
Ga	5	20	N	N	15	10	5	10	10
Hg	0.80	0.28	1.08	1.21	0.25	0.64	0.79	0.36	2.01
La	L	L	N	N	N	N	N	N	N
Mo	3400	760	760	800	270	3500	2200	2500	28
Nb	10	10	N	10	L	20	15	N	10
Ni	100	33	46	20	13	48	73	38	9.60
Pb	5000	2000	1000	500	200	3000	3000	3000	70
Sb	200	20	70	50	15	150	30	150	10
Sc	5	10	10	N	10	10	10	7	10
Sr	150	150	30	30	200	150	500	500	300
Th	<1500	<290	<510	<300	<260	<1400	<3100	<640	<1000
Tl	5	<1	3	5	2	10	7	5	<1
U	5520	1760	1910	1820	1550	6070	14,100	2530	4550
V	300	200	150	70	700	500	500	500	150
Y	30	10	10	N	15	20	30	15	30
Yb	N	N	N	N	N	N	N	N	3
Zn	2000	200	50	50	200	300	150	300	50
Zr	70	70	30	30	100	100	150	70	100
S%	NA	NA	NA	NA	NA	NA	NA	NA	NA
C carb. %	NA	NA	NA	NA	NA	NA	NA	NA	NA
C org. %	NA	NA	NA	NA	NA	NA	NA	NA	NA
W	N	N	N	N	N	N	N	N	N

N: not detected

L: present but below detection limits

NA: not analyzed for